



**TRIBHUVAN UNIVERSITY
INSTITUTE OF ENGINEERING
PULCHOWK CAMPUS**

THESIS NO: M-23-MSMDE-2017/2020

Numerical Study of Magnetohydrodynamic Flows past a Wedge Structure

by

Shailendra Rana

A THESIS

**SUBMITTED TO THE DEPARTMENT OF MECHANICAL AND
AEROSPACE ENGINEERING IN PARTIAL FULFILLMENT OF THE
REQUIREMENTS FOR THE DEGREE OF MASTER OF SCIENCE IN
MECHANICAL SYSTEMS DESIGN AND ENGINEERING**

**DEPARTMENT OF MECHANICAL AND AEROSPACE ENGINEERING
LALITPUR, NEPAL**

JULY, 2020

COPYRIGHT

The author has agreed that the library, Department of Mechanical and Aerospace Engineering, Pulchowk Campus, Institute of Engineering may make this thesis freely available for inspection. Moreover, the author has agreed that permission for extensive copying of this thesis for scholarly purpose may be granted by the professor(s) who supervised the work recorded herein or, in their absence, by the Head of the Department wherein the thesis was done. It is understood that the recognition will be given to the author of this thesis and to the Department of Mechanical and Aerospace Engineering, Pulchowk Campus, Institute of Engineering in any use of the material of the thesis. Copying or publication or the other use of this thesis for financial gain without approval of the Department of Mechanical and Aerospace Engineering, Pulchowk Campus, Institute of Engineering and author's written permission is prohibited.

Request for permission to copy or to make any other use of the material in this thesis in whole or in part should be addressed to:

Head

Department of Mechanical and Aerospace Engineering

Pulchowk Campus, Institute of Engineering

Lalitpur

Nepal

TRIBHUVAN UNIVERSITY
INSTITUTE OF ENGINEERING
PULCHOWK CAMPUS
DEPARTMENT OF MECHANICAL AND AEROSPACE ENGINEERING

The undersigned certify that they have read, and recommended to the Institute of Engineering for acceptance, a thesis entitled "**Numerical Study of Magnetohydrodynamic Flows past a Wedge Structure**" submitted by Shailendra Rana in partial fulfilment of the requirements for the degree of Master of Science in Mechanical Systems Design and Engineering.

Supervisor, Dr. Rajendra Shrestha
Professor
Department of Mechanical and Aerospace
Engineering

Supervisor, Mr. Hari Bahadur Dura
Assistant Professor
Department of Mechanical and Aerospace
Engineering

External Examiner, Dr. Sailesh Chitrakar
Lecturer
Department of Mechanical Engineering
Kathmandu University

Committee Chairperson, Dr. Nawraj Bhattarai
Head of Department
Department of Mechanical and Aerospace
Engineering

Date

ABSTRACT

The laminar viscous and incompressible flow of an electrically conducting fluid across an unconfined wedge structure in the presence of transverse magnetic field has been studied. The wedge structure is an equilateral triangular cylinder. Two-dimensional numerical simulations have been performed for Reynolds number (Re) = 1 - 150 and Hartmann number (Ha) = 0 - 10 for a fixed confinement ratio of 1/30. The fluid is assumed to have uniform physical properties. The magnetic Reynolds number is very small such that the induced magnetic field is negligible compared to the applied magnetic field. The magnetic induction method in magneto-hydrodynamics (MHD) module built in ANSYS FLUENT solver has been employed to compute the flow fields. Results show that the complete elimination of vortex shedding is achievable if the applied magnetic field is strong enough. In the steady flow regime, it has been found that the recirculation length reduces with the increase in Ha . A minimal reduction in the drag coefficient is observed with the increase in Ha as long as unsteady flow is maintained ($Ha < 7.3$). However, the drag coefficient has a tendency to significantly increase with the increase in Ha in a steady flow. Similarly, the lift amplitude decreases with the increase in Ha indicating a diminishing effect on the strength of vortices. A critical Hartmann number (Ha_{cr}) of 7.3 has been found for $Re = 100$ at which complete suppression of vortex shedding is observed.

ACKNOWLEDGEMENTS

I would like to express my sincere gratitude to Prof. Dr. Rajendra Shrestha and Asst. Prof. Hari Bahadur Dura, Pulchowk Campus for supervising my thesis work. Without their continuous support and guidance, this research would not have been completed.

I am thankful to the Department of Mechanical and Aerospace Engineering, Pulchowk Campus for technical assistance and support by providing access to computational resources. Without such assistance, I would not have completed this thesis work.

I am thankful to Er. Hemanta Dulal, Instructor, Department of Mechanical and Aerospace Engineering, Pulchowk Campus and Er. Milan Adhikari for their help and support on academic matters during my thesis period.

Moreover, I am grateful to my friends Er. Sanjay Mahat, Er. Nishant Bhatta, Er. Chiranjivi Dahal, Er. Saleen Bhattarai and Er. Janak Kumar Tharu for their continuous motivation and support during hard times.

Lastly, I will always be in debt to my beloved family; my mother Mrs. Durga Rana, my father Mr. Ram Bahadur Rana, brother and sister, Saurav and Sabina Rana for their continuous support and motivation. I would not be here today without them.

TABLE OF CONTENTS

COPYRIGHT	2
ABSTRACT	4
ACKNOWLEDGEMENTS	5
TABLE OF CONTENTS.....	6
LIST OF TABLES	10
LIST OF FIGURES	11
LIST OF SYMBOLS.....	13
LIST OF ABBREVIATIONS	15
CHAPTER ONE: INTRODUCTION.....	16
1.1. Background.....	16
1.2. Research Gap.....	20
1.3. Objectives.....	24
1.3.1. Main Objective.....	24
1.3.2. Specific Objectives.....	24
1.4. Scope and Limitations of Work.....	24
1.4.1. Scope of Work	24
1.4.2. Limitations of Work	25
CHAPTER TWO: LITERATURE REVIEW	26
2.1. Magneto-hydrodynamics.....	26
2.2. Governing Equations.....	27
2.2.1. Navier-Stokes Equations	27
2.2.2. Maxwell’s Equations.....	27
2.2.3. Magnetic Induction Formulation.....	28
2.2.4. Low- Re_m Approximation.....	29

2.3.	Fundamental Parameters	30
2.4.	Hydrodynamic Flow around Bluff Bodies	32
2.4.1.	Flow Regimes	33
2.4.2.	Vortex Shedding Phenomena.....	34
2.4.3.	Mechanism of Vortex Shedding.....	35
2.5.	Related Works	36
CHAPTER THREE: RESEARCH METHODOLOGY		39
3.1.	Research Design	39
3.2.	Research Methods.....	40
3.3.	Research Tools.....	40
3.3.1.	ANSYS Modeler	40
3.3.2.	ICEM CFD.....	40
3.3.3.	ANSYS Fluent	40
3.3.4.	Tecplot.....	41
3.4.	Study of MHD Flows past Square Cylinder.....	42
3.4.1.	Geometrical Configuration	43
3.4.2.	Mesh	44
3.4.3.	Physics Setup	46
3.4.4.	Mesh Independence Study.....	48
3.4.5.	MHD Simulations	49
3.5.	Study of Flow past Wedge without Magnetic Field	50
3.5.1.	Geometrical Configuration	50
3.5.2.	Mesh	52
3.5.3.	Physics Setup	54
3.5.4.	Mesh Resolution Study.....	55
3.6.	Study of Flow past Wedge with Magnetic Field	57
3.6.1.	Geometrical Configuration	57

3.6.2.	Mesh	58
3.6.3.	Physics Setup	59
CHAPTER FOUR: RESULTS AND DISCUSSION.....		60
4.1.	Study of MHD Flows past Square Cylinder.....	60
4.1.1.	Validation of Results	60
4.1.2.	Critical Hartmann Number	62
4.1.3.	Effects on Wake	63
4.1.4.	Effects on Drag and Lift coefficients	63
4.2.	Study of Flows past Wedge without Magnetic Field.....	69
4.2.1.	Validation of Results	69
4.2.2.	Study of Flow Patterns at Different Flow Regimes	71
4.2.3.	Study of Flow Patterns for Steady Flow Regimes	74
4.3.	Study of Flows past Wedge with Magnetic Field.....	75
4.3.1.	Calculation of Critical Hartmann Number	75
4.3.2.	Influence on Wake	76
4.3.3.	Influence on Drag and Lift coefficients.....	79
CHAPTER FIVE: CONCLUSIONS AND RECOMMENDATIONS.....		82
5.1.	Conclusions	82
5.2.	Recommendations.....	82
REFERENCES.....		83
PUBLICATIONS.....		89
APPENDIX-A: WEDGE MODEL VALIDATION DATA.....		90
APPENDIX-B: UDF CODE FOR SQUARE CYLINDER		91
APPENDIX-C: PYTHON CODE FOR STROUHAL NUMBER CALCULATION.....		92
APPENDIX-D: PRESSURE CONTOURS FOR SQUARE CYLINDER AT HA = 0 – 8.		94

APPENDIX-E: VELOCITY CONTOURS FOR SQUARE CYLINDER FOR HA = 0 - 8.....	95
APPENDIX-F: PRESSURE CONTOURS FOR SQUARE CYLINDER AT RE = 75 - 200.....	96
APPENDIX-G: VELOCITY CONTOURS FOR SQUARE CYLINDER AT RE = 75 - 200.....	97
APPENDIX-H: PRESSURE CONTOURS FOR WEDGE AT RE = 50 - 150	98
APPENDIX-I: VELOCITY CONTOURS FOR WEDGE AT RE = 50 - 150	99
APPENDIX-J: PRESSURE CONTOURS FOR WEDGE AT RE = 100 FOR HA = 0 - 10.....	100
APPENDIX-K: VELOCITY CONTOURS FOR WEDGE AT RE = 100 FOR HA = 0 - 10.....	101

LIST OF TABLES

Table 1.1: Research works on the flow past triangular cylinders	21
Table 1.2: Research works on the MHD flow past obstacles	22
Table 3.1: Details of meshes corresponding to square cylinder.....	44
Table 3.2: Mesh independence study for $Re = 100$, $\Delta t = 0.025 s$	48
Table 3.3: Computational domain for wedge.....	51
Table 3.4: Details of meshes	53
Table 3.5: Boundary conditions for the wedge model.....	55
Table 3.6: Results of mesh resolution study for $Re = 150$ at $\Delta t = 0.01 s$	56
Table 4.1: Range of critical Hartmann number for different Re	62
Table 4.2: Comparison of critical Hartmann number for $Re = 200$	63

LIST OF FIGURES

Figure 1.1: A general overview of TOKAMAKS reactor	17
Figure 1.2: Fusion reaction involving two nuclei of deuterium and tritium forming helium, neutrons and releasing tremendous amount of energy	17
Figure 1.3: A general overview of ITER reactor	18
Figure 1.4: HCLL BB in the ½ DEMO 2015 baseline	19
Figure 2.1: Mechanism showing induced current for fluid motion under magnetic field	26
Figure 2.2: Flow regimes of circular cylinder.....	32
Figure 2.3: Formation of vortex from shear layers	34
Figure 2.4: (a) Pulling of vortex B by vortex A before its shedding, (b) Pulling of vortex C by vortex B before its shedding	35
Figure 3.1: Research methodology.....	39
Figure 3.2: MHD analysis of square cylinder.....	42
Figure 3.3: Geometrical configuration for square cylinder	43
Figure 3.4: Mesh distribution and sub-computational domains.....	44
Figure 3.5: G4 mesh (a) Full view, (b) Zoomed view	45
Figure 3.6: Boundary conditions associated with square cylinder.....	46
Figure 3.7: Transverse magnetic field acting on the flow past square cylinder.....	49
Figure 3.8: Methodology for study of flow past wedge without magnetic field	50
Figure 3.9: Schematic diagram showing unconfined flow across the wedge	51
Figure 3.10: M1 mesh (a) Full view, (b) Zoomed view	52
Figure 3.11: Boundary conditions associated with the wedge.....	54
Figure 3.12: Schematic showing flow past the wedge under transverse magnetic field	57
Figure 3.13: M2 mesh (a) Full view, (b) Zoomed view	58

Figure 4.1: Validation of C_d for very low $Re = 1 - 50$	60
Figure 4.2: Validation of time-averaged C_d for $Re = 75 - 200$	61
Figure 4.3: Validation of St for $Re = 75 - 200$	61
Figure 4.4: Streamlines at $Re = 200$: (a) $Ha = 0$, (b) $Ha = 1.0$, (c) $Ha = 3.0$, (d) $Ha = 4.0$ and (e) $Ha = 8.0$	65
Figure 4.5: Vorticity contours at $Re = 200$: (a) $Ha = 0$, (b) $Ha = 1.0$, (c) $Ha = 3.0$, (d) $Ha = 4.0$ and (e) $Ha = 8.0$	66
Figure 4.6: Temporal variation of the drag coefficient with respect to the non- dimensional time at $Re = 200$: (a) $Ha = 0$, (b) $Ha = 1.0$, (c) $Ha = 3.0$, (d) $Ha = 4.0$ and (e) $Ha = 8.0$	67
Figure 4.7: Temporal variation of the lift coefficient with respect to the non- dimensional time at $Re = 200$: (a) $Ha = 0$, (b) $Ha = 1.0$, (c) $Ha = 3.0$, (d) $Ha = 4.0$ and (e) $Ha = 8.0$	68
Figure 4.8: Validation of time-averaged C_d for $Re = 50 - 150$	69
Figure 4.9: Validation of St for $Re = 50 - 150$	70
Figure 4.10: Validation of C_d for $Re = 10 - 40$	70
Figure 4.11: Streamlines for $Re = 1, 10, 30$ and 100	72
Figure 4.12: Vorticity contours for $Re = 1, 10, 30$ and 100	73
Figure 4.13: Streamlines for $Re = 10 - 40$	74
Figure 4.14: Variation of ΔC_d with Ha	75
Figure 4.15: Streamlines at $Re = 100$: (a) $Ha = 0$, (b) $Ha = 2.0$, (c) $Ha = 5.0$, (d) $Ha =$ 7.3 and (e) $Ha = 10$	77
Figure 4.16: Vorticity contours at $Re = 100$: (a) $Ha = 0$, (b) $Ha = 2.0$, (c) $Ha = 5.0$, (d) $Ha = 7.3$ and (e) $Ha = 10$	78
Figure 4.17: Temporal variation of drag coefficient at $Re = 100$: (a) $Ha = 0$, (b) $Ha =$ 2.0 , (c) $Ha = 5.0$, (d) $Ha = 7.3$ and (e) $Ha = 10$	80
Figure 4.18: Temporal variation of lift coefficient at $Re = 100$: (a) $Ha = 0$, (b) $Ha = 2.0$, (c) $Ha = 5.0$, (d) $Ha = 7.3$ and (e) $Ha = 10$	81

LIST OF SYMBOLS

μ_0	: Magnetic permeability of free space
ΔC_d	: Difference in the amplitude of drag coefficient
b	: Self-induced magnetic field
B	: Total magnetic field
B_0	: Externally imposed magnetic field
C_d	: Drag coefficient
C_l	: Lift coefficient
D	: Displacement current
d	: Side length of the triangular cylinder
D	: Side length of the square cylinder
E	: Electric field
f	: Frequency of the vortex shedding
F_d	: Drag force
F_l	: Lift force
H	: Width of the square model in the lateral direction
H	: Magnetic field strength
Ha	: Hartmann number
J	: Current density
L	: Total length for square cylinder in the axial direction
L_1	: Total length for wedge in the stream-wise direction
L_2	: Total width distance for wedge in the lateral direction
N	: Stuart number
Pr	: Prandtl number
Re	: Reynolds number
Re_m	: Magnetic Reynolds number
St	: Strouhal number
u	: Velocity field
U_0	: Parabolic maximum inlet velocity
U_{inf}	: Free-stream velocity of the fluid medium
X_d	: Downstream distance between rear surface of wedge and exit plane
X_u	: Upstream distance between inflow plane and rear side of the wedge

Δt	: Time-step size
δ	: First cell height in the mesh
ε	: Permittivity of the medium
μ	: Dynamic viscosity of the fluid medium
ρ	: Density of the fluid medium
σ	: Electrical conductivity of the fluid medium.
ϑ	: Kinematic viscosity of the fluid medium

LIST OF ABBREVIATIONS

ANSYS	: Analysis Systems
BB	: Breeding Blanket
CAD	: Computer Aided Design
CFD	: Computational Fluid Dynamics
ITER	: International Thermonuclear Experimental Reactor
MATLAB	: Matrix Laboratory
MHD	: Magneto-hydrodynamics
NASA	: National Aeronautics and Space Administration
OPENFOAM	: Open Field Operation and Manipulation
SIMPLE	: Semi-Implicit Pressure Linked Equations

CHAPTER ONE: INTRODUCTION

1.1. Background

The flow of an electrically conducting fluids in the presence of external magnetic field cannot be described by usual hydrodynamics. Such physical phenomena is explained by magneto-hydrodynamics (MHD). MHD combines the classical fluid dynamics and electro-dynamics. The field of MHD has been extensively studied through experimental and numerical approaches. For instance, one of the major works was done by Hartmann (1937) who studied the flow of a liquid metal in a duct in the presence of external magnetic field. Today, MHD has expanded into an extensive field covering several areas like liquid metal flows in fusion reactors and metallurgical industry, astrophysical solar and planetary flows etc.

Several electromagnetic methods have been applied to control and manipulate the flows of electrically conducting fluids in different fields. Some of the applications of MHD are pumps, generators, metallurgical industries, material processing etc. For instance, in metallurgical and material processing, the application of magnetic fields includes heating, melting and casting of conducting materials, stirring and levitation of liquid metals (Davidson, 1999; Davidson, 2001; Ivlev & Baranov, 1993; Kolesnichenko, 1990).

Nowadays, several material processing industries extensively make use of electromagnetic pumps to transport and dose melting metal (Ivlev & Baranov, 1993). This is because electromagnetic pumps offer several advantages over mechanical pumps such as absence of moving and rotating parts, noiseless operations, simplicity of control etc.

In the last two decades, magneto-hydrodynamics has been receiving attention owing to its applications in fusion reactors. The production of electricity using fusion technology is based on magneto-hydrodynamics. The nuclear reactor is where the nuclear reactions occurring in the Sun are reproduced, releasing tremendous amount of heat energy. Figure 1.1 shows a general overview of TOKAMAKS reactor.

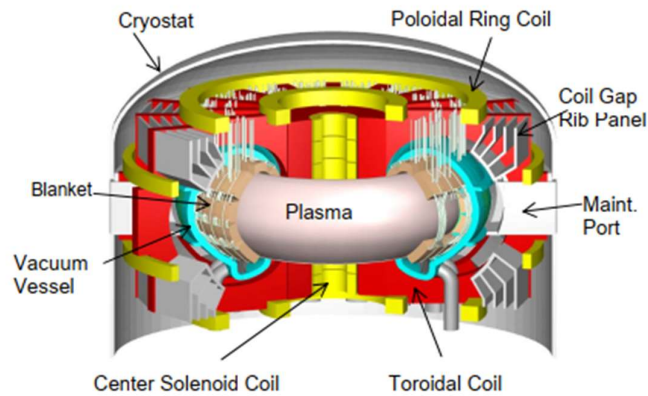


Figure 1.1: A general overview of TOKAMAKS reactor (Ligere, 2014)

Two fuels namely: deuterium and tritium are combined together in a fusion reactor for reactions to occur. The mechanism is that a nucleus of deuterium fuses with a nucleus of tritium to produce a nucleus of Helium and neutrons releasing tremendous amount of heat energy. The energy released is 17 MeV per reaction. Figure 1.2 depicts the process of fusion reaction involving two nuclei of deuterium and tritium.

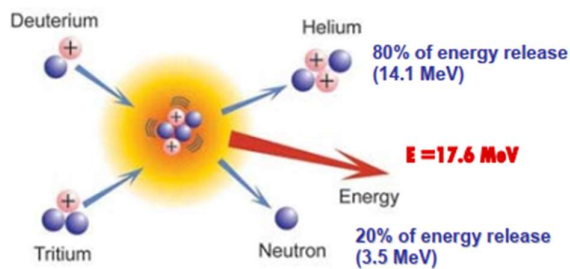


Figure 1.2: Fusion reaction involving two nuclei of deuterium and tritium forming helium, neutrons and releasing tremendous amount of energy (Ligere, 2014)

One of the major events involving the reactions between deuterium and tritium is that the temperatures reach above 100 million centigrade. Above such temperatures, the two aforementioned fuels become ionized to form an electrically highly conducting plasma which are confined inside a toroidal shell by a set of superconducting magnet coils. Several researches indicate that tokamak reactors offer impressive plasma confinement system having proven their capabilities in different experiments in several countries. But tokamak systems also had some drawbacks. Experiments showed that the duration

of plasma confinement was short and the production of energy was less than that of the energy supplied for the experiment. To overcome such drawbacks, Europe, USA, Russia and Japan developed the first thermonuclear nuclear reactor based on tokamak system known as ITER, which stands for International Thermonuclear Experimental Reactor. A general overview of ITER reactor is shown in Figure 1.3. It is the first thermonuclear reactor designed to produce more energy than it requires. For the input of 50 MW heating power, it is able to produce 500 MW of fusion power for the pulses of 400-600 seconds.

One of the key components of a nuclear reactor is blankets modules which form the walls of the vacuum vessel. Blankets modules are employed for mainly two purposes. They are designed to slow down the high-energy neutrons where their kinetic energy is converted into heat energy. This energy is used for production of electricity in nuclear power plants. And blankets modules are also used for the breeding of tritium, an isotope not naturally available, but can be extracted from liquid metal (Lielausis, 1989; Buhler, 2007).

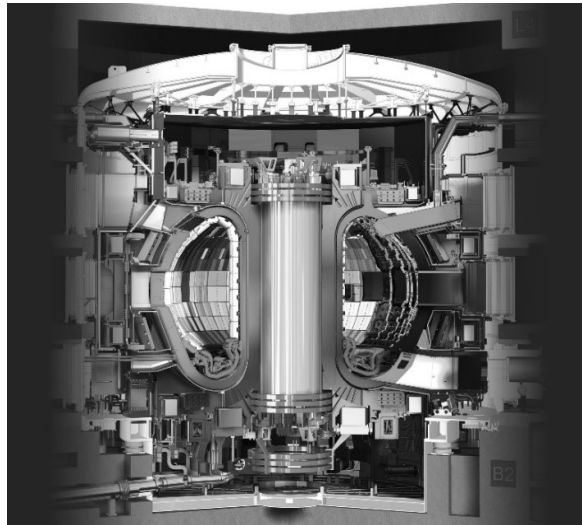


Figure 1.3: A general overview of ITER reactor (ITER Organization, 2020)

Several designs of liquid metal blankets have already been investigated. As of now, three main concepts of liquid metal blanket modules are in the phase of development. (Mistrangelo & Buhler, 2017). For the water-cooled and the helium cooled lead-lithium blankets (HCLL), the lead-lithium (PbLi) alloy is utilized for breeding purposes to produce tritium used to create plasma in a confined state. The fusion heat is removed

by a separated water or helium cooling system. At such condition, the liquid metal can be considered at rest. Instead, the dual coolant lead lithium blanket is provided with the liquid metal as tritium breeder and to remove the deposited heat in the breeding zone. Helium cools the first wall and blanket module. Following this concept, PbLi has a tendency for faster flow (10 cm/s) which contributes to rapid cooling of the breeding section. Figure 1.4 shows a typical design of the HCLL breeding blanket module in the ½ DEMO 2015 baseline.

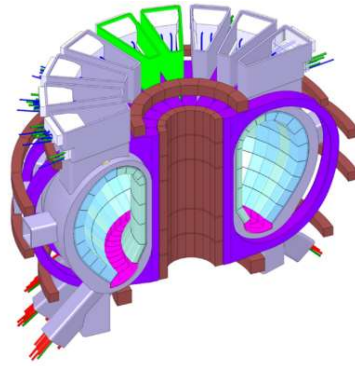


Figure 1.4: HCLL BB in the ½ DEMO 2015 baseline (Aubert, 2018)

As mentioned earlier, in HCLL blankets, the circulating liquid metal PbLi experiences the magnetic field. This magnetic field, in particular, has significant influence on the heat transfer inside these blankets. The heat transfer mechanism can be enhanced by creating a turbulent flow and a technique to introduce turbulence is placing obstacles inside the blanket modules (Dousset & Potherat, 2008; Hussam, et al., 2011; Chatterjee & Gupta, 2015). This is the fundamental concept which forms the basis of this thesis.

Thus, the study of incompressible MHD flows of an electrically conducting fluid in the presence of obstacles is of main interest in this thesis. Several studies on MHD flows of conducting fluids in confined medium i.e. inside channels and ducts in the presence of obstacles have been already conducted (Chatterjee, et al., 2012). It is to be noted that the shape of the obstacle has significant influence on flow dynamics despite offering many similarities (Dousset, 2009). This particular concept also forms the basis of research for this thesis. To conclude, this thesis focuses on incompressible MHD flows of conducting fluids in an unconfined medium in the presence of an obstacle.

1.2. Research Gap

The flow around obstacles lies at the heart of this thesis. For over a century, flow past obstacles such as circular cylinders have received tremendous attention from researchers due to practical engineering applications. Such obstacles find practical engineering applications in diverse fields such as heat exchangers, marine risers, road vehicles, pipelines, design of vortex flowmeters, cooling towers etc. Owing to their practical applications in the real world, there have been massive numerical and experimental studies for over a century. It is seen that researchers are keen on understanding the flow dynamics past such obstacles at different flow regimes. For example, one of the prominent features of the flow past such obstacles is the vortex shedding phenomena occurring at different flow regimes. Such phenomena have been massively investigated by both numerical and experimental methods.

To get a big picture of how extensive research works have been done regarding the flow past cylinders, one can refer the works done by Zdravkovich (1997). Zdravkovich (1997) made a huge compilation of the studies regarding the flow over cylinders in his book. In contrast to non-MHD flows around circular cylinders, limited information is available regarding the hydrodynamic flows past non-circular obstacles such as square, rectangular and triangular cylinders. In particular, the obstacle of interest in this thesis is the triangular cylinder. Although the shape of an obstacle has considerable effects, studies have shown that the flow dynamics of the triangular cylinders present many similarities with circular or square cylinders. For example, the hydrodynamic studies of the flow past triangular cylinders also exhibit vortex shedding mechanism, however, initiating at a low Reynolds number i.e. 39.9 (De & Dalal, 2006). A comprehensive review of the literature indicates that limited information is available regarding the flow past triangular cylinders.

Several studies on the hydrodynamic flows past triangular cylinders are available. Jackson (1987) numerically investigated the two dimensional laminar flow past bodies of different shapes such as circular cylinder, triangular prism of different shapes, flat plates and elliptical cylinders. Johansson, et al. (1993) studied the turbulent flow around triangular-shaped flameholders for Reynolds number (Re) = 45000 using finite volume code with k- ϵ turbulence model. He observed unsteady flow past the flameholders evidenced by the presence of von-Karman vortex streets having a Strouhal frequency

of 0.27. Wesfried & Zielinska (1995) performed a numerical investigation regarding the flow past an equilateral triangular obstacle for Reynolds numbers up to 50 using spectral finite element code. Wesfried, et al. (1996) experimentally and numerically studied the flow past equilateral triangular obstacle to investigate the two dimensional structure of the global mode of the longitudinal component of the velocity using spectral finite element code. Abbasi, et al. (2001) numerically studied the laminar flow and heat transfer past a triangular prism placed in a confined channel for Reynolds number ranging from 20 to 250 at Prandtl number (Pr) = 0.71. De & Dalal (2006) conducted a numerical study of the laminar incompressible flow past an equilateral triangular obstacle for $Re = 50 - 250$ to investigate wake dynamics. Chattopadhyay (2007) numerically investigated the turbulent flow and heat transfer in a channel consisting of a triangular prism for Reynolds numbers up to 40000. Other studies regarding the flow past triangular obstacle were conducted by De & Dalal (2007), Dalal, et al. (2008) and Dhiman & Shyam (2011). A quick overview of the past research works done by some researchers regarding the flow past triangular cylinders can be found in Table 1.1.

Table 1.1: Research works on the flow past triangular cylinders

S.N.	Authors	Type of research	Reynolds number	Spatial dimensions
1.	(Jackson, 1987)	Numerical	Up to 50	2D
2.	(Johansson, et al., 1993)	Numerical	45,000	2D
3.	(Wesfried & Zielinska, 1995)	Numerical	Up to 50	2D
4.	(Wesfried, et al., 1996)	Experimental , Numerical	-	2D
5.	(Abbasi, et al., 2001)	Numerical	20 - 250	2D
6.	(De & Dalal, 2006)	Numerical	10 - 250	2D
7.	(Chattopadhyay, 2007)	Numerical	Up to 40,000	2D
8.	(De & Dalal, 2007)	Numerical	80 - 200	2D
9.	(Dalal, et al., 2008)	Numerical	10 - 200	2D, 3D
10.	(Dhiman & Shyam, 2011)	Numerical	50 - 150	2D

Table 1.2: Research works on the MHD flow past obstacles

S.N.	Authors	Research approach	Reynolds number	Spatial dimensions	Obstacle shape
1.	(Mutschke, et al., 1998)	Numerical	50 - 300	2D/3D	Circular
2.	(Weier, et al., 1998)	Numerical, Experimental	200	2D/3D	Circular
3.	(Posdziech & Grundmann, 2001)	Numerical	10 - 300	2D	Circular
4.	(Chen & Aubry, 2005)	Numerical	200	2D	Circular
5.	(Singha , et al., 2007)	Numerical	50 - 250	2D	Square
6.	(Singha & Sinhamahapatra , 2011)	Numerical	50 - 250	2D	Circular
7.	(Chatterjee, et al., 2012)	Numerical	10 - 40	2D	Circular, Square
8.	(Zhang, et al., 2014)	Numerical	150	2D	Circular
9.	(Hussam, et al., 2018)	Numerical	3000	2D	Triangular

The main interest of this thesis is the magnetohydrodynamic flows past cylinders. Just as limited studies on the flow dynamics past triangular cylinders are available, studies pertaining to MHD flows past obstacles like circular or square cylinders are also scarce. A thorough review of literature regarding MHD flows past obstacles has been done. Table 1.2 provides a list of works regarding MHD flows past obstacles of different shapes. The review of the literature suggests that most of the MHD flows focussed more on circular cylinders while a few research works on MHD flows past square cylinders are also available. It can be observed that researchers are keen on investigating the influence of magnetic field on wake dynamics behind such obstacles. Studies involve both steady and unsteady MHD flows in the laminar flow regime for small Hartmann

numbers to investigate the effects on drag and lift coefficients, Strouhal number, vorticity contours etc. Numerical and experimental MHD flows past circular cylinders for unsteady laminar flow regime were conducted by several researchers like Mutschke, et al. (1998), Weier, et al. (1998), Chen & Aubry (2005), Singha & Sinhamahapatra (2011) and Zhang, et al. (2014). Posdziech & Grundmann (2001) numerically investigated the steady and unsteady magnetohydrodynamic flows past circular cylinders for Reynolds numbers ranging from 10 to 300. Chatterjee, et al. (2012) numerically investigated the influence of magnetic field on the two-dimensional steady separated flows across circular and square cylinders for low Reynolds number ranging from 10 to 40 in unbounded configurations. Singha, et al. (2007) studied the two-dimensional MHD flows past square cylinders for $Re = 50 - 250$. Recently, Hussam, et al. (2018) numerically studied the influence of aligned magnetic field on fluid flow and heat transfer of an electrically conducting fluid past triangular cylinder for $Re = 100 - 3000$ at high Hartmann numbers (Ha) ranging upto 2400.

From above discussions, it can be concluded that there is still a gap in numerical and experimental MHD flows past triangular cylinders. This thesis attempts to close such gap by numerically investigating laminar, incompressible and unsteady MHD flows past an equilateral triangular cylinder (wedge) in an unconfined medium for $Re = 1 - 150$ and $Ha = 0 - 10$.

1.3. Objectives

In order to successfully complete a thesis, several objectives associated with the thesis problem has to be met. This thesis shall be completed by fulfilling the following objectives as follows:

1.3.1. Main Objective

The main objective of this research is to study the effects of magneto-hydrodynamics on vortex shedding past the wedge structure at low Hartmann numbers.

1.3.2. Specific Objectives

To accomplish the main objective, the following specific objectives shall be met as follows:

- i) To study and validate the MHD flows past square cylinder at $Re = 1 - 200$ for low Hartmann numbers i.e. $Ha = 0 - 8$.
- ii) To find the critical Hartmann number for MHD flows past the square cylinder at $Re = 200$.
- iii) To study and validate the flow past wedge structure without magnetic field at low Reynolds numbers i.e. $Re = 1 - 150$.
- iv) To study the flow past the wedge structure with magnetic field at $Re = 100$ for low Hartmann numbers i.e. $Ha = 0 - 10$ and determine the critical Hartmann number.

1.4. Scope and Limitations of Work

The scope and limitations of thesis works are explained as follows:

1.4.1. Scope of Work

Many space propulsion vehicles such as Ion Propulsion and Variable Specific Impulse Magnetoplasma Rocket (VASIMR) exploit the principles of magneto-hydrodynamics. In particular, relevant to this thesis, the nuclear fusion power plant technologies also make use of MHD principles with the aim of cleaner way of generating electricity. The placement of promoters like triangular cylinder inside the blanket modules of a fusion reactor aims to enhance the heat transfer since such promoters offer qualities that promote turbulence. The present work considers the flow of an electrically conducting

fluid past a wedge at low Reynolds numbers i.e. $Re = 1 - 150$, evident in nuclear reactors which employ liquid metals. Moreover, such flow conditions are also present in microfluidic devices, semi-conductors etc. and thus find the applications. Hence, the current research will provide a theoretical framework in understanding the wake dynamics past the wedge structure in a magneto-hydrodynamics flow.

1.4.2. Limitations of Work

The limitations of this work are enlisted as follows:

- i) All the research works are solely based on CFD analysis.
- ii) Although the experimental analysis has not been done, the numerical results obtained from CFD analysis have been verified against the past research studies.

CHAPTER TWO: LITERATURE REVIEW

2.1. Magneto-hydrodynamics

Magneto-hydrodynamics comprises of classical fluid mechanics and electromagnetism. A magneto-hydrodynamic flow can be described as the motion of electrically conducting fluids under imposed magnetic field (Davidson, 2001). Figure 2.1 provides a pictorial description of MHD phenomena involving plasma as the conducting fluid.

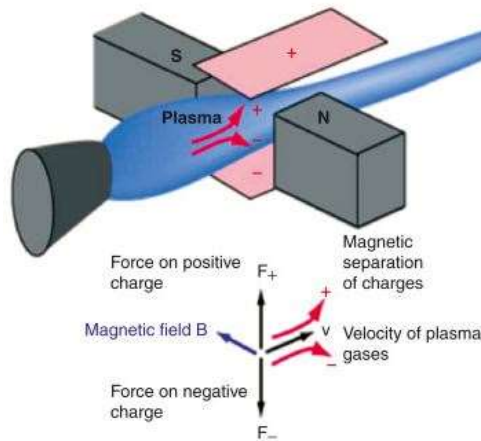


Figure 2.1: Mechanism showing induced current for fluid motion under magnetic field (Sheikholeslam & Domairry, 2016)

The mechanism of MHD flow can be described by the following points:

- i) For an electrically conducting fluid moving with velocity u under the influence of an externally imposed magnetic field B_0 , the mutual interaction between the magnetic field B_0 and the velocity field u develops an electromotive force according to Faraday's law of induction. This, in turn, induces electric currents, the current density being of order $\sigma(u \times B_0)$ and σ being the electrical conductivity of the fluid medium.
- ii) These induced currents, in accordance with Ampere's law, give rise to induced magnetic field b . Then, the net magnetic field is the summation of original magnetic field (B_0) and induced magnetic field (b).

iii) Now, the interaction between the total magnetic field B (imposed and induced ones) and the induced current density J , produces a Lorentz force per unit volume, $J \times B$.

2.2. Governing Equations

A laminar viscous incompressible flow of an electrically conducting fluid under externally imposed magnetic field can be described by a set of Navier-Stokes and Maxwell's equations. Consider the flow of a conducting fluid of density ρ , kinematic viscosity ν and electrical conductivity σ under externally imposed magnetic field B_0 . The governing equations regarding the MHD flow are described as follows:

2.2.1. Navier-Stokes Equations

For incompressible fluids, the mass conservation equation is defined as:

$$\nabla \cdot u = 0 \quad \text{Equation 2.1}$$

The momentum equation is given by:

$$\frac{\partial u}{\partial t} + u \cdot \nabla u = -\nabla (p / \rho) + \mathcal{G} \nabla^2 u \quad \text{Equation 2.2}$$

If the magnetic field is present, an additional term is added to the momentum equation i.e. Equation 2.2 in order to describe the incompressible MHD flows. Thus, the following equation is obtained as follows:

$$\frac{\partial u}{\partial t} + u \cdot \nabla u = -\nabla (p / \rho) + \mathcal{G} \nabla^2 u + (J \times B) / \rho \quad \text{Equation 2.3}$$

In Equation 2.3, the term $J \times B$ describes the Lorentz force acting on the flow field.

2.2.2. Maxwell's Equations

Maxwell's equations can be described under four different equations which represent the field of electromagnetics. Maxwell's equations can be described by Equations 2.4-2.7 as follows:

$$\nabla \cdot B = 0 \quad \text{Equation 2.4}$$

$$(\nabla \times E) = -\frac{\partial B}{\partial t} \quad \text{Equation 2.5}$$

$$\nabla \cdot D = 0 \quad \text{Equation 2.6}$$

$$\nabla \times H = J + \frac{\partial D}{\partial t} \quad \text{Equation 2.7}$$

The induction fields H and D are defined as:

$$H = \frac{1}{\mu} B \quad \text{Equation 2.8}$$

$$D = \varepsilon E \quad \text{Equation 2.9}$$

All the MHD simulations have been conducted using the magnetic induction method in MHD module built in ANSYS Fluent. The magnetic induction method describing the MHD flows can be derived using Ohm's law, Ampere's law and Maxwell's equations.

2.2.3. Magnetic Induction Formulation

The theoretical framework regarding magnetic induction method is provided by Altintas & Ozkol (2015) as follows:

Mathematically, for a stationary conducting medium, Ohm's law defines the current density as follows:

$$J = \sigma E \quad \text{Equation 2.10}$$

When an external magnetic field is present, the fluid motion described by velocity field u gives the current density as follows:

$$J = \sigma(E + u \times B) \quad \text{Equation 2.11}$$

From Equation 2.5,

$$\frac{\partial B}{\partial t} = -\nabla \times E \quad \text{Equation 2.12}$$

From Equation 2.11,

$$E = \left(\frac{J}{\sigma} - u \times B \right) \quad \text{Equation 2.13}$$

Taking the curl on both sides in Equation 2.13, we obtain,

$$\nabla \times E = \nabla \times \left(\frac{J}{\sigma} - u \times B \right) \quad \text{Equation 2.14}$$

Inserting Equation 2.14 into Equation 2.12, we obtain,

$$\frac{\partial B}{\partial t} = -\nabla \times \left(\frac{J}{\sigma} - u \times B \right) \quad \text{Equation 2.15}$$

$$\frac{\partial B}{\partial t} = -\nabla \times \left(\frac{J}{\sigma} \right) + \nabla \times (u \times B) \quad \text{Equation 2.16}$$

Without considering the effects of displacement current, Equation 2.7 becomes:

$$\nabla \times H = J \quad \text{Equation 2.17}$$

Using Equation 2.8,

$$\frac{1}{\mu} (\nabla \times B) = J \quad \text{Equation 2.18}$$

Substituting Equation 2.18 into Equation 2.16, we get,

$$\frac{\partial B}{\partial t} = -\frac{1}{\mu\sigma} \nabla \times (\nabla \times B) + \nabla \times (u \times B) \quad \text{Equation 2.19}$$

Equation 2.19 can be rewritten as:

$$\frac{\partial B}{\partial t} = -\frac{1}{\mu\sigma} (\nabla(\nabla \cdot B) - B(\nabla \cdot \nabla)) + u(\nabla \cdot B) - B(\nabla \cdot u) \quad \text{Equation 2.20}$$

Using Equation 2.4, we get,

$$\frac{\partial B}{\partial t} = \frac{1}{\mu\sigma} \nabla^2 B + u(\nabla \cdot B) - B(\nabla \cdot u) \quad \text{Equation 2.21}$$

Equation 2.21 can be rewritten as:

$$\frac{\partial B}{\partial t} = \nabla \times (u \times B) + \frac{1}{\mu\sigma} \nabla^2 B \quad \text{Equation 2.22}$$

Equation 2.22 represents the mathematical formulation of the magnetic induction method. By solving Equation 2.22, we can obtain B , and using B , we can compute J .

2.2.4. Low- Re_m Approximation

As stated earlier, the total magnetic field B acting in the flow domain is the summation of imposed magnetic field B_0 and induced magnetic field b . Mathematically, it can be expressed as:

$$B = B_0 + b \quad \text{Equation 2.23}$$

The induced magnetic field b in Equation 2.23 is negligible under low magnetic Reynolds number (Re_m) approximation. Under such approximation, Re_m is assumed to be very small i.e. $Re_m \ll 1$.

Here, Equations 2.1, 2.3, 2.22 and 2.23 completely describe the incompressible MHD flows. If low- Re_m approximation is considered, Equation 2.22 reduces as follows:

$$\frac{\partial B}{\partial t} = \frac{1}{\mu\sigma} \nabla^2 B \quad \text{Equation 2.24}$$

For example, in liquid metal flows, $Re_m \ll 1$ condition is generally observed which satisfies the low Re_m approximation. It is to be noted that such low- Re_m approximation has been considered for all MHD simulations in this work.

2.3. Fundamental Parameters

For an incompressible MHD flow, the essential parameters of interest are briefly described as follows:

- i) Magnetic Reynolds number (Re_m)

Magnetic Reynolds number is the ratio of induction of a magnetic field by fluid motion to magnetic diffusion. Mathematically, it is expressed as:

$$Re_m = \frac{\text{Momentum advection}}{\text{Magnetic diffusivity}} = \mu_0 \sigma U_\infty d \quad \text{Equation 2.25}$$

where, U_∞ , σ and d represent freestream fluid velocity, electrical conductivity and characteristic length of the obstacle respectively.

- ii) Hartmann number (Ha)

The Hartmann number expresses the relation between electromagnetic and viscous forces acting on the fluid. Mathematically, it is given by:

$$Ha = \left(\frac{\text{Electromagnetic forces}}{\text{Viscous forces}} \right)^{1/2} = B_0 d \sqrt{\frac{\sigma}{\mu}} \quad \text{Equation 2.26}$$

- iii) Reynolds number (Re)

The Reynolds number expresses the relation between inertial and viscous forces acting on the fluid. Mathematically, it can be expressed as:

$$Re = \frac{\text{Inertial forces}}{\text{Viscous forces}} = \frac{\rho U_{\infty} d}{\mu} \quad \text{Equation 2.27}$$

iv) Strouhal number (St)

The frequency of vortex shedding is expressed by a dimensionless Strouhal number. Mathematically, it can be expressed as:

$$St = \frac{fd}{U_{\infty}} \quad \text{Equation 2.28}$$

where, f represents the vortex shedding frequency.

v) Stuart Number (N)

Stuart number, also referred as the interaction parameter, is defined as the ratio of electromagnetic to inertial forces. Mathematically, it can be expressed as:

$$N = \frac{B_0^2 d \sigma}{\rho U_{\infty}} \quad \text{Equation 2.29}$$

vi) Drag coefficient (C_d)

Drag coefficient describes the resistive force offered by an obstacle in a fluid flow. Mathematically, it can be expressed as:

$$C_d = \frac{2F_d}{\rho U_{\infty}^2 A} \quad \text{Equation 2.30}$$

where, F_d is the drag force acting the object and A is the reference area.

vii) Lift coefficient (C_l)

Lift coefficient describes the lift generated by an object in a flow fluid. Mathematically, it can be expressed as:

$$C_l = \frac{2F_l}{\rho U_{\infty}^2 A} \quad \text{Equation 2.31}$$

where, F_l is the force due to lift acting on the object.

2.4. Hydrodynamic Flow around Bluff Bodies

This section provides a concise introduction to the hydrodynamic flows around bluff bodies where no magnetic field is applied. Despite dissimilar geometry of bluff bodies such as circular, square or triangular cylinders, they offer many similarities in terms of wake structure. Since this thesis is concerned with MHD flows past such bodies, firstly, it is important to be familiar with the flow regimes and related flow patterns around such bodies when no magnetic field is present.


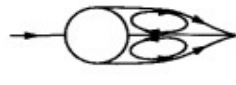




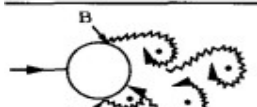
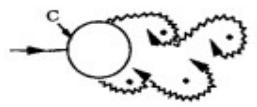

	No separation. Creeping flow	$Re < 5$
	A fixed pair of symmetric vortices	$5 < Re < 40$
	Laminar vortex street	$40 < Re < 200$
	Transition to turbulence in the wake	$200 < Re < 300$
	Wake completely turbulent. A: Laminar boundary layer separation	$300 < Re < 3 \times 10^5$ Subcritical
	A: Laminar boundary layer separation B: Turbulent boundary layer separation; but boundary layer laminar	$3 \times 10^5 < Re < 3.5 \times 10^5$ Critical (Lower transition)
	B: Turbulent boundary layer separation; the boundary layer partly laminar partly turbulent	$3.5 \times 10^5 < Re < 1.5 \times 10^6$ Supercritical
	C: Boundary layer com- pletely turbulent at one side	$1.5 \times 10^6 < Re < 4 \times 10^6$ Upper transition
	C: Boundary layer com- pletely turbulent at two sides	$4 \times 10^6 < Re$ Transcritical

Figure 2.2: Flow regimes of circular cylinder (Sumer & Fredsoe, 2006)

2.4.1. Flow Regimes

The motion of an incompressible Newtonian fluid across a circular cylinder in an unconfined medium is considered. The flow is described by Reynolds number defined

as: $Re = \frac{\rho U_{\infty} d}{\mu}$. It has been experimentally and numerically established that there exists

a critical Re at which the flow makes successive transitions between flow regimes.

With reference to Figure 2.2, different flow regimes established based on Reynolds number are discussed. A short description of different flow regimes based on variation of Re is provided in the following points:

- i) At $Re < 5$, a creeping flow mechanism or Stokes flow is observed. At this regime, the flow remains attached to the surface of the cylinder and takes the shape of the cylinder since the viscous forces are more dominant than the inertial forces. No flow separation and recirculation bubbles are observed.
- ii) At $4 < Re < 40$, a recirculating wake with the presence of twin vortices known as ‘recirculation bubble’ is observed. The length of the recirculating wake increases with the increment of Reynolds number.
- iii) At $40 < Re < 200$, the flow can be described by the presence of laminar vortex shedding. As the Reynolds number is further increased i.e. $Re > 40$, the wake becomes unstable to exhibit vortex shedding phenomena where vortices shed alternately from the upper and lower regions of the cylinder.

This thesis is concerned only with the first three flow regimes. Hence, other flow regimes based on Reynolds number are not discussed here.

2.4.2. Vortex Shedding Phenomena

One of the distinguishing flow characteristics around cylinders is the vortex shedding phenomena occurring at particular flow regimes. Beyond $Re = 40$, the arising of wake instability leads to the formation of von-Karman vortex streets behind the cylinder.

The adverse pressure gradient arising at the back side of the cylinder causes the boundary layer on the surface of the cylinder to separate, forming shear layers on the upper and lower regions of the cylinder. These shear layers roll up to form vortices on the upper and lower regions of the cylinder. These formed vortices rotate in opposite direction to each other. In Figure 2.3, vortex A and B are the two vortices formed on the upper and lower regions of the cylinder respectively.

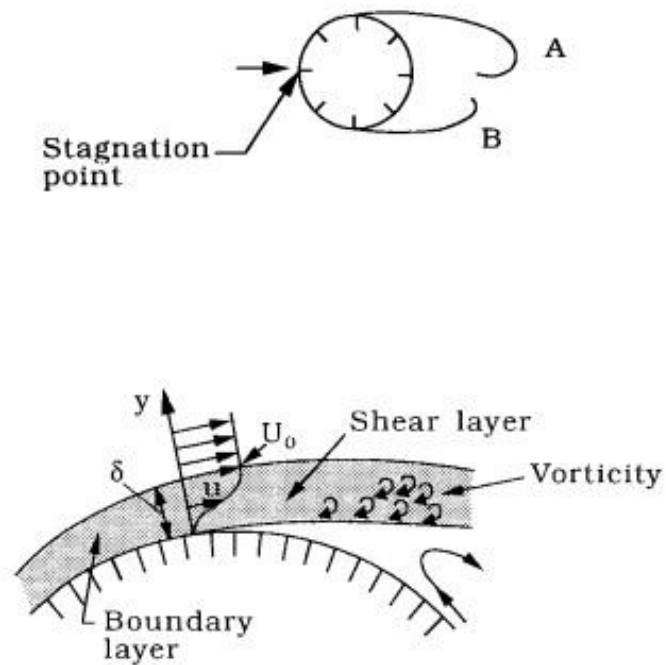


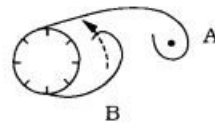
Figure 2.3: Formation of vortex from shear layers (Sumer & Fredsoe, 2006)

2.4.3. Mechanism of Vortex Shedding

A widely accepted theory regarding the formation of vortex shedding was well described by Gerrard (1966). His theory was based on the notion that vortex shedding phenomena occur as a result of interaction between shear layers formed on both the upper and lower regions of the cylinder. Processes that lead to the formation of alternating vortex shedding are described as follows:

- i) The large-sized vortex A of high strength has the capacity to pull vortex B having opposite sign in the wake region as shown in Figure 2.4 (a). The vortex A rotates in the clockwise direction whereas vortex B rotates in the anti-clockwise direction. The vorticity originating in the boundary layer is supplied to vortex A which is then interrupted by the opposite vorticity present in vortex B. These processes lead to the shedding of vortex A and is convected downstream of the wake as shown in Figure 2.4 (b).
- ii) After the vortex A is shed off, a forming vortex C is being pulled by the larger vortex B. Now, the vortex B growing in size and strength, plays the same role as vortex A. The vortex B gets cut off and convected downstream of the wake. This process continues to occur in a cyclic manner leading to the formation of alternating vortex shedding phenomena.

(a)



(b)

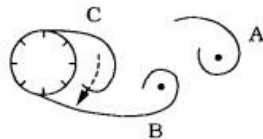


Figure 2.4: (a) Pulling of vortex B by vortex A before its shedding, (b) Pulling of vortex C by vortex B before its shedding (Sumer & Fredsoe, 2006)

2.5. Related Works

Bramley (1974) conducted the steady two-dimensional incompressible magneto-hydrodynamic flow across a circular cylinder under the influence of axial magnetic field using the series truncation method. It was seen that the flow attaches to the cylinder longer and no separation was observed until the rear stagnation point.

Zachariah & Singh (1983) studied the flow of a conducting fluid around a circular cylinder placed in a channel under externally imposed axial magnetic field. It was seen that the channel walls have significant influence on the drag force acting on the cylinder, the force increasing with the blockage parameter. Presence of the walls also tends to flatten the streamlines and also reduce the upstream and downstream wakes seen in the absence of the walls.

Kumari & Bansal (1985) studied the incompressible viscous flow of an electrically conducting fluid past a circular cylinder under the influence of axial magnetic field for two Reynolds numbers i.e. 0.05 and 0.1 using series truncation method. It was concluded that the tangential drag coefficient is increased with the increase in interaction parameter.

Josserand, et al. (1993) numerically studied the influence of an aligned magnetic field on the flow of a liquid metal across a cylinder and found out that the reduction of drag on the cylinder could be achieved by the magnetic field and a sufficient magnetic field suppressed von-Karman street behind the cylinder.

Mutschke, et al. (1998) investigated the effects on wake instabilities due to external magnetic field in the flow of a conducting fluid across a circular cylinder.

Rao & Sekhar (2000) carried out the study of steady magnetohydrodynamic flows of a conducting fluid across a circular cylinder up to Reynolds number of 500 with aligned magnetic field using finite difference method. It was found that with the increment of interaction parameter, the flow separation is suppressed. The drag coefficient is found to decrease for the small values of interaction parameter and has a tendency to increase as the interaction parameter is further increased.

Midya, et al. (2003) studied the effects of magnetic field in a channel flow with constriction. They found that the separated zone downstream of the constriction was

reduced under the influence of transverse magnetic field and the complete elimination of separation is achievable if stronger magnetic field is applied.

Sekhar, et al. (2003) investigated the magnetohydrodynamic flow past a sphere under the influence of parallel magnetic field for the Reynolds number up to 100 and interaction parameter up to 0.7. The drag coefficient has a tendency to increase with the increment of the interaction parameter.

Sekhar, et al. (2005) conducted numerically studied the steady incompressible flow around a circular cylinder in the presence of an aligned magnetic field for Reynolds numbers up to 40 and interaction parameter up to 15. It was found that the boundary layer separation at the rear stagnation point for $Re = 10$ was completely suppressed when $N \geq 9$ and it started growing again when $N \geq 9$. For $Re = 20$ and 40, the suppression is not completed. The drag coefficient decreases for small values of interaction parameter and then increases with increase of N . It was also found that the upstream and downstream pressures on the surface of the cylinder increases for low values of N (< 0.1) and rear pressure aversion occurs with further increase of N .

Kumar & Rajathy (2006) numerically investigated the steady viscous flow of a conducting fluid around a circular cylinder in the presence of axial magnetic field for Reynolds number up to 100. It was observed that the recirculation bubble decreases and the drag coefficient is found to increase with the increment of Hartmann number.

Sekhar, et al. (2006) studied the steady viscous incompressible flow of a conducting fluid past a circular cylinder under the influence of imposed magnetic field at high Reynolds numbers. Their study concluded that the drag coefficient increases with the increase of interaction parameter.

Sekhar, et al. (2007) studied the steady viscous flow around a circular cylinder with an aligned magnetic field for the range of Reynolds numbers $100 < Re < 500$. It was found that the recirculation bubble decreases and drag coefficient increases as the Hartmann number is increased. It was also observed that the upstream base pressure increases slightly with increase of Hartmann number whereas the downstream base pressure decreases with increase of Hartmann number.

Singha, et al. (2007) investigated the laminar viscous flow of a conducting fluid past a square cylinder in the presence of magnetic field applied in a cross-flow direction for $Re = 50 - 250$. Within the steady flow regime, the recirculation zone formed behind the

cylinder reduces with the increment of magnetic field. Within the unsteady flow regime, a marginal increment in the Strouhal number is observed with the increase in magnetic field and the lift coefficient has a tendency to decrease implying decrement in vortex strength. They also suggested that the complete elimination of vortex shedding is achievable for higher strength of magnetic field.

Sekhar, et al. (2009) studied the effect of magnetic Reynolds number on the steady, two-dimensional, viscous, incompressible and electrically conducting flow around a circular cylinder in the presence of aligned magnetic field. In their study, the effects of the magnetic field and electrical conductivity on the recirculation bubble, drag coefficient, standing vortex and pressure were discussed. It was observed that for low interaction parameter $N < 1$, the suppression of the flow-separation is nearly independent of the conductivity of the fluid, whereas for large interaction parameters, the conductivity of the fluid strongly influences the control of flow-separation.

Grigoriadis, et al. (2009) studied the magnetohydrodynamic flows across a circular cylinder for steady and unsteady flow regimes under the influence of stream-wise and cross-flow magnetic field using immersed boundary method. It was concluded that a non-monotonic variation of the drag coefficient and recirculation length was observed in both 2-D and 3-D cases. As a result, for wide range of interaction parameters, the drag coefficient was found smaller than the corresponding hydrodynamic value.

Singha, et al. (2011) studied the flow of a conducting fluid past a circular cylinder under magnetic field at $Re = 50 - 250$. It was concluded that the imposed transverse magnetic field significantly reduced the lift coefficient implying decrement of vortex strength. It was also observed that the periodic vortex shedding at higher Reynolds numbers can be completely suppressed if sufficiently strong magnetic field is imposed. The separated zone behind the cylinder in a steady flow was reduced with the increment of the magnetic field strength.

Esfahani, et al. (2015) carried out the study of two-dimensional flow around a circular obstacle under the influence of external magnetic field. They performed studies for the Reynolds number of $1 < Re < 200$ and Stuart number ranging $0 < N < 10$. For higher Stuart number i.e. $N = 5$, a rapid increase in the drag coefficient is observed.

CHAPTER THREE: RESEARCH METHODOLOGY

This chapter provides a detailed description of research outlines, tools and methods required to successfully conduct the research.

3.1. Research Design

This research is solely based on CFD analysis. Firstly, CFD simulations without magnetic field have been conducted and MHD analysis afterwards. A general methodology required to conduct the research is provided in Figure 3.1.

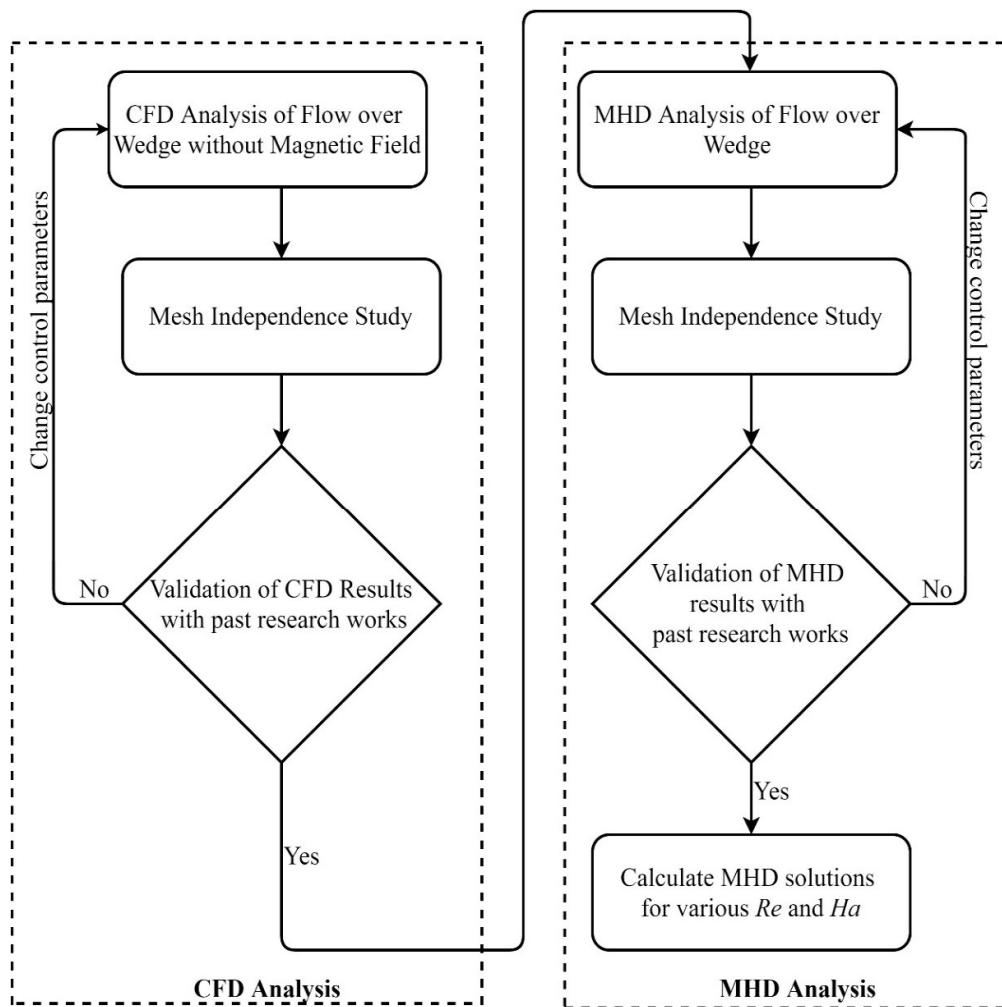


Figure 3.1: Research methodology

3.2. Research Methods

Research methods can be understood as all the methods or techniques employed by the researcher to carry out his research. This research is solely based on numerical simulations using CFD. CFD stands for ‘Computational Fluid Dynamics’. In recent years, with the development of powerful computing systems, it has become easier for researchers to carry out numerical studies using CFD on a large scale.

3.3. Research Tools

Research tools are the set of instruments or software or experimental tools used to collect, generate or process the data. Depending on the nature of the research, one sets a number of research tools necessary to carry out the research. Since this research is entirely based on numerical simulations using CFD, all the works here make use of the CFD software. Tools used in this research are described below.

3.3.1. ANSYS Modeler

ANSYS Modeler is useful for creating a physical model i.e. geometry. Both 2D and 3D models can be easily developed using this software. This software has been used to create all the geometrical configurations required in this thesis.

3.3.2. ICEM CFD

ICEM CFD is an interactive grid generation software developed by ICEM CFD. It is equipped with efficient tools for grid generation, post-processing and mesh optimization. It is widely used for applications like structural analysis, heat transfer analysis etc. Several types of grids such as structured, unstructured, hybrid grids etc can be generated using this software. It reads geometries from different CAD software like AutoCAD, Solidworks, Nastran, etc. and creates meshes for CFD codes likes Fluent, OpenFOAM, etc. This software is widely used by big companies like TOYOTA, NASA etc.

In this thesis, all the meshes have been generated using this software.

3.3.3. ANSYS Fluent

ANSYS Fluent is a powerful CFD tool capable of modelling fluid flows, heat transfer analysis, multiphase flows, turbulence etc. It employs finite volume method where a volume is divided into small volumes and governing equations being valid for all the

volumes. A typical CFD simulation consists of three major steps namely: (i) Pre-processing, (ii) Solvers and (iii) Post-processing.

3.3.4. Tecplot

Tecplot is a CFD visualization and analysis software capable of generating pictorial and graphical representation of large data sets. This software is user-friendly and users can easily present their results through 2D and 3D plots. All the post-processing works have been carried out using this software.

3.4. Study of MHD Flows past Square Cylinder

A flowchart showing the methodology regarding the study of MHD flows past square cylinder is shown in Figure 3.2 below.

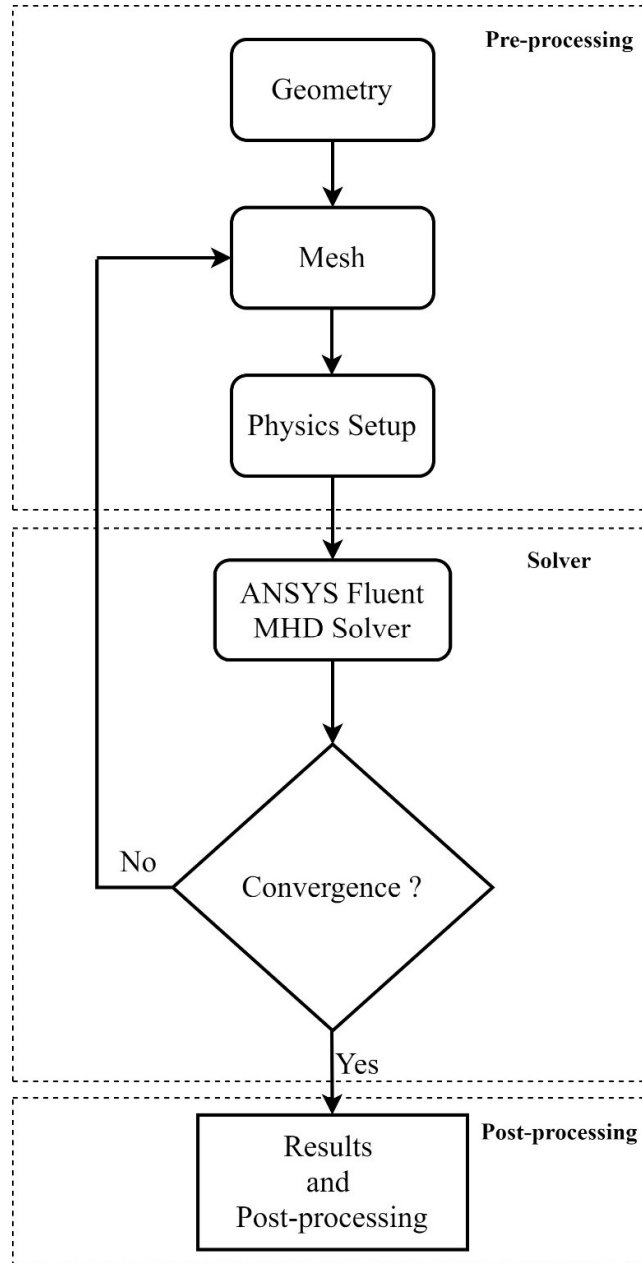


Figure 3.2: MHD analysis of square cylinder

3.4.1. Geometrical Configuration

The problem under consideration is shown in Figure 3.3. Two-dimensional laminar viscous flow of an electrically conducting incompressible fluid having electrical conductivity σ , dynamic viscosity μ and density ρ around a square cylinder placed in rectangular channel is considered. A parabolic velocity inlet is assigned at the inlet. The flow Reynolds number has been defined on the basis of maximum inlet velocity U_0 . The physical model corresponds to that used by Breuer, et al. (2000). The width of the channel is H and L represents the axial length of the computational domain. In Figure 3.3, L_u and L_d represent the upstream and downstream distances of the cylinder respectively. The origin is set at the centre of the cylinder. Details about the assumptions considered in this study are presented as follows:

- i) The flow is two-dimensional, laminar and incompressible.
- ii) The total length of the channel in an axial direction is set to $L/D = 50$.
- iii) Upstream and downstream distances of the channel is set to $L_u = 12.5D$ and $L_d = 37.5D$ respectively.
- iv) The confinement ratio is set to $D/H = 0.125$.
- v) All the solid walls are insulated.

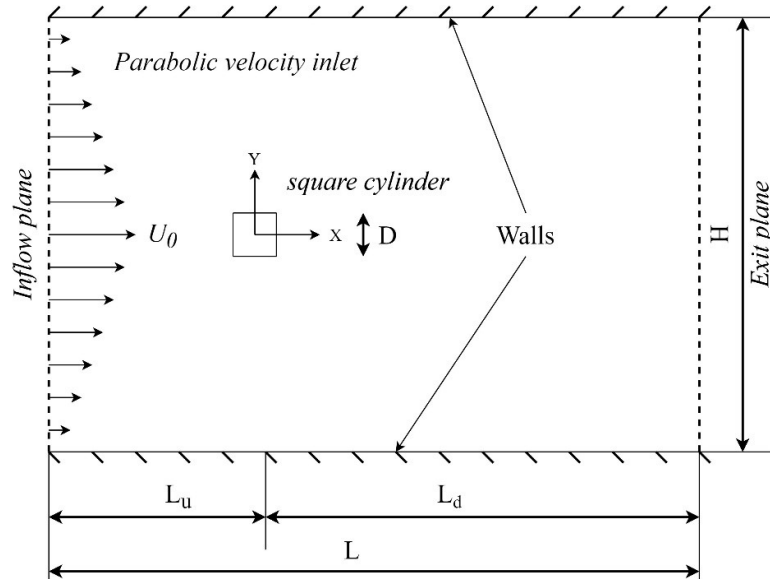


Figure 3.3: Geometrical configuration for square cylinder

3.4.2. Mesh

In order to create a structured mesh, the physical model has been divided into five sub-domains, D1, D2, D3, D4 and D5 as shown in Figure 3.4. After importing the model into ICEM CFD environment, non-uniform grids have been created with mesh refinement on the vicinity of the cylinder surface and the walls of the channel. In order to obtain the finest grid, the refined cells have been created with size of the first grid point of $0.01D$ units on all sides of the cylinder and $0.02D$ units in the vicinity of channel walls. Figure 3.5 (a) shows the full view of the computational mesh corresponding to G4 mesh. Figure 3.5 (b) shows the zoomed view of the G4 mesh around the surface of the cylinder. Table 3.1 provides a complete detail of the computational meshes created for this study.

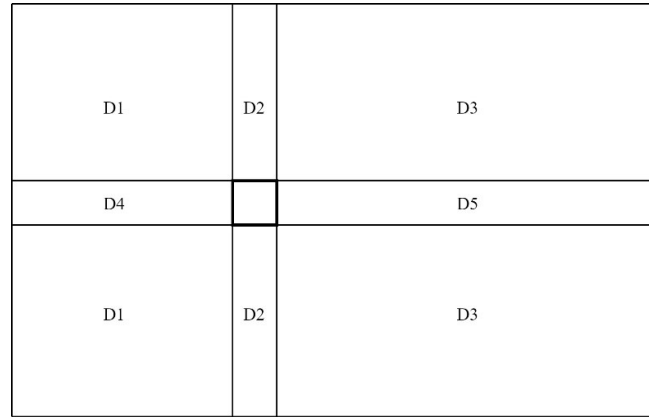


Figure 3.4: Mesh distribution and sub-computational domains

Table 3.1: Details of meshes corresponding to square cylinder

S.N.	Name of the mesh	Total no of elements	Length of first grid point around the sides of square cylinder	Length of first grid point in upper and lower walls
1.	G1	14972	0.01D	0.02D
2.	G2	27022	0.01D	0.02D
3.	G3	42172	0.01D	0.02D
4.	G4	60422	0.01D	0.02D

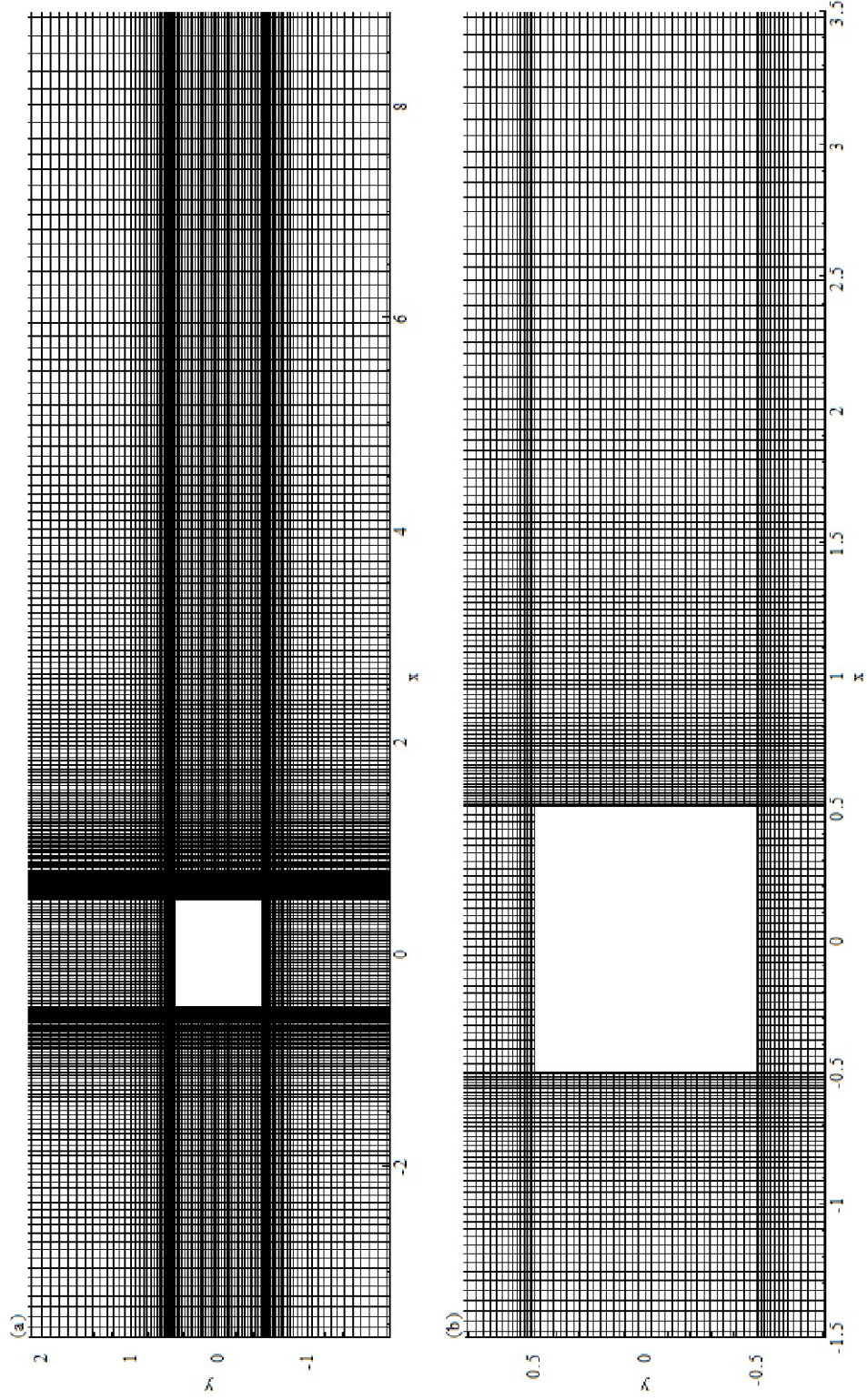


Figure 3.5: G4 mesh (a) Full view, (b) Zoomed view

3.4.3. Physics Setup

The present simulations have been carried out by ANSYS Fluent which utilizes the finite volume method. The coupling between continuity and momentum equations is done by SIMPLE algorithm. For temporal discretization, the second-order implicit scheme has been used. In case of spatial discretization, the second-order upwind scheme has been employed for convective terms while the central difference scheme has been employed for diffusive terms. A convergence criterion of 10^{-7} has been set. The convergence of the solution is assumed to have reached if more than 10 periodic cycles in the temporal variation of the flow parameters is observed.

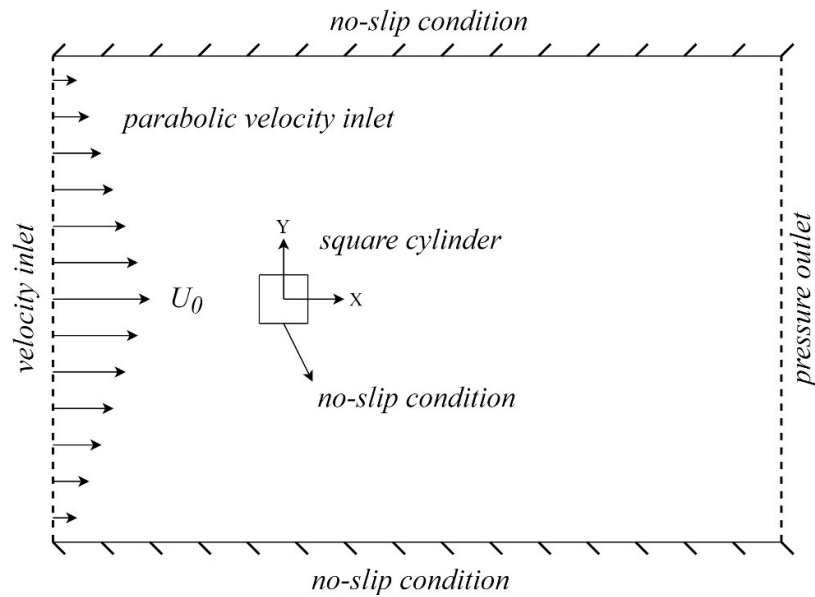


Figure 3.6: Boundary conditions associated with square cylinder

Figure 3.6 depicts the boundary conditions associated with the computational model of square cylinder. The boundary conditions associated in this study can be explained in the following points:

- i) *At the inflow plane:* A parabolic velocity inlet depicting fully developed laminar flow is considered at the inlet of the channel. In order to assign the parabolic velocity distribution, the following boundary condition has been imposed at the inlet which is given by,

$$u = \frac{u^*}{U_0} = \left(1 - \left(\frac{2y}{H}\right)^2\right), \quad v = 0 \quad \text{Equation 3.1}$$

where, U_0 represents the maximum inlet velocity.

- ii) *On the upper and lower walls:* To simulate the confined flow past the square cylinder, a *no-slip* boundary condition, that is, $u = 0, v = 0$ at a distance of $4D$ from the origin of the cylinder has been applied on the upper and lower walls.
- iii) *On the surface of square cylinder:* *No-slip* condition has been applied on the solid surface of the square cylinder, that is, $u = 0, v = 0$.
- iv) *At the exit plane:* *Pressure outlet* boundary condition has been applied at the exit plane.

3.4.4. Mesh Independence Study

For mesh independence studies, simulations have been performed for $Re = 100$ taking time step size of $\Delta t = 0.025 s$ for all simulations. The test has been conducted for four progressively refined grids namely G1, G2, G3 and G4. Table 3.2 shows the comparison of Strouhal number and drag coefficient for $Re = 100$ obtained for four grids. In the table, $x \times y$ defines the number of grid points in the horizontal and vertical directions respectively.

Table 3.2: Mesh independence study for $Re = 100, \Delta t = 0.025 s$

Grid number							
Mesh	D1 ($x \times y$)	D2 ($x \times y$)	D3 ($x \times y$)	D4 ($x \times y$)	D5 ($x \times y$)	C_d	St
G1	80×30	5×30	150×30	80×5	150×5	1.447524	0.14
G2	95×40	15×40	180×40	95×15	180×15	1.3869	0.14
G3	110×50	25×50	210×50	110×25	210×25	1.37345	0.139
G4	125×60	35×60	240×60	125×35	240×35	1.3704	0.139

It can be observed that the variation in C_d as we move from G1 mesh to G2 mesh is 4.18%. Again, as we move from G2 mesh to G3 mesh, the variation in C_d is less than 1%. As we move further from G3 mesh to G4 mesh, the variation in C_d is 0.23%. Similarly, the difference in Strouhal number (St) between G3 and G4 meshes is less than 1%. Hence, for conservative analysis, G4 mesh has been chosen for the rest of simulations.

3.4.5. MHD Simulations

Figure 3.7 represents the schematic of physical domain for all MHD simulations. A transverse magnetic field acting on the flow past square cylinder has been considered. Taking $Re = 200$ as the representative Reynolds number, MHD simulations have been performed for $Ha = 0 - 8$ using ANSYS Fluent MHD module. The magnetic induction method in MHD module built in ANSYS Fluent has been selected for all simulations.

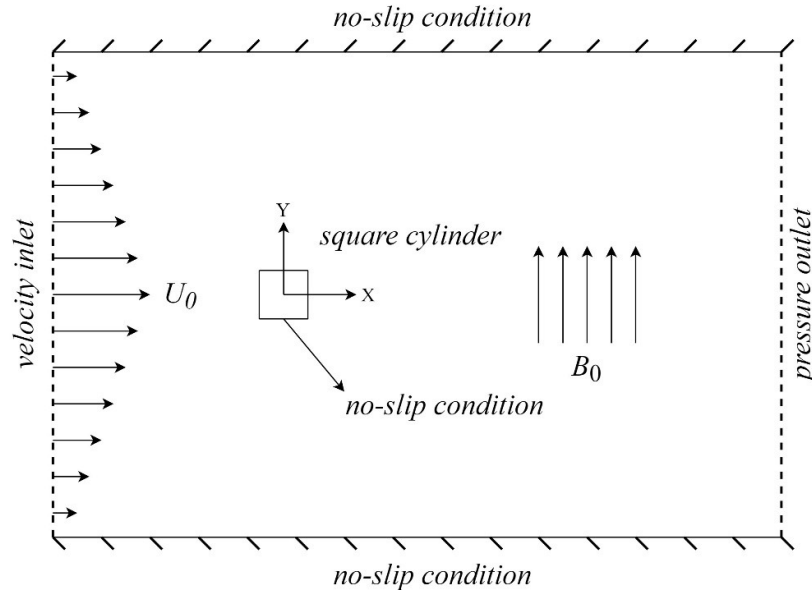


Figure 3.7: Transverse magnetic field acting on the flow past square cylinder

On the application of transverse magnetic field past square cylinder at $Re = 200$ for $Ha = 0 - 8$, the effects of magnetic field on wake dynamics have been observed. The effects of magnetic field on vorticity, streamlines and drag and lift coefficients are studied. Also, previous studies confirm that there exists a critical value of Hartmann number at which complete vortex suppression is observed. Simulations have been conducted to determine the value of critical Hartmann number for $Re = 200$ and compared with the values reported by Singha, et al. (2007) and Farjallah, et al. (2011). Such comparative analysis has been carried out to demonstrate the solution capabilities of MHD module built in ANSYS Fluent. After that, rest of the MHD simulations for the square cylinder have been conducted.

3.5. Study of Flow past Wedge without Magnetic Field

The methodology adopted for numerical simulation of the flow past wedge without magnetic field is shown in Figure 3.8.

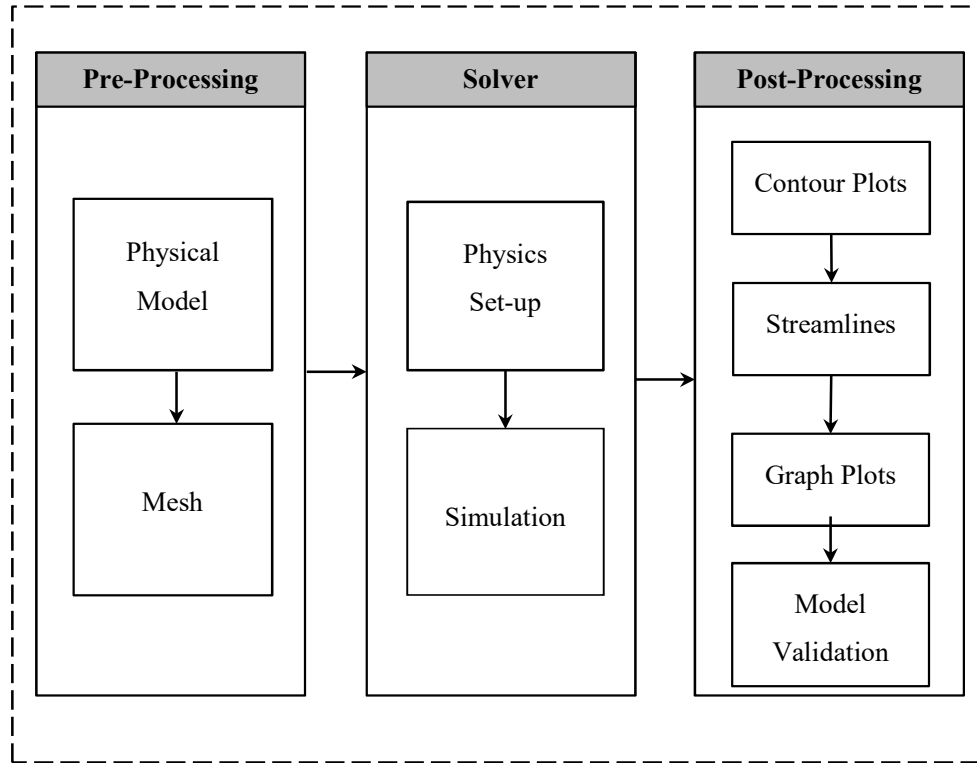


Figure 3.8: Methodology for study of flow past wedge without magnetic field

3.5.1. Geometrical Configuration

The wedge structure is an equilateral triangular cylinder of side d . The wedge model was created in ANSYS Modeler software. The wedge is placed in a channel with fictitious boundaries on the upper and lower regions of the computational domain. However, to create a domain with finite boundaries, the normalised upstream length (X_u/d) is set to 12, and the normalised downstream length between the back side of the wedge and the exit plane (X_d/d) is set to 20. The total normalised axial length of the computational domain (L_1/d) is of 32 whereas the normalised height of the computational domain (L_2/d) is used as 30. All the solid walls are insulated. The geometrical configuration is shown in Figure 3.9. It corresponds to the schematics used by Dhiman, et al. (2011).

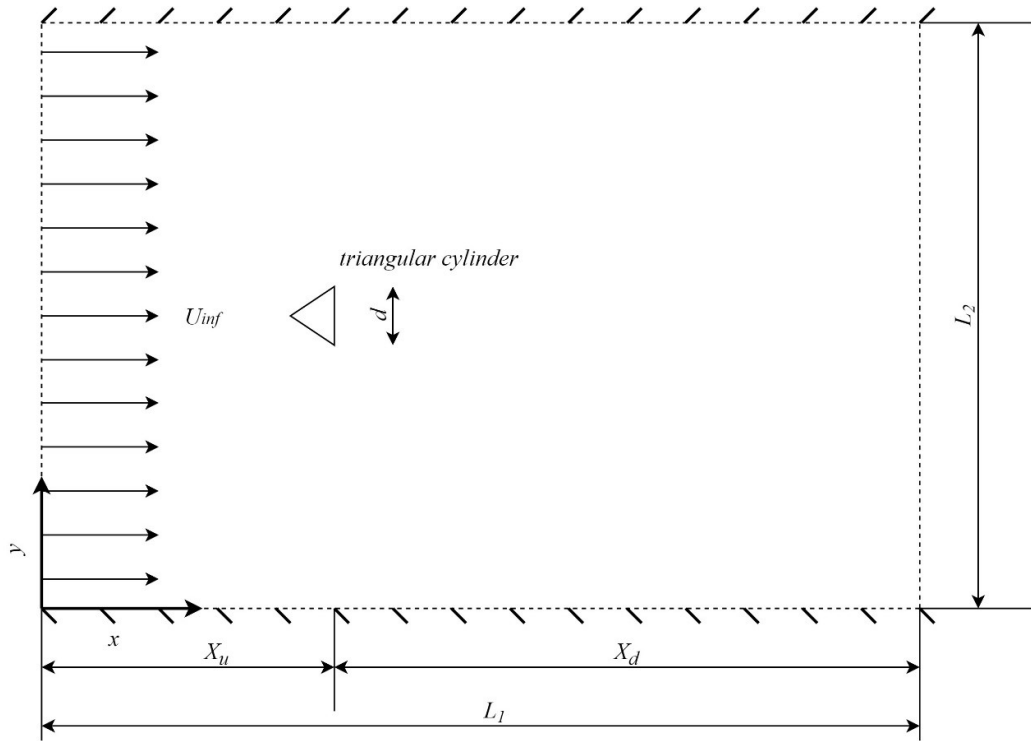


Figure 3.9: Schematic diagram showing unconfined flow across the wedge

The flow over the wedge structure is studied with the normalized computational domain dimensions. The side of the triangular wedge structure is used to normalise all the other dimensions. Table 3.3 gives the values of the normalized dimensions of the geometrical configuration used in this study.

Table 3.3: Computational domain for wedge

S.N.	Geometrical parameters	Values
1.	Upstream length (X_u / d)	12
2.	Downstream length (X_d / d)	20
3.	Total axial length (L_1 / d)	32
4.	Domain height (L_2 / d)	30

3.5.2. Mesh

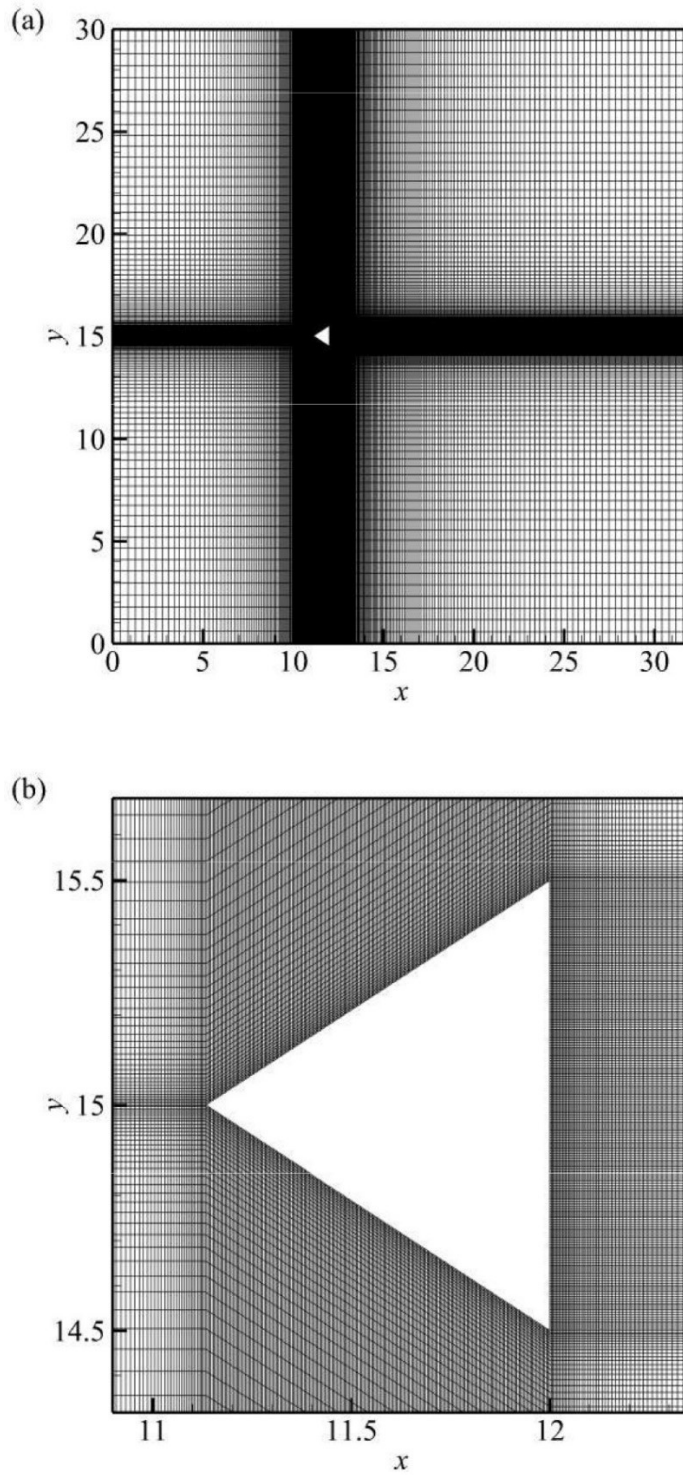


Figure 3.10: M1 mesh (a) Full view, (b) Zoomed view

The model was imported into ICEM CFD environment to create structured meshes. Non-uniform grids having 114147 cells with 200 grid points on the surface of the wedge have been created. Three structured meshes have been generated namely: M1, M2 and M3 each having 114147 cells with size of the first grid point from the cylinder of $0.004d$, $0.0015d$ and $0.001d$ units respectively. A detailed view of the M1 mesh is shown in Figure 3.10. Figure 3.10 (a) shows the full view of M1 mesh whereas Figure 3.10 (b) provides a zoomed view of the same mesh. A detailed description of the meshes can be found in Table 3.4 below.

Table 3.4: Details of meshes

S.N.	Name of the mesh	Total no of cells	No of nodes	No of nodes around the side of the triangular cylinder	Size of the first grid point from the cylinder (δ)
1.	M1	114147	115200	200	$0.004d$
2.	M2	114147	115200	200	$0.0015d$
3.	M3	114147	115200	200	$0.001d$

3.5.3. Physics Setup

At this stage, after successful geometry and mesh creation, the computational model is ready for simulation.

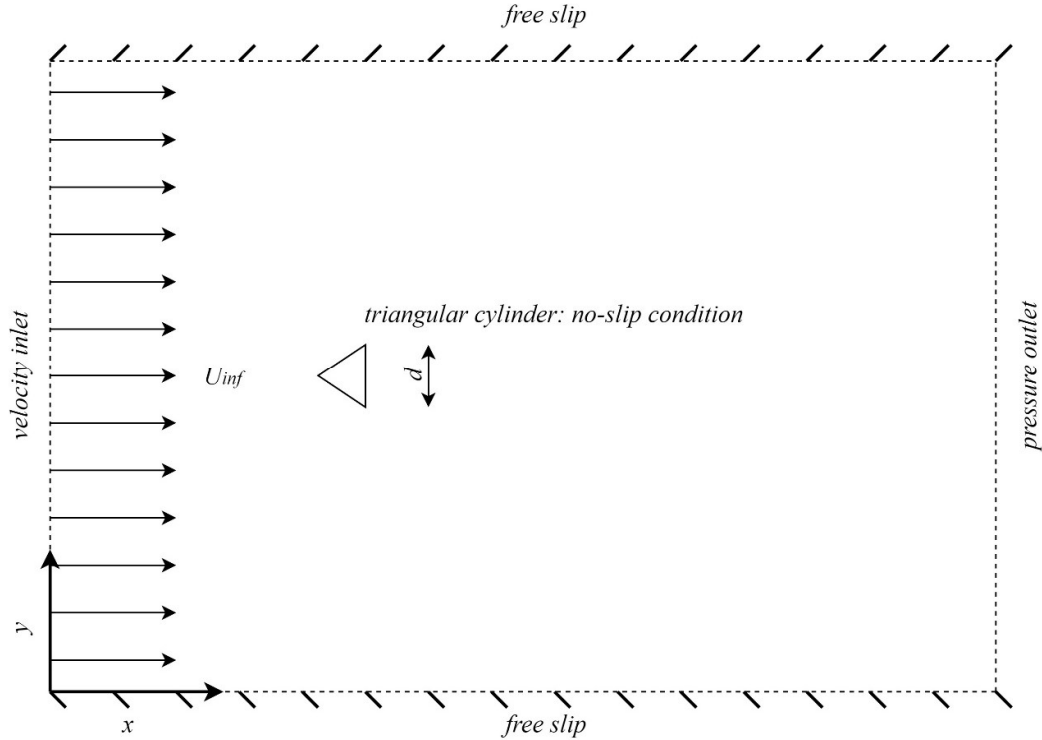


Figure 3.11: Boundary conditions associated with the wedge

Consider an unconfined two-dimensional laminar viscous flow of an electrically conducting incompressible fluid of density ρ , dynamic viscosity μ and electrical conductivity σ with free-stream velocity U_{inf} across the wedge in the absence of magnetic field as shown in Figure 3.11. The Reynolds number is defined on the basis of side length of the wedge, free-stream velocity and fluid properties. The values of free-stream velocity and fluid properties were adjusted so as to conduct simulations at required flow conditions.

Firstly, the meshes were imported into ANSYS Fluent environment. The boundary conditions associated with the wedge model is shown in Figure 3.11. The boundary conditions implemented correspond to flow simulations without magnetic field. A detailed description of the boundary conditions implemented for this model is explained below:

- i) *At the inlet boundary:* A uniform fluid flow in free-stream condition is considered from left to right, that is, $u = 1$, $v = 0$. This boundary condition is applied in ANSYS Fluent by assigning the inlet boundary with *velocity inlet* condition.
- ii) *On the upper and lower boundaries:* Since the present study considers an unconfined flow across the wedge, a *slip* boundary condition at a distance of $L_2 = 15d$ from the centre has been applied on the top and bottom boundaries.
- iii) *On the surface of triangular cylinder:* *No-slip* condition has been applied on the solid surface of the triangular cylinder, that is, $u = 0$, $v = 0$.
- iv) *At the exit boundary:* *Pressure outlet* boundary condition has been applied at the exit boundary.

Table 3.5 provides a quick overview of the boundary conditions implemented in ANSYS Fluent for the given problem description.

Table 3.5: Boundary conditions for the wedge model

S.N.	Patch	Boundary condition
1.	INLET	<i>Velocity inlet</i>
2.	OUTLET	<i>Pressure outlet</i>
3.	WEDGE	<i>No-slip</i>
4.	TOP	<i>Slip</i>
5.	BOTTOM	<i>Slip</i>

3.5.4. Mesh Resolution Study

A computational model is required to be validated against analytical or numerical or experimental results. After setting up the physics in ANSYS Fluent, our computational model is ready for mesh resolution studies. Mesh resolution studies ensure that the solution is independent of the mesh resolution. The SIMPLE algorithm is used for coupling between continuity and momentum equations. For temporal discretization, the second-order implicit scheme has been used. For spatial discretization, the second-order upwind scheme has been used for convective terms while the central difference scheme has been employed for diffusive terms. A convergence criterion of 10^{-5} for continuity equation and 10^{-6} for momentum equation has been set to determine the flow

parameters. The convergence of the solution is said to have been achieved if it shows more than 10 periodic cycles in the temporal variation of drag and lift coefficients.

For mesh resolution studies, simulations have been performed for $Re = 150$ taking time step size, $\Delta t = 0.01 s$ for three different meshes namely: M1, M2 and M3. Each of the meshes i.e. M1, M2 and M3 comprise of 114147 cells having the first grid point of $0.004d$, $0.0015d$ and $0.001d$ units around the cylinder respectively. The results of the grid resolution studies for $Re = 150$ are summarized in Table 3.6 below. The time-averaged values of drag coefficient (C_d) and Strouhal number (St) for three meshes have been computed and shown in Table 3.6. It is observed that the percentage differences in the values of the mean drag coefficient and the Strouhal number between M1 and M3 grids are found to be 0.27% and 5.21% respectively. Similarly, for M2 and M3 grids, the percentage difference in the value of the mean drag coefficient has been found to be 0.05%, but no further changes in the Strouhal number has been observed. Hence, the computational model is valid and therefore, the medium mesh M2 has been selected for all subsequent simulations.

Table 3.6: Results of mesh resolution study for $Re = 150$ at $\Delta t = 0.01 s$

S.N.	Name of the mesh	Total number of cells	Size of the first grid point from the cylinder	Time-averaged drag coefficient (C_d)	Strouhal number (St)
1.	M1	114147	$0.004d$	1.9188	0.211
2.	M2	114147	$0.0015d$	1.9231	0.2
3.	M3	114147	$0.001d$	1.9240	0.2

3.6. Study of Flow past Wedge with Magnetic Field

A general methodology for conducting MHD flow simulations in case of wedge structure is similar to that of the methodology adopted for square cylinder depicted in Figure 3.2. After the validation of the wedge model through mesh resolution studies, the model is ready for MHD simulations.

3.6.1. Geometrical Configuration

In this study, the two-dimensional laminar viscous flow of an electrically conducting incompressible fluid having electrical conductivity σ , dynamic viscosity μ and density ρ past the wedge placed in free-stream condition in the presence of external magnetic field B_0 is considered. The fluid flow is under the presence of transverse magnetic field. Figure 3.12 provides schematic showing transverse magnetic field imposed in the fluid flow occurring from the left to right direction.

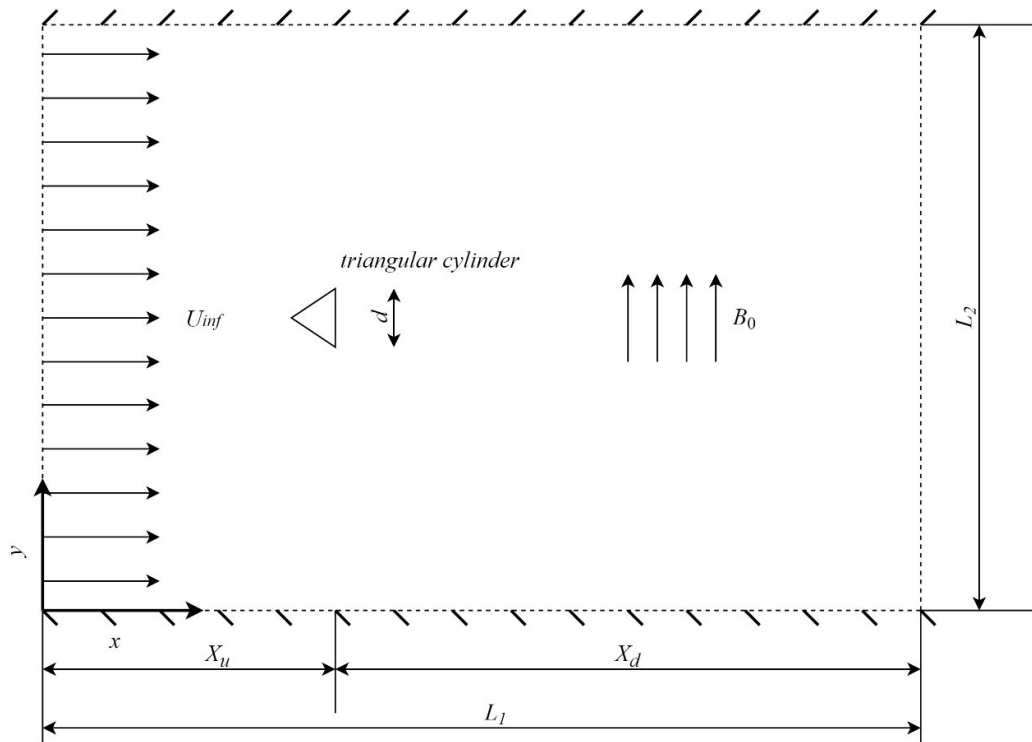


Figure 3.12: Schematic showing flow past the wedge under transverse magnetic field

3.6.2. Mesh

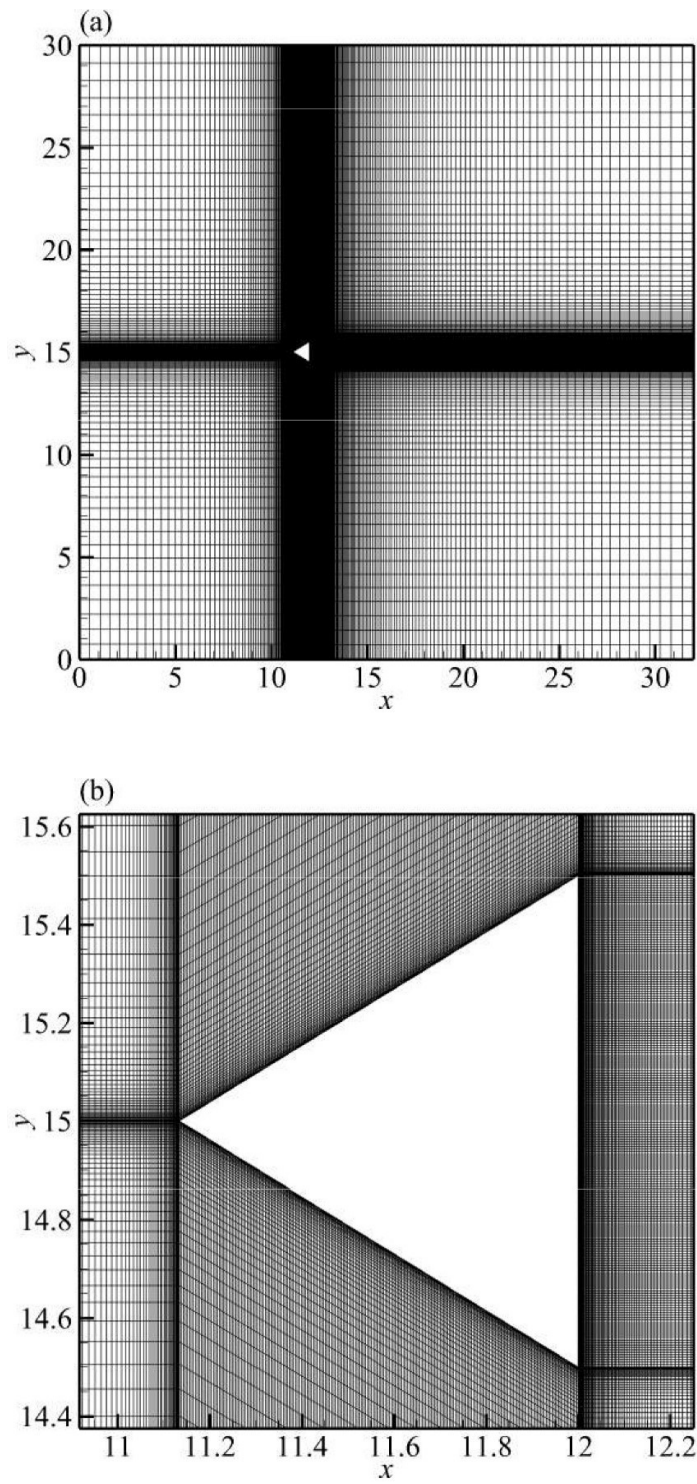


Figure 3.13: M2 mesh (a) Full view, (b) Zoomed view

The medium mesh M2 has been chosen for all subsequent MHD simulations. The medium mesh M2 contains 114147 cells with size of the first grid point of $0.0015d$ units around the surface of the cylinder. Figure 3.13 (a) shows the full view of the medium mesh M2 whereas Figure 3.13 (b) shows the zoomed view of the mesh.

3.6.3. Physics Setup

The magnetic induction method available in MHD module built in ANSYS Fluent has been used for all MHD simulations. The schematic shown in Figure 3.12 represents the physical domain for MHD simulations. Simulations have been performed for $Re = 100$ considering $Ha = 0 - 10$. The boundary conditions associated with MHD simulations are same as that used for non-MHD simulations performed for the wedge model. The effects of transverse magnetic field on wake structure and flow parameters such as drag and lift coefficients have been investigated.

CHAPTER FOUR: RESULTS AND DISCUSSION

4.1. Study of MHD Flows past Square Cylinder

In this section, the results of numerical study of MHD flows past confined square cylinder are discussed to understand the solution capabilities of ANSYS Fluent MHD solver. The effects of magnetic field on wake dynamics past the square cylinder are also discussed.

4.1.1. Validation of Results

After the selection of G4 mesh, simulations have been performed for $Re = 1 - 200$. The values of drag coefficient and Strouhal number belonging to respective Reynolds numbers have been computed and compared with the published literature. Figure 4.1 depicts the comparison of drag coefficient for $Re = 1 - 50$ against the results of Breuer, et al. (2000). An excellent agreement has been obtained between the present results and the published results of Breuer, et al. (2000). For instance, the average difference between the present results and the published literature of drag coefficient for $Re = 1 - 50$ is 1.83%.

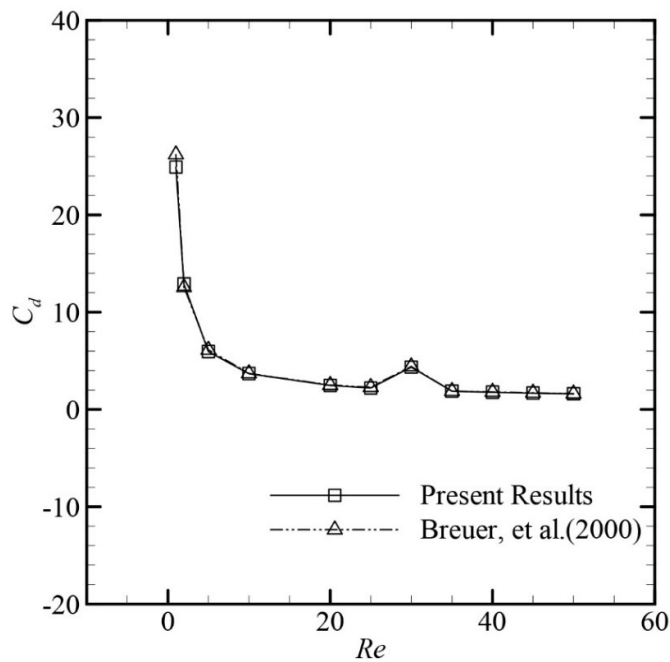


Figure 4.1: Validation of C_d for very low $Re = 1 - 50$

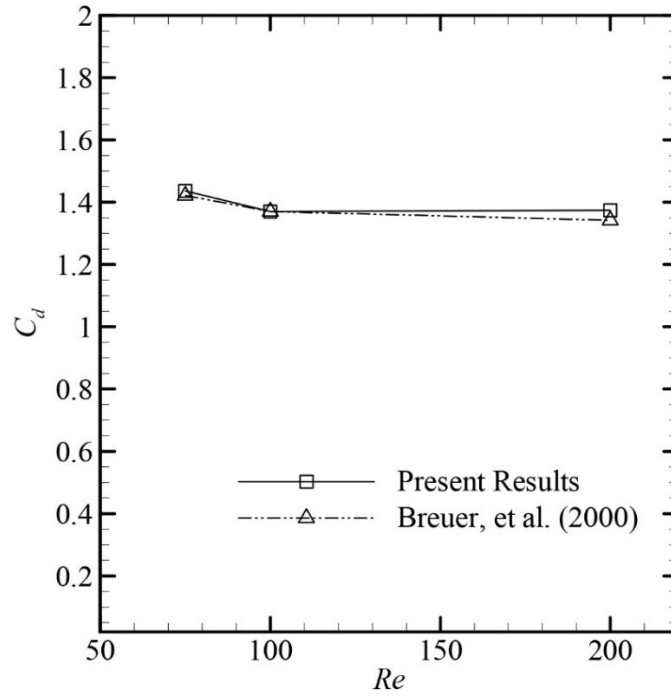


Figure 4.2: Validation of time-averaged C_d for $Re = 75 - 200$

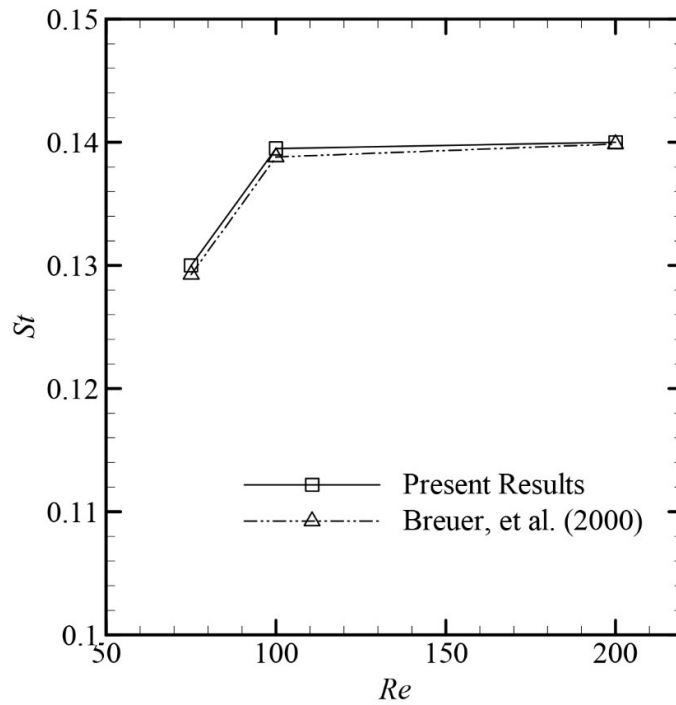


Figure 4.3: Validation of St for $Re = 75 - 200$

Similarly, the time-averaged values of drag coefficient and Strouhal number for $Re = 75 - 200$ has been computed and compared with the results of Breuer, et al. (2000) as shown in Figure 4.2 and Figure 4.3 respectively. An excellent agreement has been achieved between the present results and the results of Breuer, et al. (2000). For instance, the average difference between the present results and the published literature of time-averaged drag coefficient and Strouhal number for $Re = 75 - 200$ is 1.15% and 0.39% respectively. Hence, the computational model of square cylinder has been validated.

4.1.2. Critical Hartmann Number

Critical Hartmann number (Ha_{cr}) refers to the value of Hartmann number at which the unsteady flow transitions to a steady flow. In order to demonstrate the solution capabilities of ANSYS Fluent MHD solver, the study of MHD flows past confined square cylinder under transverse magnetic field has been conducted and the value of critical Hartmann number has been compared with the results of Singha, et al. (2007) and Farjallah, et al. (2011). Singha, et al. (2007) reported a range of minimum Hartmann numbers for several Re in case of confined square cylinder under transverse magnetic field. Table 4.1 presents the required range of minimum Hartmann numbers for several Re which converts unsteady flow to steady flow reported by Singha, et al. (2007).

Table 4.1: Range of critical Hartmann number for different Re

S.N.	Re	Range of Ha_{cr}
1.	150	2.0 - 3.0
2.	200	3.0 - 4.0
3.	250	4.0 - 5.0

The value of critical Hartmann number has been obtained for $Re = 200$ and compared with the values reported by Singha, et al. (2007) and Farjallah, et al. (2011). Table 4.2 shows the comparison of present results of critical Hartmann number with the published literature. It is clear that an excellent agreement has been obtained between the present results and the published literature of critical Hartmann number. Furthermore, the study of the effects of transverse magnetic field on vorticity, streamlines, drag and lift coefficients has also been carried out.

Table 4.2: Comparison of critical Hartmann number for $Re = 200$

S.N.	Re	Singha, et al. (2007)	Farjallah, et al. (2011)	Present results
1.	200	3.0-4.0	3.662	3.6

4.1.3. Effects on Wake

Figures 4.4 - 4.5 depict the contours of streamline and vorticity of the flow at $Re = 200$ under different transverse magnetic fields. At $Re = 200$, the flow is time-dependent with the presence of alternate shedding of vortices from the upper and lower regions of square cylinder. Figures 4.4 (a) - (c) clearly depict that the unsteady nature of the flow shown by the presence of alternate vortex shedding remains still intact up to certain Hartmann numbers. However, beyond certain Hartmann number, the flow converts from unsteady to steady nature depicted by the presence of wake consisting of recirculation bubbles and the recirculation length is reduced with further increment in Hartmann number as shown in Figure 4.4 (d) - (e). The physical interpretation is that the transverse magnetic field produces an opposing force known as Lorentz force in the upstream direction capable of suppressing the vortices and hence, the wake is reduced. On the increment of Hartmann number, the strength of vortices is reduced as depicted by Figures 4.5 (a) - (c). On further increment of Hartmann number, it can be observed that the vortex shedding phenomena is completely suppressed at $Ha = 3.6$ and the flow assumes the steady state evidenced by the presence of symmetric and closed recirculating wake as shown in Figures 4.4 (d) - (e).

4.1.4. Effects on Drag and Lift coefficients

Figures 4.6 (a) - (e) shows the temporal variations of the average drag coefficient at $Re = 200$ for different Hartmann numbers. It is seen that there is a minimal reduction in the drag coefficient with the increasing Hartmann number within the unsteady flow regime. But beyond the critical Hartmann number, the flow assumes the steady state and the average drag coefficient marginally increases with further increment of Hartmann number as shown by Figures 4.6 (d) - (e). The possible explanation is that at steady state, the mass flow across the channel is constant causing the pressure drop to increase with the increased amount of Lorentz force. Such increment in pressure drop

may be due to the increase in pressure on the front section of the cylinder, which contributes to the pressure drag on the body.

The temporal variations of the lift coefficient for $Re = 200$ at different Hartmann numbers are shown in Figure 4.7 (a) - (e). It is observed that up to certain Hartmann numbers, the flow remains unsteady depicted by the presence of alternating shedding of vortices as shown in Figures 4.7 (a) - (c). The lift amplitude decreases with the increment of Hartman number. If the strength of magnetic field is sufficient, the unsteadiness present in the flow is completely eliminated as evidenced by Figures 4.7 (d) - (e). It is also seen that the lift amplitude becomes zero after initial unsteady duration.

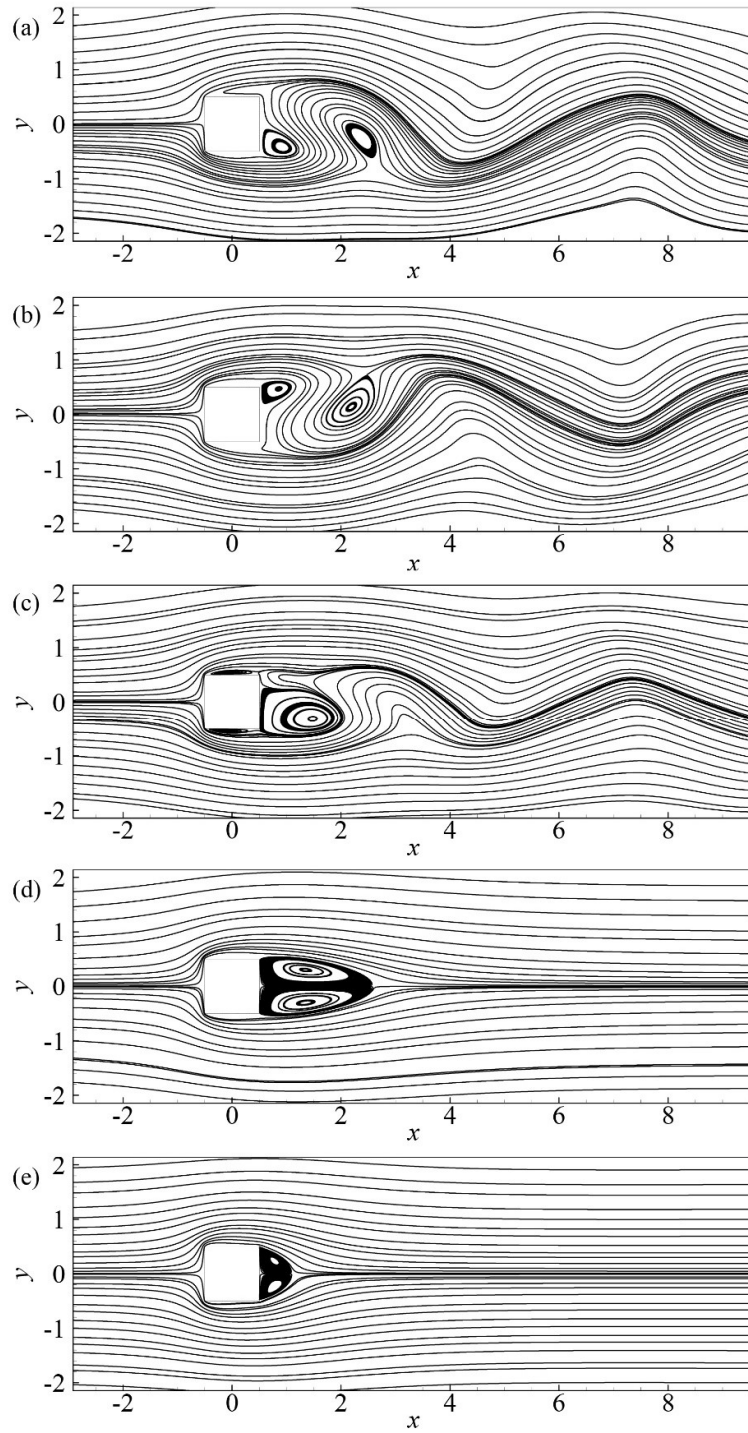


Figure 4.4: Streamlines at $Re = 200$: (a) $Ha = 0$, (b) $Ha = 1.0$, (c) $Ha = 3.0$, (d) $Ha = 4.0$ and (e) $Ha = 8.0$

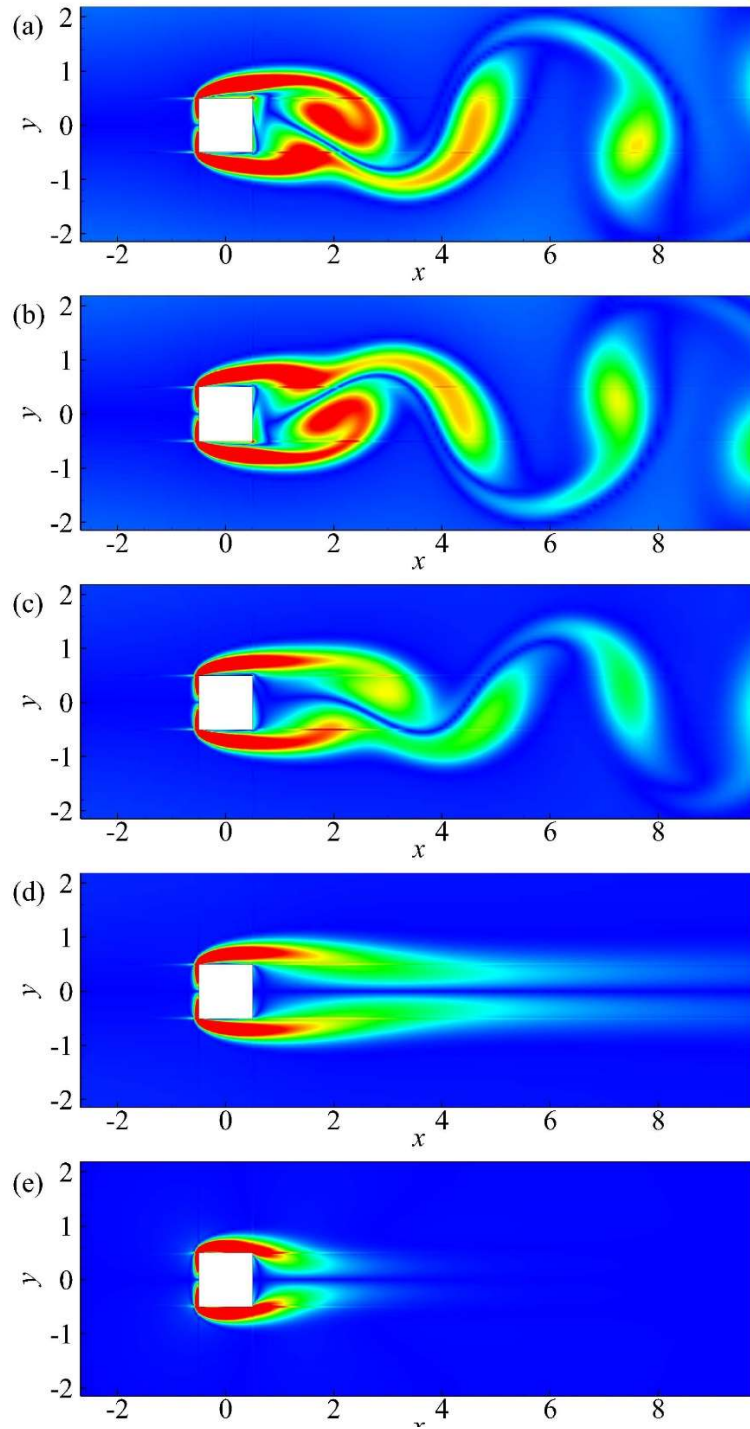


Figure 4.5: Vorticity contours at $Re = 200$: (a) $Ha = 0$, (b) $Ha = 1.0$, (c) $Ha = 3.0$, (d) $Ha = 4.0$ and (e) $Ha = 8.0$

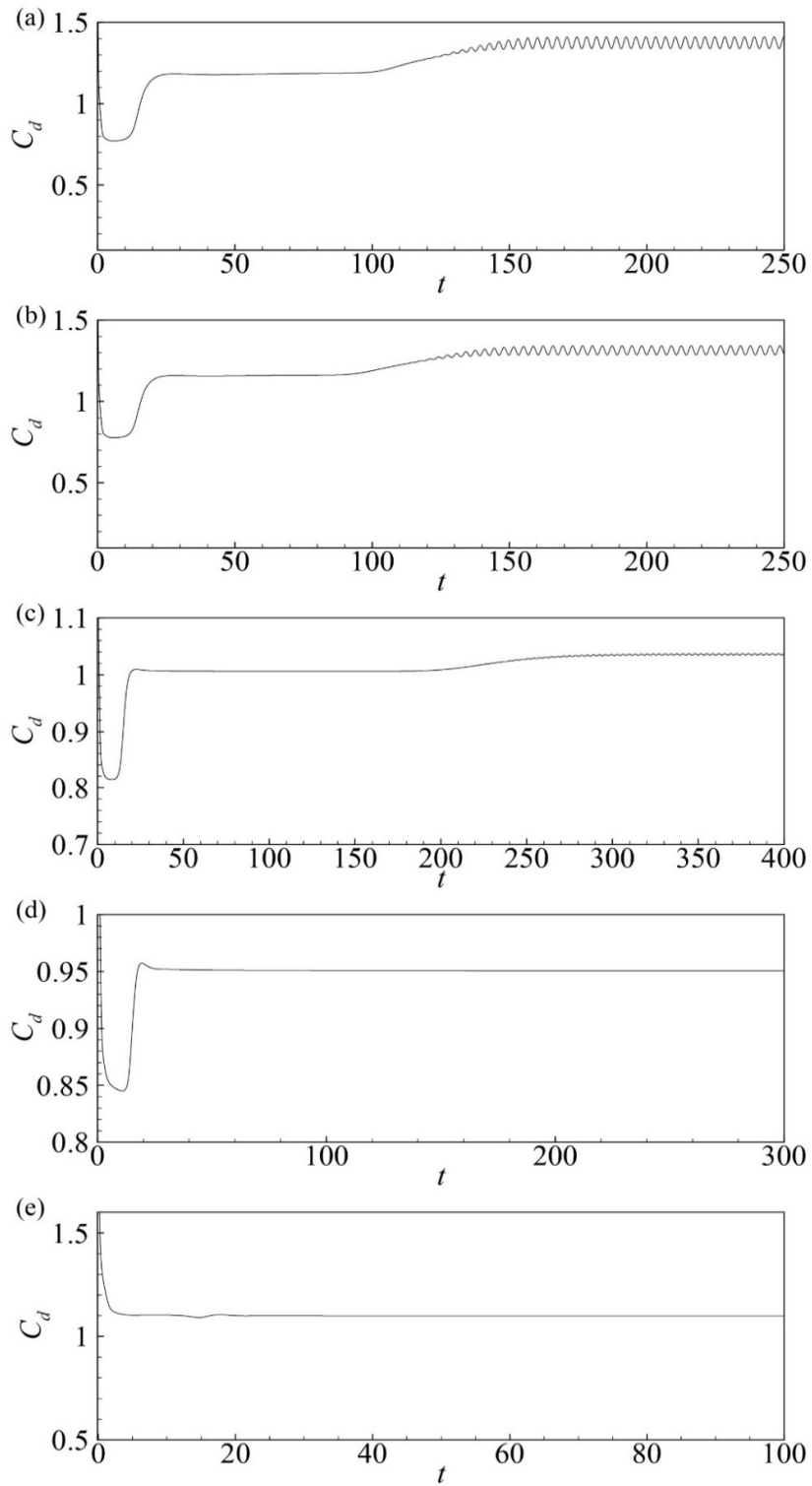


Figure 4.6: Temporal variation of the drag coefficient with respect to the non-dimensional time at $Re = 200$: (a) $Ha = 0$, (b) $Ha = 1.0$, (c) $Ha = 3.0$, (d) $Ha = 4.0$ and (e) $Ha = 8.0$

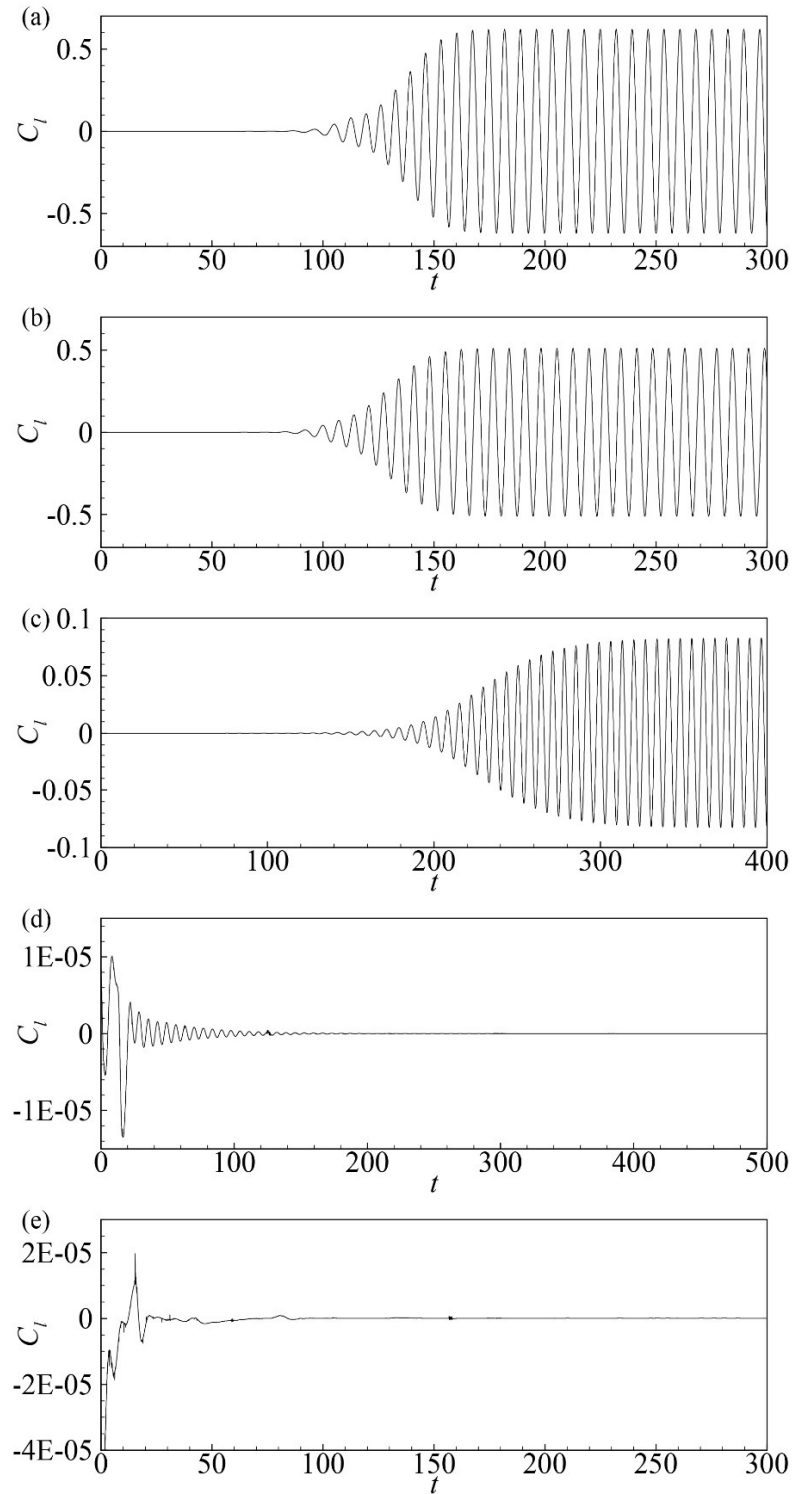


Figure 4.7: Temporal variation of the lift coefficient with respect to the non-dimensional time at $Re = 200$: (a) $Ha = 0$, (b) $Ha = 1.0$, (c) $Ha = 3.0$, (d) $Ha = 4.0$ and (e) $Ha = 8.0$

4.2. Study of Flows past Wedge without Magnetic Field

Flow past the wedge without magnetic field can be understood as purely hydrodynamic flow. Since simulations were conducted for $Re = 1 - 150$, results are presented in terms of streamlines and vorticity depicting various flow regimes. The flow patterns behind the wedge for the aforementioned range of Reynolds number are explained.

4.2.1. Validation of Results

Using M2 mesh belonging to wedge model, simulations have been carried out for $Re = 10 - 150$ to obtain the values of drag coefficient and Strouhal number and perform comparative analysis. The comparison of present results with the published literature of time-averaged drag coefficient for $Re = 50 - 150$ is depicted in Figure 4.8. An excellent agreement of present results against the reported data of De & Dalal (2006) and Dhiman, et al. (2011) can be clearly observed. For instance, the average difference between the present results and that of De & Dalal (2006) of mean drag coefficient for $Re = 50 - 150$ is 1.23%.

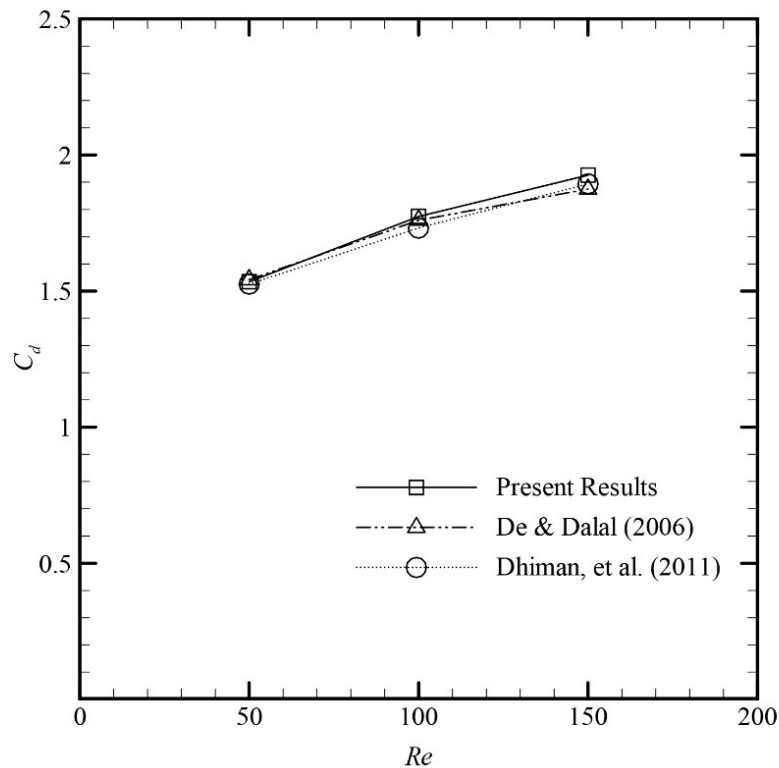


Figure 4.8: Validation of time-averaged C_d for $Re = 50 - 150$

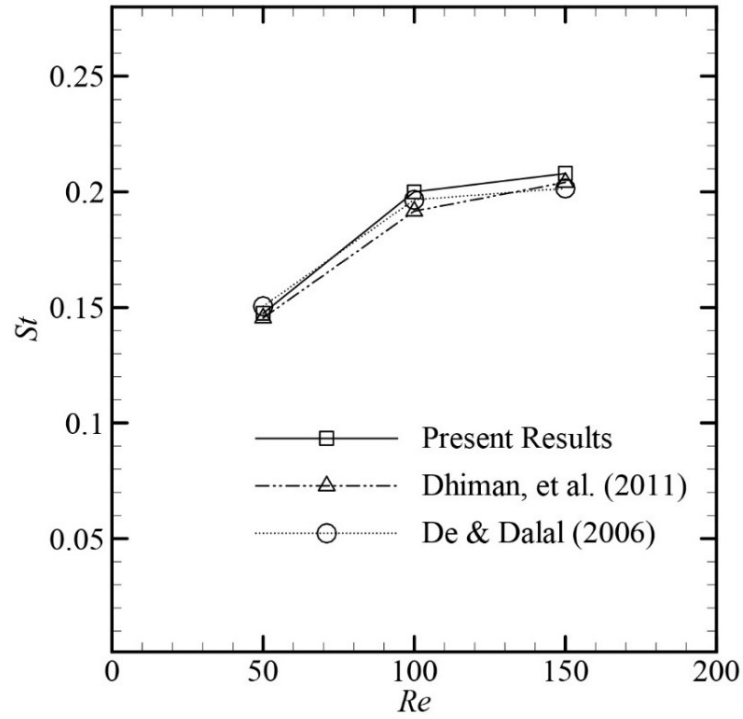


Figure 4.9: Validation of St for $Re = 50 - 150$

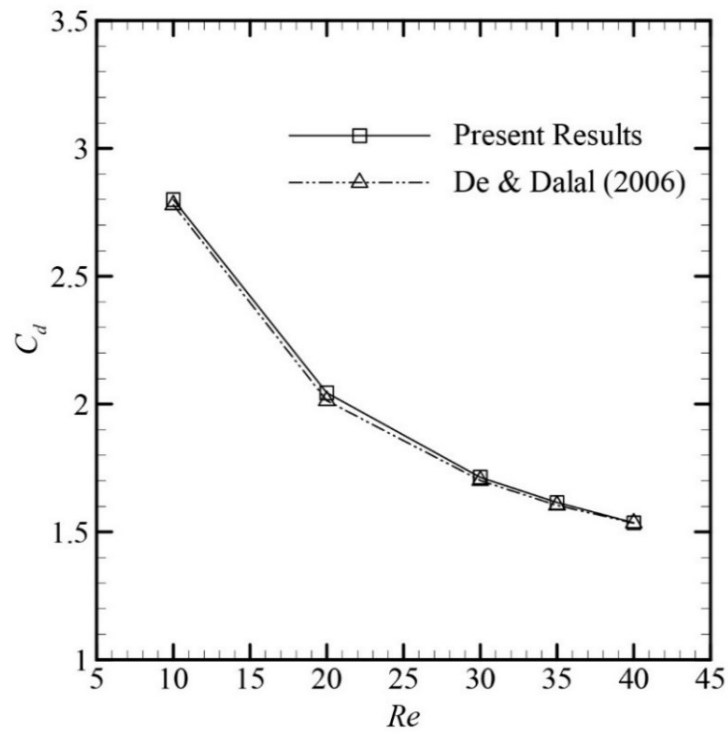


Figure 4.10: Validation of C_d for $Re = 10 - 40$

Figure 4.9 shows the comparison of Strouhal number for $Re = 50 - 150$ against the published literature. An excellent agreement between the present results of Strouhal number against the results of De & Dalal (2006) and Dhiman, et al. (2011) has been obtained. For instance, the average difference between the present results and that of De & Dalal (2006) of Strouhal number is 2.32%. Similarly, simulations have been performed for $Re = 10 - 40$ have also been conducted. The values of drag coefficient for the aforementioned Reynolds numbers have been computed and compared with the published literature. An excellent agreement has been obtained between the present values of drag coefficient against the results of De & Dalal (2006) as shown in Figure 4.10. For instance, the average difference between the present results and that of De & Dalal (2006) of drag coefficient is 2.24%. Hence, the computational model of wedge has been validated.

4.2.2. Study of Flow Patterns at Different Flow Regimes

Before imposing external magnetic field, the purely hydrodynamic flows have been numerically investigated. Figures 4.11 and 4.12 provide the contours of streamlines and vorticity for $Re = 1, 10, 30$ and 100 around the wedge without magnetic field ($Ha = 0$). It can be observed that for $Re = 1$, the flow of creeping nature is observed. At this Reynolds number, the viscous forces are more dominant than the inertial forces and as a consequence, the fluid particles follow the shape of the wedge. Hence, the flow attaches to the wedge surface with no flow separation behind the wedge. As we move to higher Reynolds numbers, the flow patterns behind the wake of the wedge changes. For $Re = 30$, it can be observed that a closed separated zone known as ‘recirculation bubble’ is formed behind the wedge. Such flow patterns observed in this case seem consistent with the usual hydrodynamic flows at Re ranging from 5 up to 40 in other bluff bodies. Now, as we go from $Re = 30$ to 100 , the flow patterns transition to unsteady laminar flow regime depicting alternate vortex shedding. De & Dalal (2006) reported the critical Reynolds number, Re_{cr} to be 39.9 in his paper. Critical Reynolds number, Re_{cr} provides distinction between the steady flow and unsteady flow, and, is defined as the Reynolds number for which the onset of vortex shedding is observed. For $Re = 100$, it is evident that the recirculating wake behind the wedge is time-dependent and flow patterns constantly change with time. It is observed that the periodic vortex shedding

phenomena begin to take place and vortices from the upper and lower regions of the wedge start to shed continuously.

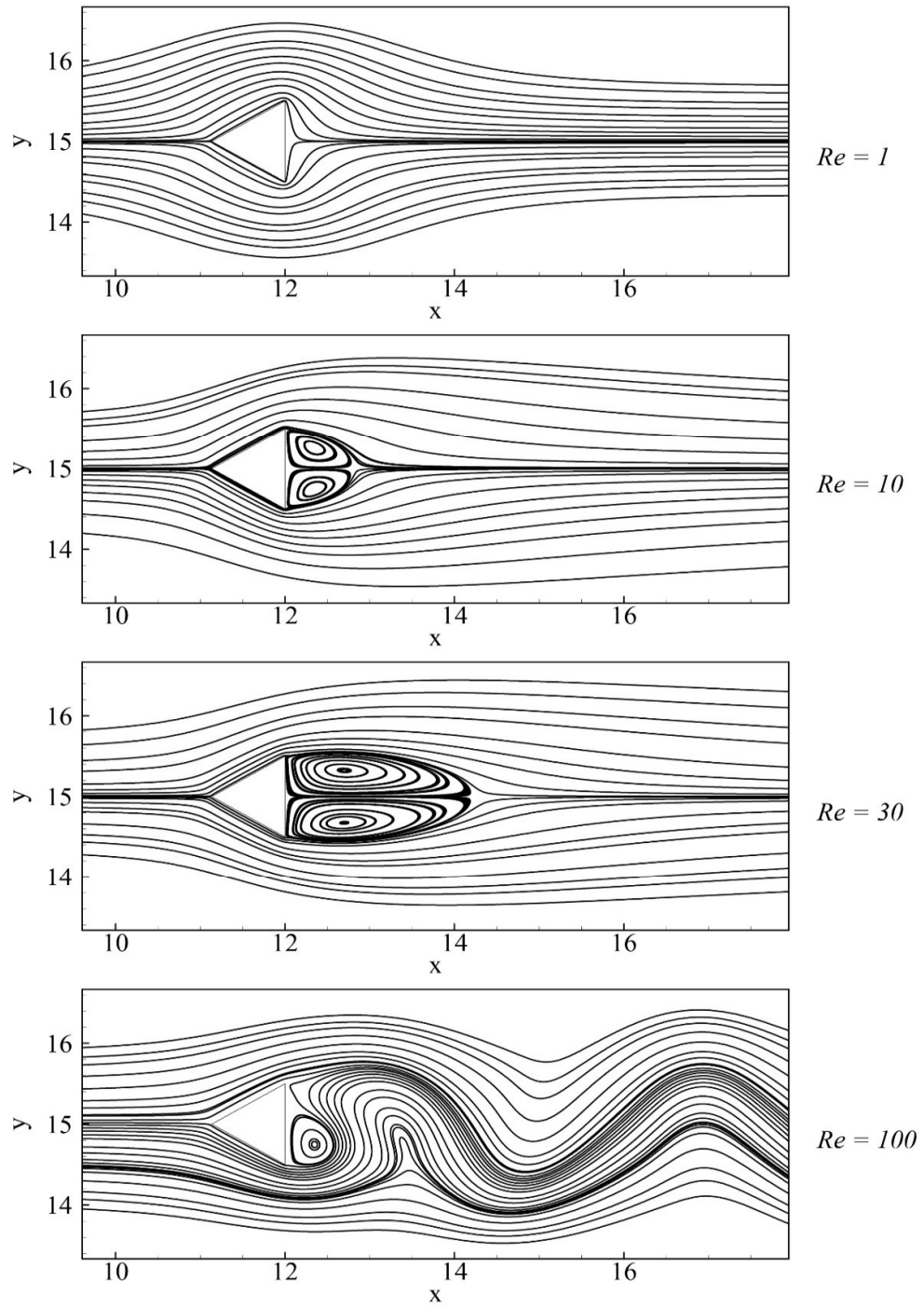


Figure 4.11: Streamlines for $Re = 1, 10, 30$ and 100

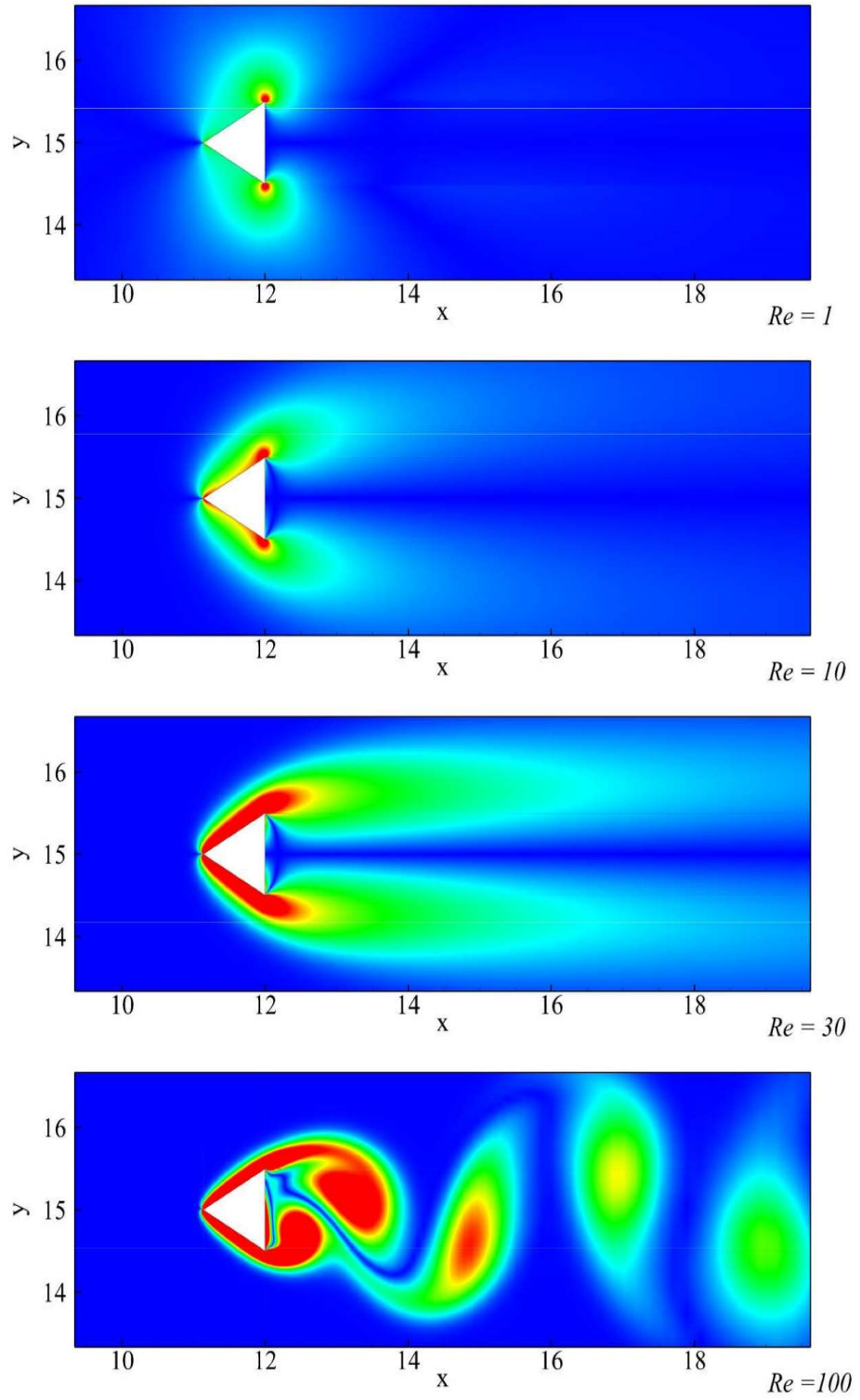


Figure 4.12: Vorticity contours for $Re = 1, 10, 30$ and 100

4.2.3. Study of Flow Patterns for Steady Flow Regimes

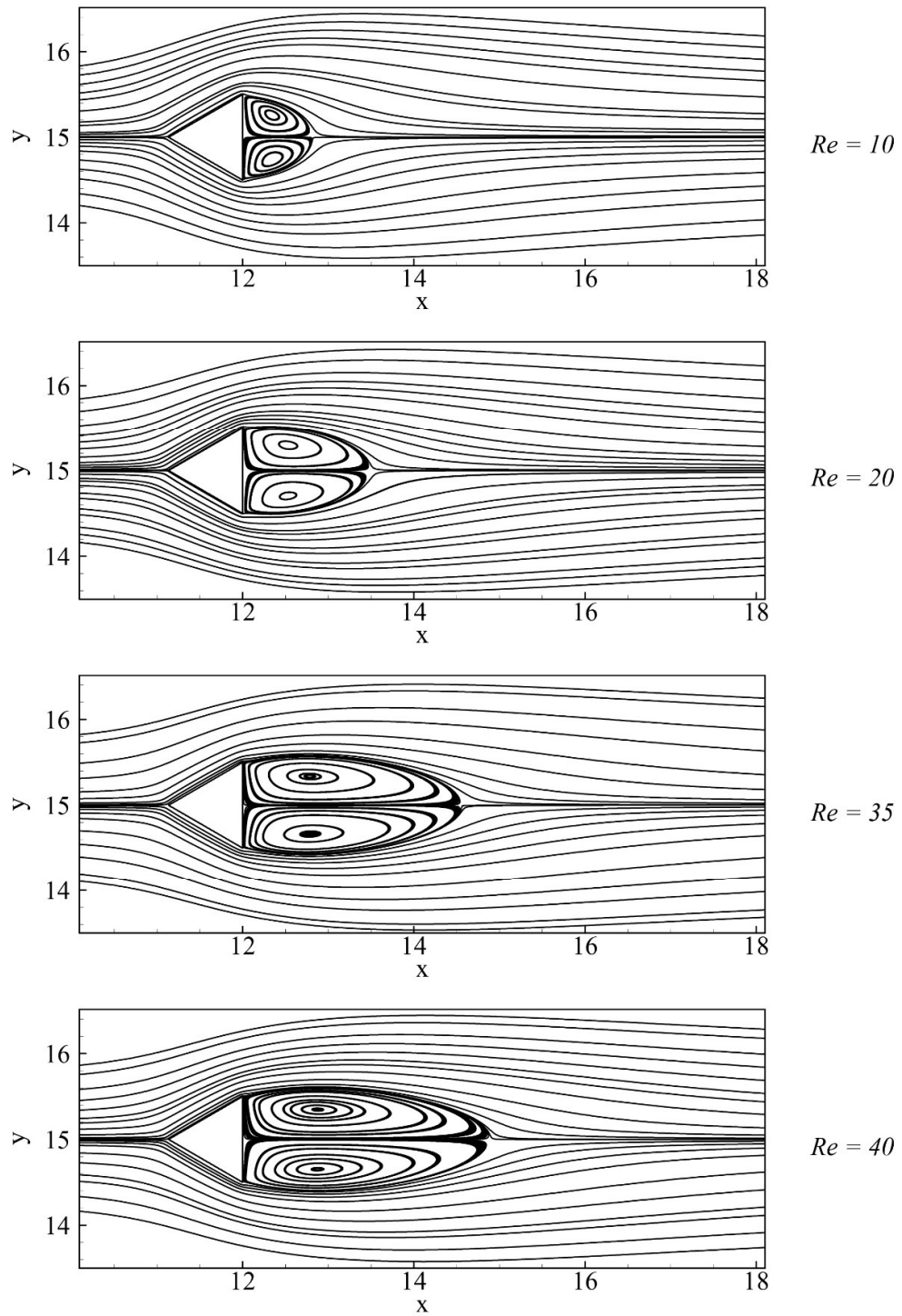


Figure 4.13: Streamlines for $Re = 10 - 40$

The study of flow patterns for steady flow regime for $Re = 10 - 40$ is discussed. As mentioned earlier, at this sub-critical range i.e. $5 < Re < 40$, the region of wake behind the obstacle is characterized by the presence of a closed steady recirculating bubble consisting of symmetric twin vortices. Another important feature of this flow regime is the recirculation length which increases with the Reynolds number. Figure 4.13 presents the streamlines in the vicinity of wedge for $Re = 10 - 40$. It can be observed that the two steady symmetrical vortices are formed behind the wedge and the growth of the recirculating wake with increasing Reynolds number is clearly seen.

4.3. Study of Flows past Wedge with Magnetic Field

This section focuses on the study of flow past the wedge at $Re = 100$ for $Ha = 0 - 10$. The effects of transverse magnetic field on wake structure and flow coefficients are presented in detail.

4.3.1. Calculation of Critical Hartmann Number

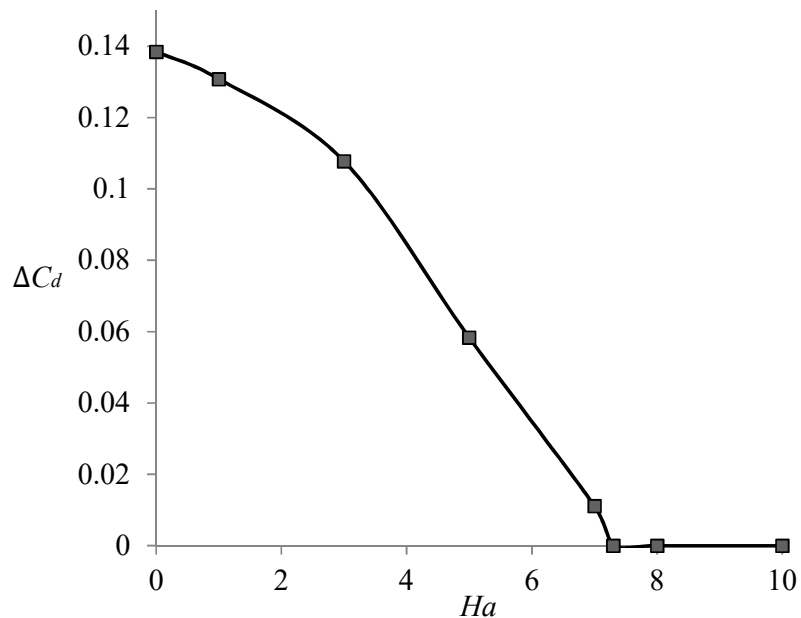


Figure 4.14: Variation of ΔC_d with Ha

To calculate the value of critical Hartmann number at $Re = 100$, an analysis has been done to study the behavior of the amplitude of drag coefficient with the increasing Hartmann number. Here, ΔC_d represents the difference between the maximum and

minimum amplitudes of the oscillating drag coefficient. With increasing Hartmann number, it is observed that the magnitude of ΔC_d decreases up to certain Hartmann number as shown in Figure 4.14. However, on further increment of Hartmann number, the magnitude of ΔC_d becomes zero, indicating the attainment of the steady flow regime. Analysis shows that the flow attains the steady state at $Ha = 7.3$. Also, at $Ha_{cr} = 7.3$, the oscillating lift, after some time, becomes zero indicating the attainment of the steady flow as evidenced by the presence of symmetric twin vortices in the wake region of the wedge. Hence, the alternate shedding of vortices is completely suppressed.

4.3.2. Influence on Wake

At $Re = 100$, the profiles of streamline and vorticity for different strengths of magnetic field in crossflow direction is shown in Figures 4.15 – 4.16. The shedding of alternate vortices from the upper and the lower regions of the wedge is evident which implies the unsteady nature of the flow. For higher magnetic field, the unsteady nature of the flow evidenced by the presence of alternate vortex shedding still remains undisturbed up to certain Hartmann number as shown by Figure 4.15 (a) - (c). However, beyond certain Hartmann number, the flow converts from unsteady to steady nature shown by the presence of a recirculating wake and with further increment in Hartmann number, the wake length reduces as shown in Figure 4.15 (d) - (e). This is due to the resistive Lorentz force in the upstream direction arising on the application of transverse magnetic field which dampens the vortices. On the increment of Hartmann number, the strength of vortices is reduced as depicted by Figures 4.16 (a) - (c). At $Ha = 7.3$, the shedding of vortices is completely eliminated resulting in steady state as evidenced by the presence of symmetric and closed recirculating wake as shown in Figure 4.15 (d).

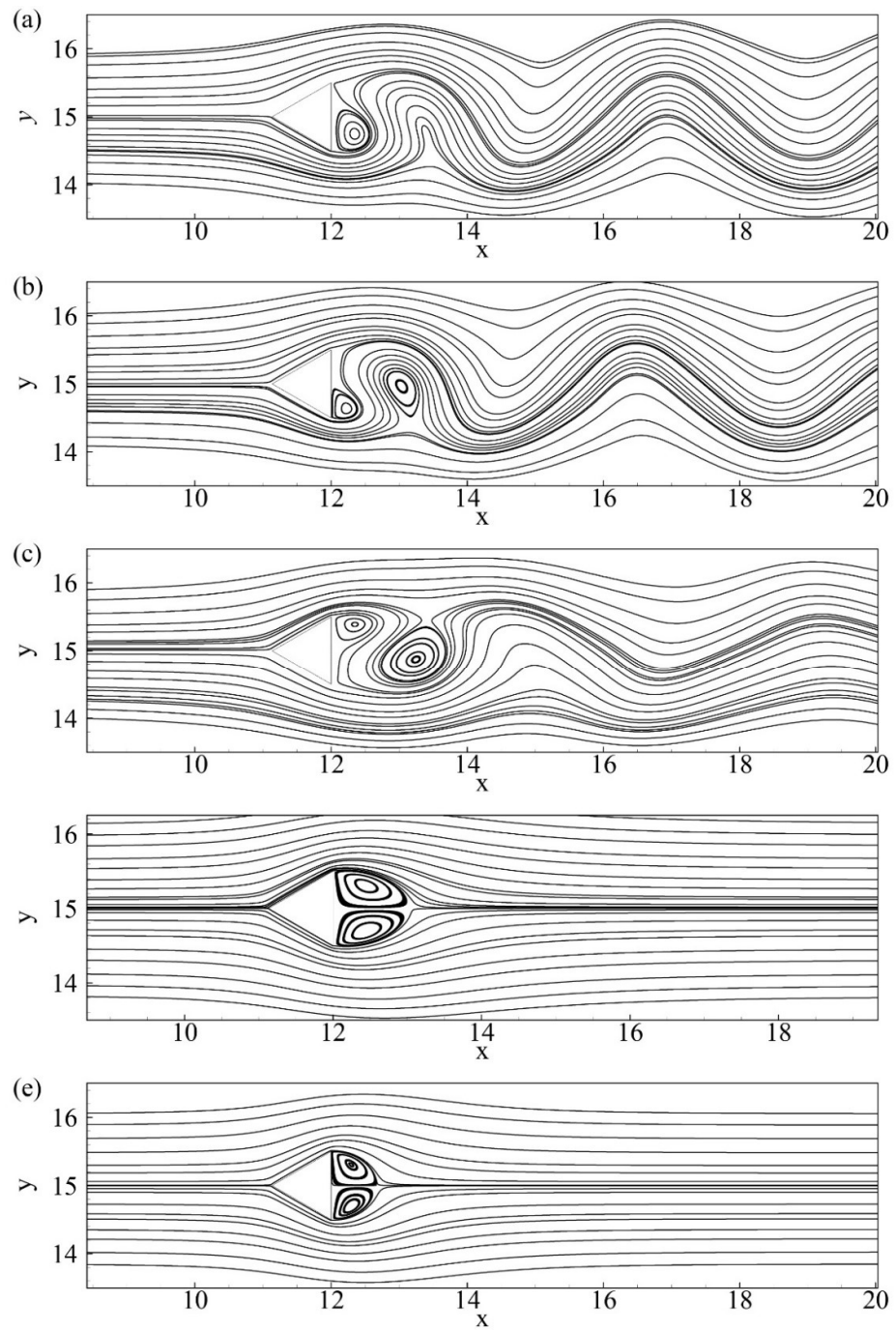


Figure 4.15: Streamlines at $Re = 100$: (a) $Ha = 0$, (b) $Ha = 2.0$, (c) $Ha = 5.0$, (d) $Ha = 7.3$ and (e) $Ha = 10$

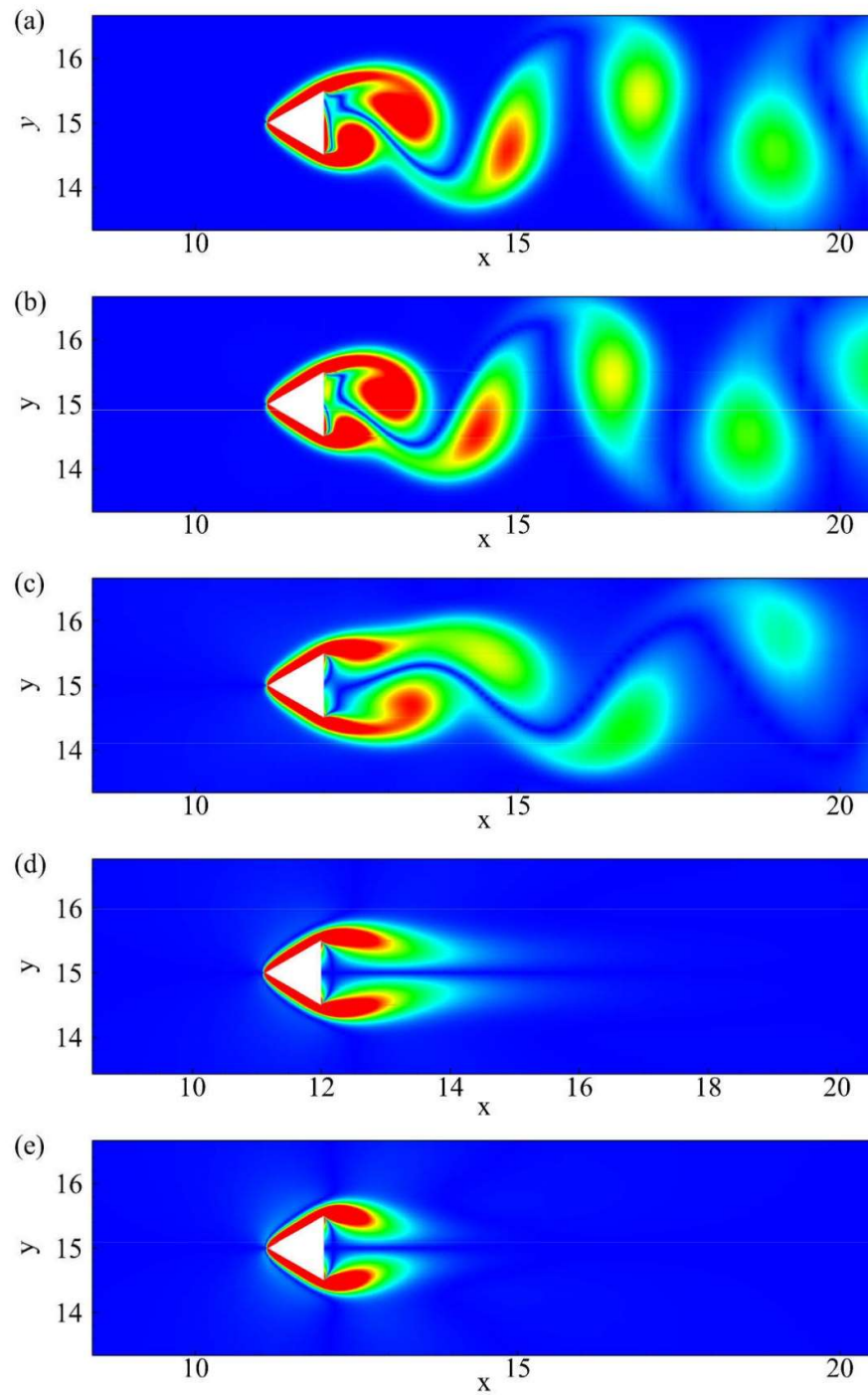


Figure 4.16: Vorticity contours at $Re = 100$: (a) $Ha = 0$, (b) $Ha = 2.0$, (c) $Ha = 5.0$,
 (d) $Ha = 7.3$ and (e) $Ha = 10$

4.3.3. Influence on Drag and Lift coefficients

Figures 4.17 (a) - (e) shows the time history profiles of the mean drag coefficient at $Re = 100$ for different Hartmann numbers. At $Ha = 0$ i.e. without magnetic field, the mean drag coefficient for $Re = 100$ has been found to be 1.7745. Within the unsteady flow regime, the mean drag coefficient minimally decreases from 1.7745 to 1.5237 with the increment in Hartmann number from 0 to 5. The drop in drag coefficient continues for $Ha < 7.3$. Such drop in drag coefficient can be attributed to the increase in pressure in the wake region behind the wedge (Yoon, et al., 2004). At critical Hartmann number i.e. $Ha = 7.3$, the flow assumes the steady state and the average drag coefficient is found to increase with further increment of Hartmann number as shown by Figures 4.17 (d) - (e). The possible explanation is that at steady state, the velocity field is significantly suppressed, causing the boundary layer thickness to increase and hence the drag. Also, the pressure drop increases is due to the pressure increase on the front region of the wedge, consequently increasing the pressure drag on the body. The time history profiles of the lift coefficient for $Re = 100$ at different Hartmann numbers are shown in Figure 4.18 (a) - (e). It is seen that the lift amplitude decreases when Ha is increased from 0 to 10. For instance, at $Ha = 10$, after an initial unsteady period, the mean lift coefficient becomes zero as shown in Figure 4.18 (e).

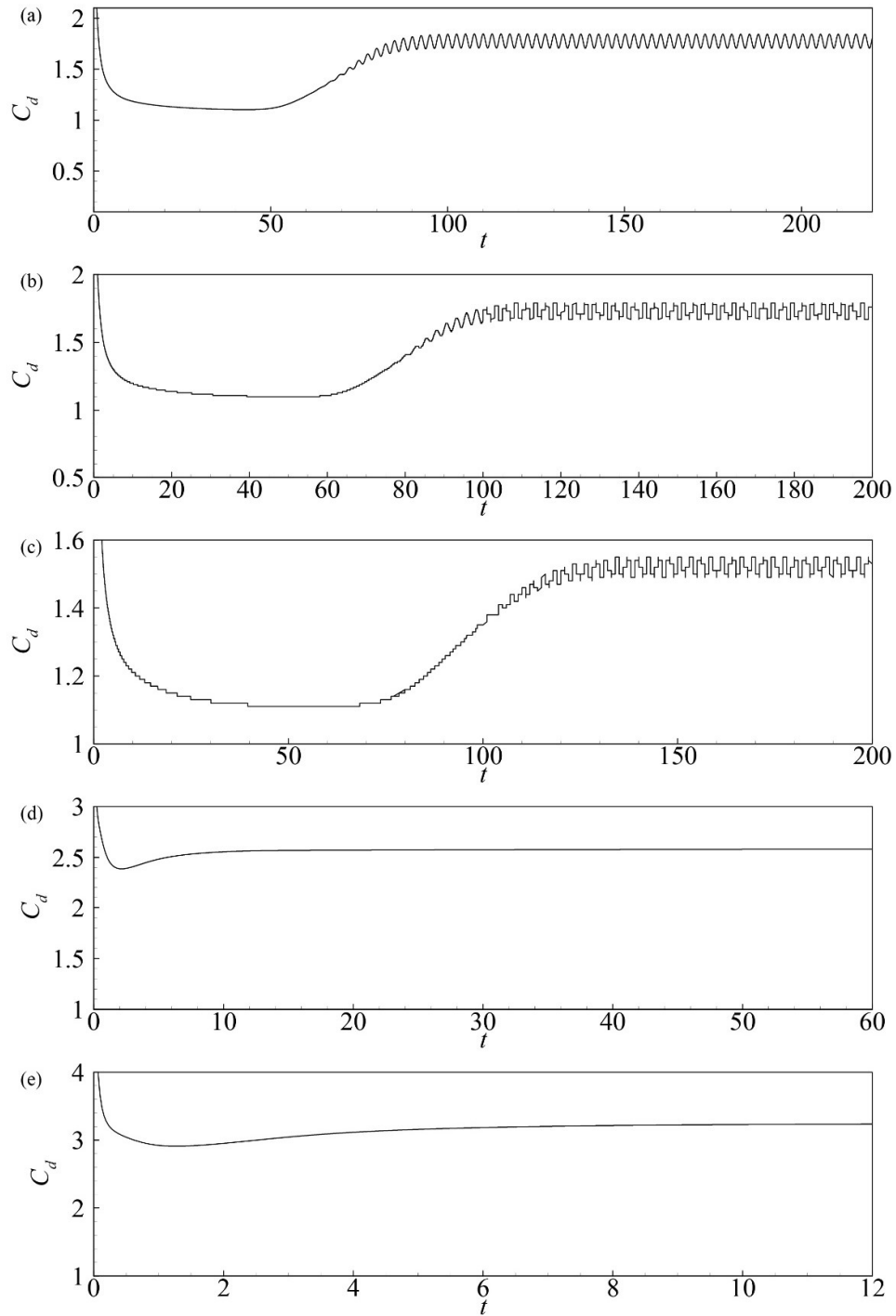


Figure 4.17: Temporal variation of drag coefficient at $Re = 100$: (a) $Ha = 0$, (b) $Ha = 2.0$, (c) $Ha = 5.0$, (d) $Ha = 7.3$ and (e) $Ha = 10$

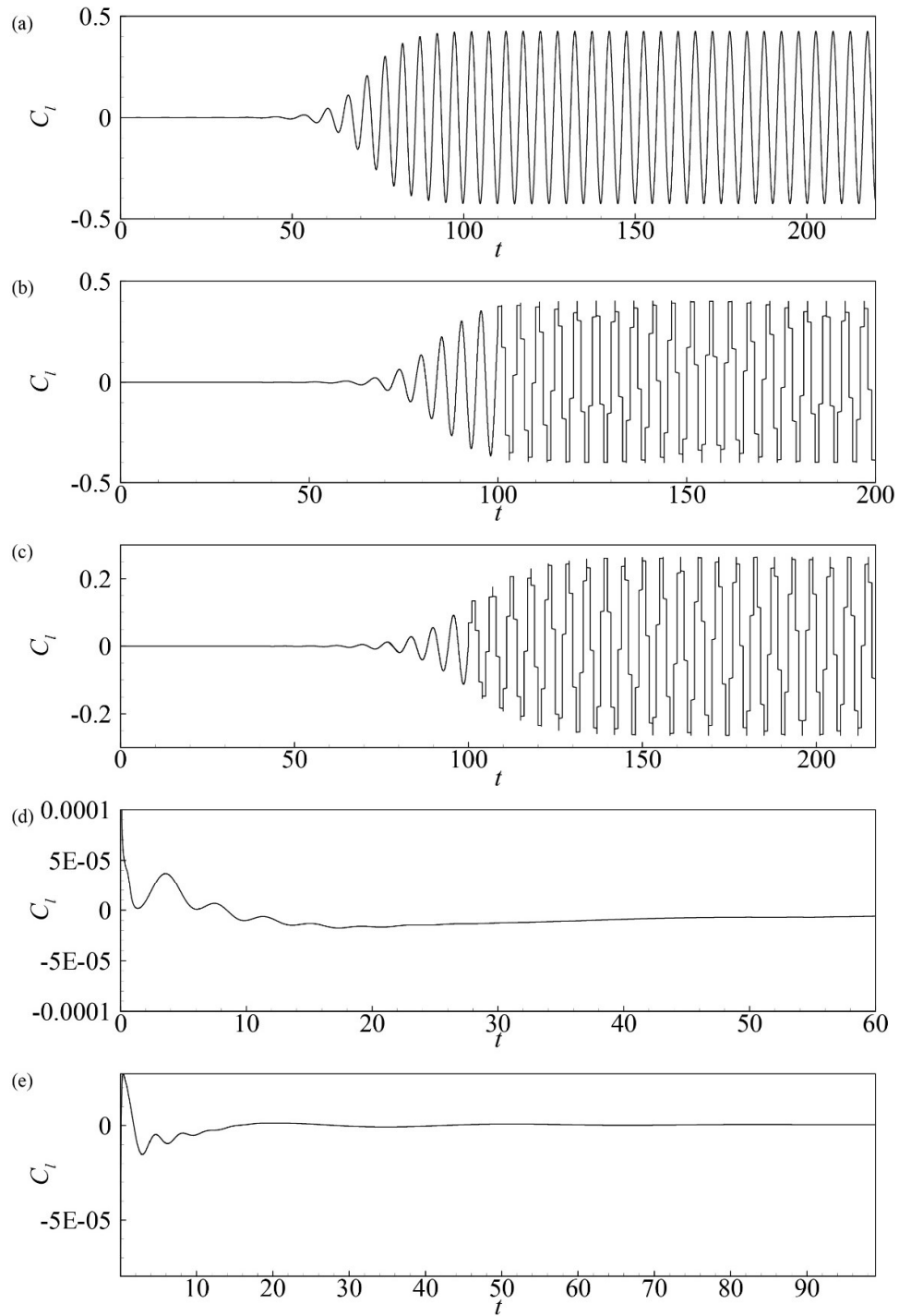


Figure 4.18: Temporal variation of lift coefficient at $Re = 100$: (a) $Ha = 0$, (b) $Ha = 2.0$, (c) $Ha = 5.0$, (d) $Ha = 7.3$ and (e) $Ha = 10$

CHAPTER FIVE: CONCLUSIONS AND RECOMMENDATIONS

5.1. Conclusions

Two-dimensional laminar incompressible viscous flow of an electrically conducting fluid past an unconfined wedge structure under the presence of transverse magnetic field has been studied. The fluid is assumed to have uniform electrical conductivity. The magnetic Reynolds number is assumed to be very small such that the induced magnetic field is negligible compared to the applied magnetic field. The magnetic induction method in MHD module built in ANSYS Fluent has been chosen for all MHD simulations. Several conclusions can be drawn from this study. Results indicate that the magnetic induction method in MHD module built in ANSYS Fluent offers good solution capabilities regarding MHD simulations. It can be concluded that the vortex shedding can be completely eliminated if a sufficiently strong magnetic field is applied. In the steady flow regime, the length of the wake is reduced with the increase in Hartmann number. The mean drag coefficient is found to decrease with the increment of Hartmann number as long as the flow remains in the periodic laminar regime. However, the drag coefficient has a tendency to increase with the increase in Hartmann number once the flow assumes the steady flow regime. Similarly, the amplitude of lift coefficient decreases with the increase in Hartmann number indicating the reduction of strength of vortices. The flow-induced vibrations could be completely eliminated with the application of magnetic field. There exists a critical Hartmann number at which complete suppression of vortex shedding is observed. For the wedge in an unconfined medium, a critical Hartmann number for $Re = 100$ has been found to be 7.3.

5.2. Recommendations

The following recommendations are suggested for further study.

- i) Effects of aligned magnetic field on wake dynamics past an unconfined wedge can be studied.
- ii) Effects of magneto-hydrodynamics on the confined flow past the wedge for low Hartmann numbers can be studied.
- iii) Study of MHD flows past the confined wedge for low Reynolds numbers i.e. 10 - 40 can also be conducted. Heat transfer can also be incorporated in this study.

REFERENCES

- Abbasi, H., Turki, S. & Nasrallah , S., 2001. Numerical Investigation of forced convection in a plane channel with a built-in trinagular prism. *International Journal of Thermal Sciences* , Volume 40, pp. 649-658.
- Altintas, A. & Ozkol, I., 2015. Magneto-hydrodynamic Flow of Liquid-Metal in Circular Pipes for Externally Heated and Non-heated Cases. *Journal of Applied Fluid Mechanics*, 8(3), pp. 507-514.
- Aubert, J., 2018. Status of the EU DEMO HCLL breeding blanket design development. *Fusion Engineering and Design*, pp. 1-5.
- Bramley, J. S., 1974. Magneto-hydrodynamic flow past a circular cylinder. *Journal of Applied Mathematics and Physics*, 25(3), pp. 409-416.
- Breuer, M., Bernsdorf, J., Zeiser, T. & Durst, F., 2000. Accurate computations of the laminar flow past a square cylinder based on two different methods: lattice-Boltzmann and finite-volume. *International Journal of Heat and Fluid Flow*, Volume 21, pp. 186-196.
- Buhler, L., 2007. Liquid metal magneto-hydrodynamics for fusion blankets. In: S. Molokov, R. Moreau & K. Moffat, eds. *Magneto-hydrodynamics. Historical Evolution and Trends*. Dordrecht: Springer, pp. 171-194.
- Chatterjee, D., Chatterjee, K. & Mondal, B., 2012. Control of Flow Separation Around Bluff Obstacles by Transverse Magnetic Field. *Journal of Fluids Engineering*, September.134(9).
- Chatterjee, D. & Gupta, S. K., 2015. MHD Flow and Heat Transfer Behind a Square Cylinder in a Duct under Strong Axial Magnetic Field. *International Journal of Heat and Mass Transfer*, Volume 88, pp. 1-13.
- Chattopadhyay, H., 2007. Augmentation of heat transfer in a channel using a triangular prism. *International Journal of Thermal Sciences*, August, Volume 46, pp. 501-505.
- Chen, Z. & Aubry, N., 2005. Active control of cylinder wake. *Communications in Nonlinear Science and Numerical Simulation*, 10(2), pp. 205-216.

- Dalal, A., Eswaran, V. & Biswas, G., 2008. A Finite-Volume Method for Navier-Stokes Equations on Unstructured Meshes. *Numerical Heat Transfer, Part B: Fundamentals*, 54(3), pp. 238-259.
- Davidson, P., 1999. Magneto-hydrodynamics in Material Processing. *Annual Reviews of Fluid Mechanics*, Volume 31, pp. 273-300.
- Davidson, P., 2001. *An Introduction to Magneto-hydrodynamics*. 1st ed. New York: Cambridge University Press.
- De, A. & Dalal, A., 2006. Numerical simulation of unconfined flow past a triangular cylinder. *International Journal of Numerical Method in Fluids* , Volume 52, pp. 801-821.
- De, A. K. & Dalal, A., 2007. Numerical Study of Laminar Forced Convection Fluid Flow and Heat Transfer From a Triangular Cylinder Placed in a Channel. *Transactions of the ASME*, May. Volume 129.
- Dhiman, A. & Shyam, R., 2011. Unsteady Heat Transfer from an Equilateral Triangular Cylinder in the Unconfined Flow Regime. *International Scholarly Research Network*, 14 February.
- Dousset, V., 2009. *Numerical Simulations of MHD Flows Past Obstacles in a Duct under Externally Applied Magnetic Field*, Coventry: s.n.
- Dousset, V. & Potherat, A., 2008. Numerical simulations of a cylinder wake under a strong axial magnetic field. *Physics of Fluids*, 23 January.20(1).
- Esfahani, J. A. et al., 2015. Control of Wake and Vortex Shedding behind Solid Circular Obstacle by Magneto-hydrodynamics. *Journal of Thermal Engineering*, February, 1(2), pp. 593-597.
- Farjallah , H., Abbassi, H. & Tuki, S., 2011. Vortex Shedding of Electrically Conducting Fluid Flow Behind Square Cylinder under Magnetic Field. *Engineering Applications of Computational Fluid Mechanics*, 5(3), pp. 349-356.
- Grigoriadis, D., Sarris, I. & Kassinos, S., 2009. MHD flow past a circular cylinder using the immersed boundary method. *Computers and Fluids*, 23 September.

- Hartmann, J., 1937. Hg-dynamics I. Theory of the laminar flow of an electrically conductive liquid in a homogeneous magnetic field. *Det Kgl. danske videnskabernes selskab. Matematisk-fysiske meddelelser*, 15(6), pp. 1-27.
- Hussam , W. K., Thompson, M. C. & Sheard, G. J., 2010. *Quasi-2D Simulation of Liquid Metal Flow Past a Cylinder in a Duct Exposed to a Magnetic Field*. Auckland, s.n.
- Hussam, W. K., Hamid, A. H., Ng, Z. Y. & Sheard, G. J., 2018. Effect of vortex promoter shape on heat transfer in MHD duct flow with axial magnetic field. *International Journal of Thermal Sciences*, 8 June, Volume 134, pp. 453-464.
- Hussam, W. K., Thompson, M. C. & Sheard, G. J., 2011. Dynamics and Heat Transfer in a Quasi-Two-Dimensional MHD Flow Past a Circular Cylinder in a Duct at High Hartmann Numbers. *International Journal of Heat and Mass Transfer*, 54(5), pp. 1091-1100.
- ITER Organization, 2020. *The ITER Tokamak*. [Online] Available at: <https://www.iter.org/mach> [Accessed 18 February 2020].
- Ivlev, V. & Baranov, N., 1993. Research and Development in the Field of MHD Devices Utilizing Liquid Working Medium for Process Applications. In: H. Branover & Y. Unger, eds. *Metallurgical Technologies, Energy Conversion, and Magnetohydrodynamic Flows*. Washington DC: American Institute of Aeronautics and Astronautics, pp. 3-23.
- Jackson, C., 1987. A finite-element study of the onset of vortex shedding in flow past variously shaped bodies. *Journal of Fluid Mechanics*, 13 January, Volume 182, pp. 23-45.
- Johansson, S., Davidson, L. & Olsson, E., 2005. Numerical simulation of vortex shedding past triangular cylinders at high Reynolds numbers using k-e turbulence model. *International Journal for Numerical Methods in FLuids* , 16(10), pp. 859-878.
- Johansson, S. H., Davidson, L. & Olsson, E., 1993. Numerical Simulation of Vortex Shedding past Triangular Cylinders at High Reynolds Number using k-e Turbulence Model. *International Journal for Numerical Methods in Fluids*, Volume 16, pp. 859-878.

- Josserand, J., Marty, P. & Alemany, A., 1993. Pressure and drag measurements on a cylinder in a liquid metal flow with an aligned magnetic field. *Fluid Dynamics Research*, pp. 107-117.
- Kolesnichenko, A. F., 1990. Electromagnetic Process in Liquid Material in the USSR and Eastern European Countries. *Iron and Steel Institute of Japan*, 30(1), pp. 8-26.
- Kumar , H. & Rajathy, R., 2006. Numerical Study of MHD Flow Past a Circular Cylinder at Low and Moderate Reynolds Numbers. *International Journal of Computational Methods in Engineering Science and Mechanics* , Volume 7, pp. 461-473.
- Kumari, R. & Bansal, J. L., 1985. Slow magnetohydrodynamic flow past a circular cylinder. *Proceedings- Mathematical Sciences* , September, 94(1), pp. 51-60.
- Lavrentiev , I. V., 1989. MHD-Flows at High R_m , N and Ha . In: J. Lielpeteris & R. Moreau, eds. *Liquid Metal Magneto-hydrodynamics. Mechanics of Fluids and Transport Processes*. Dordrecht: Kluwer Academic Publishers, pp. 21-27.
- Lielausis, O., 1989. Liquid Metal in a Strong Magnetic Field. In: J. Lielpeteris & R. Moreau, eds. *Liquid Metal Magneto-hydrodynamics. Mechanics of Fluids and Transport Processes*. Dordrecht: Kluwer Academic Publishers, pp. 3-12.
- Ligere, J., 2014. *Analytical Solutions of Magnetohydrodynamical Problems on a Flow of Conducting Fluid in the Entrance Region of Channels in a Strong Magnetic Field*, Riga: s.n.
- Mistrangelo, C. & Buhler, L., 2017. Magnetohydrodynamic flows in liquid metal blankets for fusion reactors. *Proceedings in Applied Mathematics and Mechanics*, Volume 17, pp. 115-118.
- Muck, B., Gunther, C., Muller, U. & Buhle, L., 2000. Three-Dimensional MHD Flows in Rectangular Ducts with Internal Obstacles. *Journal of Fluid Mechanics*, Volume 418, pp. 265-295.
- Mutschke, G., Gerbeth, G., Albrecht, T. & Grundmann, R., 2006. Separation control at hydrofoils using Lorentz forces. *European Journal of Mechanics - B/Fluids* , 25(2), pp. 137-152.

- Mutschke, G., Shatrov, V. & Gerbeth, G., 1998. Cylinder wakes control by magnetic fields in liquid metal flows. *Experimental Thermal and Fluid Science*, 16(1-2), pp. 92-99.
- Posdziech, O. & Grundmann, R., 2001. Electromagnetic control of seawater flow around circular cylinders. *European Journal of Mechanics - B/Fluids*, 20(2), pp. 255-274.
- Povkh, I. L., Kapusta, A. B. & Chekin, B. V., 1974. *Magnetic Hydrodynamics in Metallurgy*. Moscow: Metallurgy.
- Rajani, B., Kandasamy, A. & Majumdar, S., 2008. Numerical simulation of laminar flow past a circular cylinder. *Applied Mathematical Modelling*, pp. 1228-1247.
- Rao, C. R. & Sekhar, T., 2000. MHD Flow past a circular cylinder- a numerical study. *Computational Mechanics*, Volume 26, pp. 430-436.
- Sekhar, T., Ravikumar, T. & Kumar, H., 2003. MHD flow past a sphere at low and moderate Reynolds numbers. *Computational Mechanics*, Volume 31, pp. 437-444.
- Sekhar, T., Sivakumar, R., Kumar, H. & Kumar, T., 2007. Effect of aligned magnetic field on the steady viscous flow past a circular cylinder. *Applied Mathematical Modelling*, Volume 31, pp. 130-139.
- Sekhar, T., Sivakumar, R. & Kumar, T. R., 2005. Drag and Pressure Fields for the MHD Flow around a Circular Cylinder at Intermediate Reynolds numbers. *Journal of Applied Mathematics*, Volume 3, pp. 183-203.
- Sekhar, T., Sivakumar, R. & Kumar, T. R., 2009. Effect of magnetic Reynolds number on the two-dimensional hydromagnetic flow around a cylinder. *International Journal for Numerical Methods in Fluids*, Volume 59, pp. 1351-1368.
- Sheikholeslam, M. & Domairry, D., 2016. *External Magnetic Field Effects on Hydrothermal Treatment of Nanofluid*. The Boulevard, Langford Lane, Kidlington, Oxford, OX5 1GB, UK: Elsevier Science.
- Singha, S., Sinhamahapatra, K. & Mukherjea, S., 2007. Control of Vortex Shedding From a Bluff Body Using Imposed Magnetic Field. *Journal of Fluids Engineering*, Volume 129, pp. 517-523.

- Singha, S. & Sinhamahapatra, K., 2011. Control of vortex shedding from a circular cylinder using imposed transverse magnetic field. *International Journal of Numerical Methods for Heat & Fluid Flow*, 21(1), pp. 32-45.
- Sivakumar, R., Sekhar, T. & Ravi Kumar, T., 2006. Flow around a circular cylinder in an external magnetic field at high Reynolds numbers. *International Journal of Numerical Methods for Heat & Fluid Flow*, 16(6), pp. 740-759.
- Sumer, B. M. & Fredsoe, J., 2006. *Hydrodynamics Around Cylindrical Structures*. Revised ed. 5 Toh Tuck Link: World Scientific Publishing Co. Ltd. Ltd..
- Weier, T. & Gerbeth, G., 2004. Control of separated flows by time periodic Lorentz forces. *European Journal of Mechanics - B/Fluids*, 23(6), pp. 835-849.
- Weier, T. et al., 1998. Experiments on cylinder wake stabilization in an electrolyte solution by means of electromagnetic forces localized on the cylinder surface. *Experimental Thermal and Fluid Science*, 16(1-2), pp. 84-91.
- Wesfried, J., Goujon-Durand, S. & Zielinska, B., 1996. Global Mode Behaviour of the Streamwise Velocity in Wakes. *Journal de Physique*, 4 July, pp. 1343-1357.
- Wesfried, J. & Zielinska, B., 1995. On the spatial structure of global modes in wake flow. *Physics of Fluids*, 8 February, Volume 7, pp. 1418-1424.
- Yoon, H. S., Chun, H. H., Ha, M. Y. & Lee, H. G., 2004. A numerical study on the fluid flow and heat transfer around a circular cylinder in an aligned magnetic field. *International Journal of Heat and Mass Transfer*, Volume 47, pp. 4075-4087.
- Zachariah, J. & Singh, R. K., 1983. MHD Flow past a Circular Cylinder in a Channel. *Journal of the Physical Society of Japan*, pp. 2742-2750.
- Zdravkovich, M., 1997. Flow around Circular Cylinders. *Oxford Science Publications*, p. 692.
- Zhang, H., Fan, B.-c. & Li, H.-z., 2014. Numerical study of the suppression mechanism of vortex-induced vibration by symmetric Lorentz forces. *Journal of Fluids and Structures*, Volume 48, pp. 62-80.
- Zielinska, B. & Wesfried, J., 1995. On the spatial structure of global modes in wake flow. *Physics of Fluids*, Volume 7, pp. 1418-1424.

PUBLICATIONS

Rana, S., Dura, H.B., & Shrestha, R., 2020. *Effects of Magneto-hydrodynamics on Vortex Shedding past a Square Cylinder*. IOE Graduate Conference.

APPENDIX-A: WEDGE MODEL VALIDATION DATA

Table A.1 Drag coefficient and Strouhal number data for $Re = 50 - 150$

S.N.	Present Results			De & Dalal (2006)			Dhiman,et al. (2011)		
	<i>Re</i>	<i>C_d</i>	<i>St</i>	<i>Re</i>	<i>C_d</i>	<i>St</i>	<i>Re</i>	<i>C_d</i>	<i>St</i>
1.	50	1.5342	0.1475	50	1.542	0.1505	50	1.5257	0.1455
2.	100	1.774504	0.200	100	1.7607	0.1966	100	1.7316	0.1916
3.	150	1.9231	0.200	150	1.875	0.2015	150	1.8937	0.2041

Table A.2 Drag coefficient data for $Re = 10 - 40$

S.N.	Present Results		De & Dalal (2006)	
	<i>Re</i>	<i>C_d</i>	<i>Re</i>	<i>C_d</i>
1.	10	2.8	10	2.70
2.	20	2.044	20	1.98148
3.	30	1.7139	30	1.68765
4.	35	1.6151	35	1.59259
5.	40	1.5357	40	1.51481

APPENDIX-B: UDF CODE FOR SQUARE CYLINDER

```

/*****
/
/* vprofile.c
*/
/* UDF for specifying unsteady-state velocity profile boundary condition */
/*****
***/
#include "udf.h"

DEFINE_PROFILE(inlet_x_velocity, thread, position)
{
    real x[ND_ND];      /* this will hold the position vector */
    real y;
    face_t f;

    begin_f_loop(f, thread)
    {
        F_CENTROID(x,f,thread);
        y = x[1];
        F_PROFILE(f, thread, position) = 0.125*(1. - (4*y*y)/(64));
    }
    end_f_loop(f, thread)
}

```

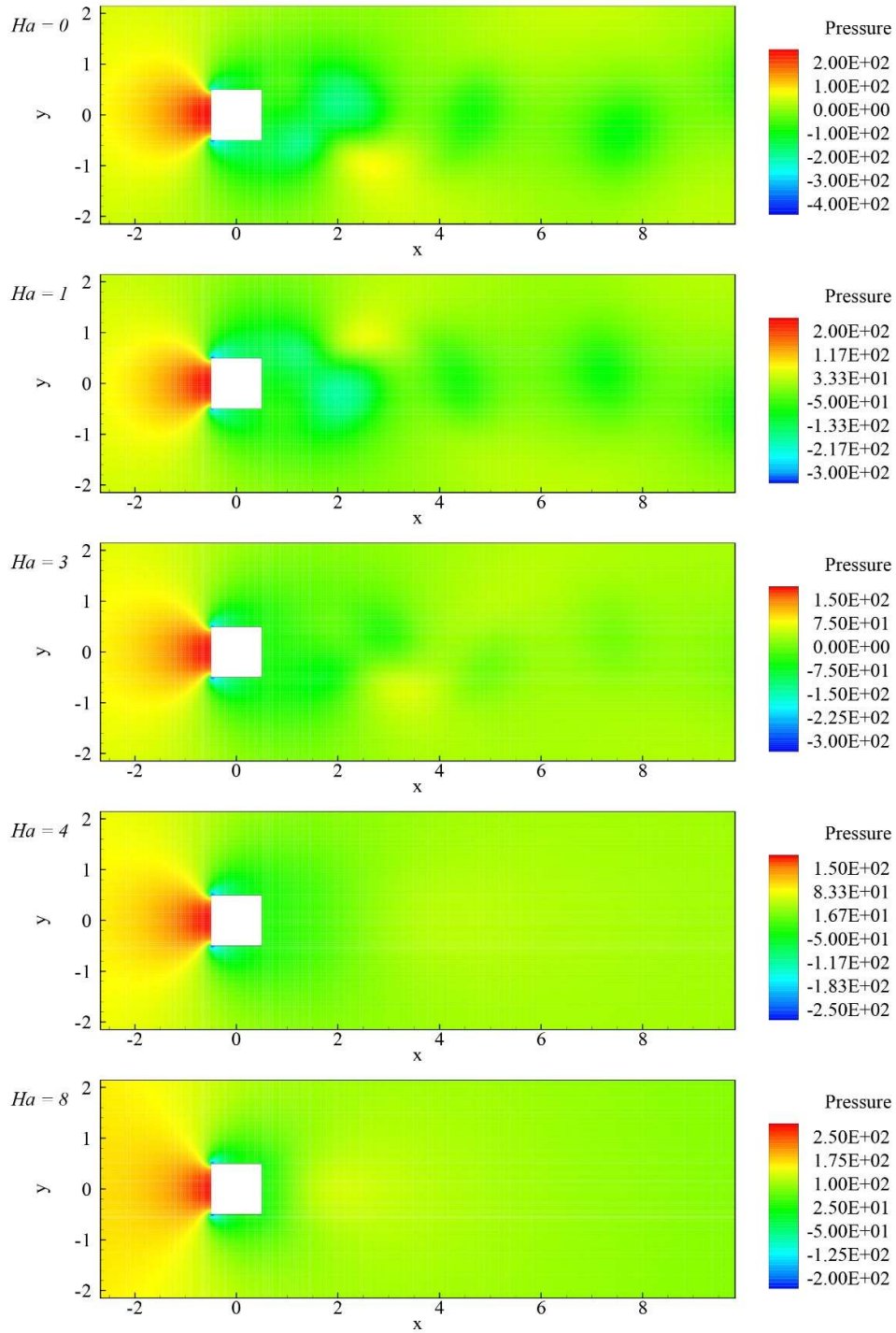
APPENDIX-C: PYTHON CODE FOR STROUHAL NUMBER CALCULATION

```
/******  
  
import numpy as np  
import scipy.signal as signal  
import matplotlib.pyplot as plt  
  
## Read Results  
data = np.loadtxt('cl.txt')  
  
L   = 1           # L = D - Diameter  
V   = 1           # Velocity  
time = data[:,0]  
Cd  = data[:,2]  
Cl  = data[:,3]  
  
# Compute FFT  
N    = len(time)  
dt   = time[2] - time[1]  
# freq = np.fft.fftfreq(N, dt)  
# Cd_fft = np.fft.fft(Cd)  
# Cl_amp = np.fft.fft(Cl)  
# plt.plot(freq, Cl_amp)  
# plt.show()  
## Better stable FFT  
nmax = 12000      # no. of points in the fft  
# freq, Cd_amp = signal.welch(Cd, 1./dt, nperseg=nmax)  
freq, Cl_amp = signal.welch(Cl, 1./dt, nperseg=nmax)  
plt.plot(freq, Cl_amp)  
plt.show()  
## Strouhal Number  
# Find the index corresponding to max amplitude
```



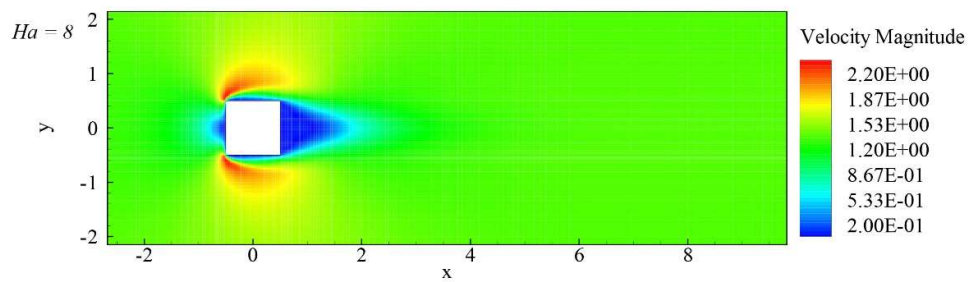
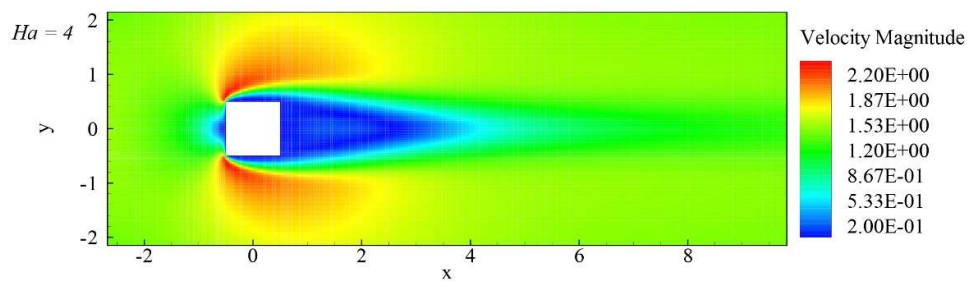
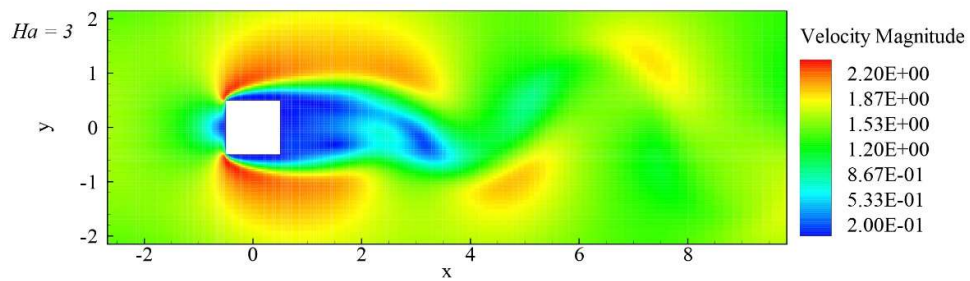
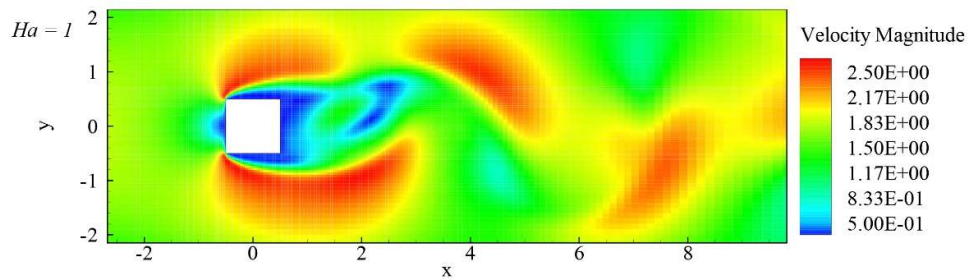
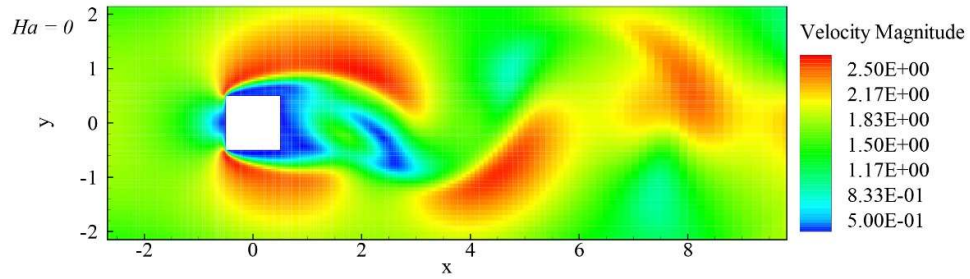
```
Cl_max_fft_idx = np.argmax(abs(Cl_amp))
freq_shed     = freq[Cl_max_fft_idx ]
St           = freq_shed * L / V
print "Vortex shedding freq: %.3f [Hz]" % (freq_shed)
print "Strouhal Number: %.3f" % (St)
```

**APPENDIX-D: PRESSURE CONTOURS FOR SQUARE CYLINDER AT HA =
0 - 8**

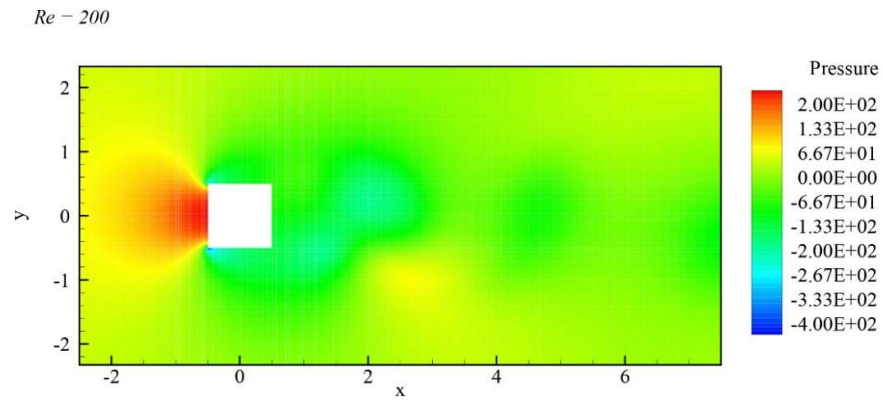
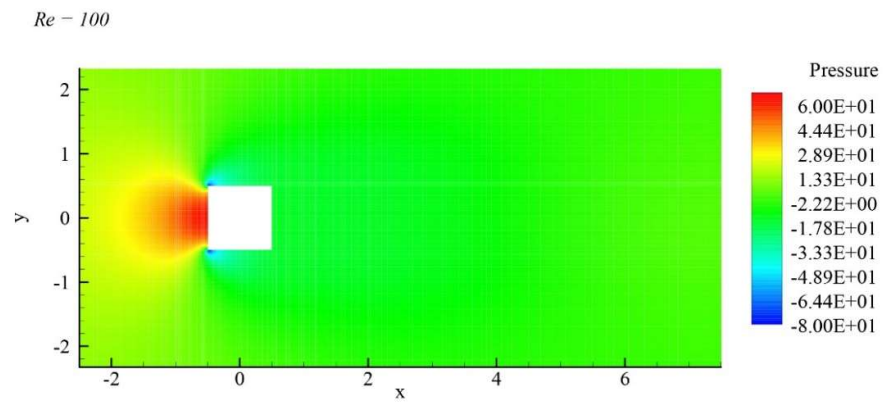
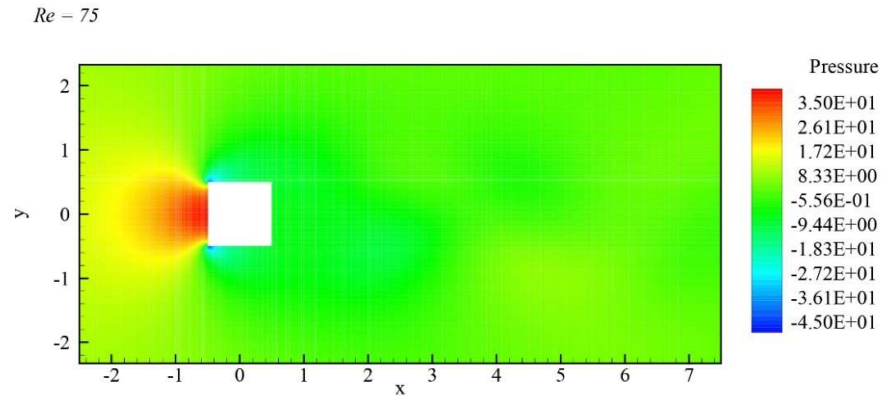


APPENDIX-E: VELOCITY CONTOURS FOR SQUARE CYLINDER FOR HA

= 0 - 8

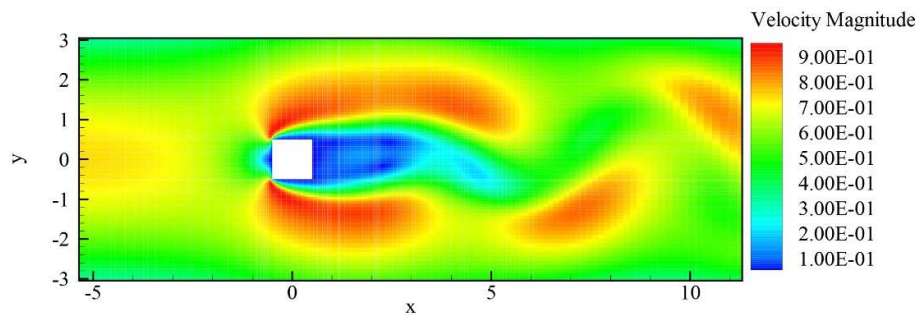


APPENDIX-F: PRESSURE CONTOURS FOR SQUARE CYLINDER AT RE =
75 - 200

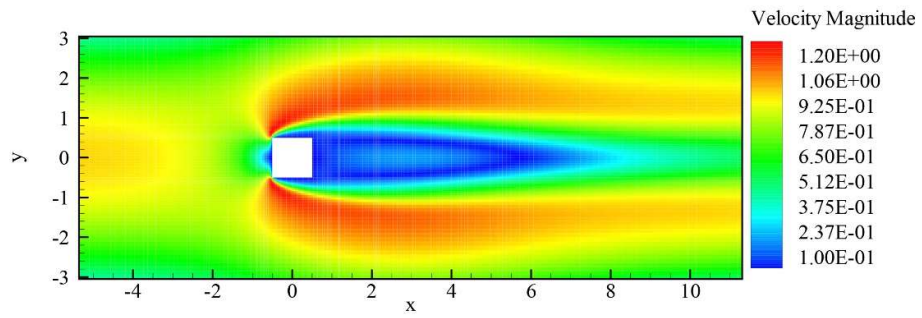


**APPENDIX-G: VELOCITY CONTOURS FOR SQUARE CYLINDER AT $Re =$
75 - 200**

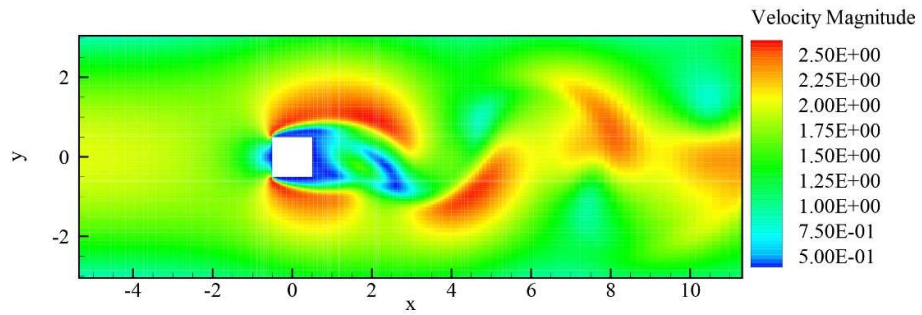
Re = 75



Re = 100

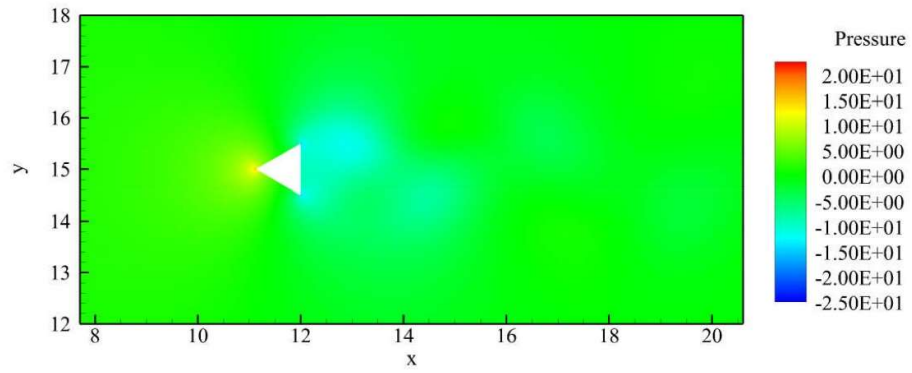


Re = 200

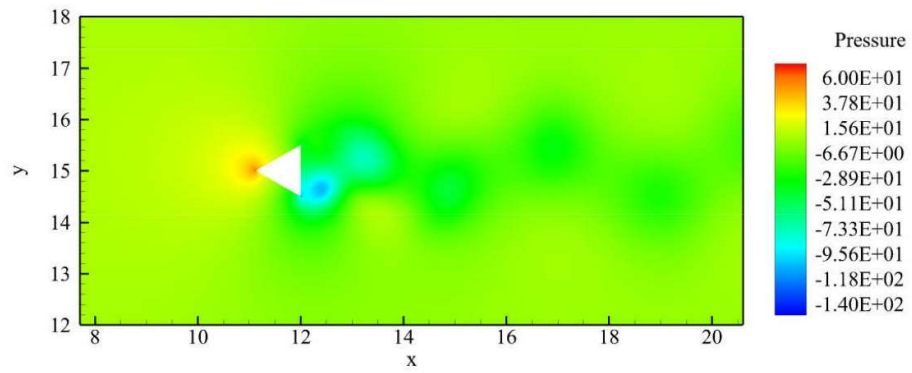


APPENDIX-H: PRESSURE CONTOURS FOR WEDGE AT RE = 50 - 150

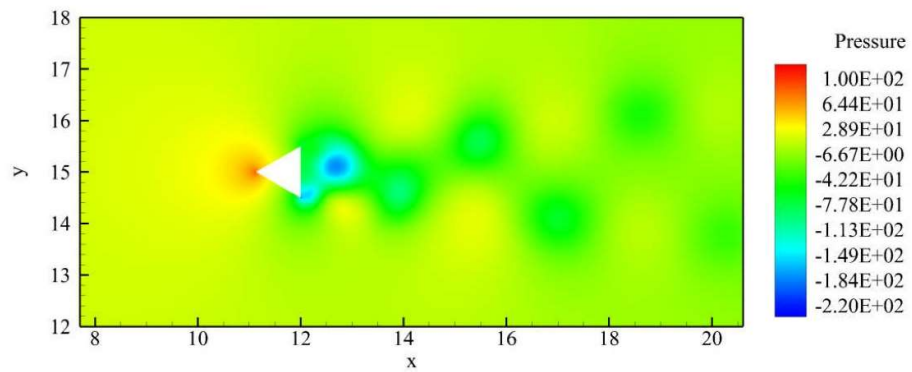
$Re = 50$



$Re = 100$

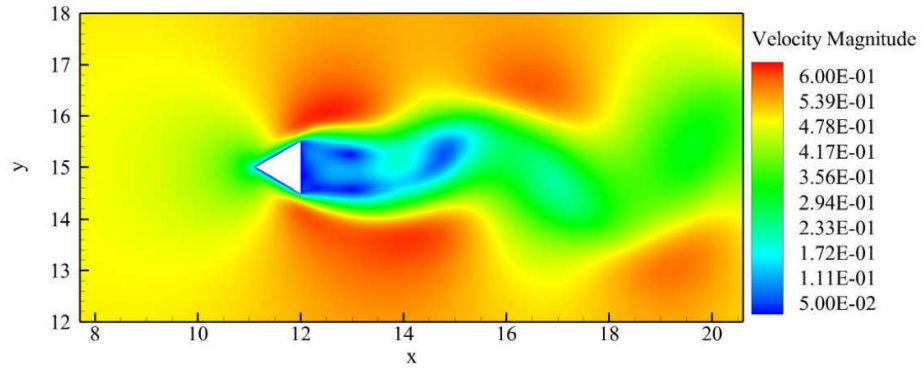


$Re = 150$

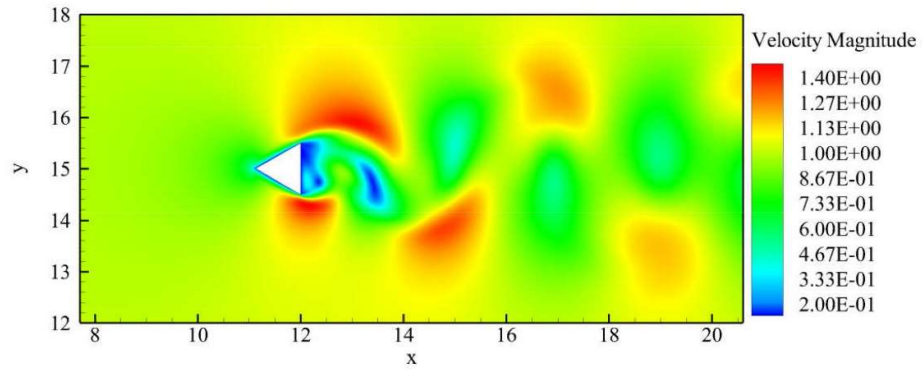


APPENDIX-I: VELOCITY CONTOURS FOR WEDGE AT RE = 50 - 150

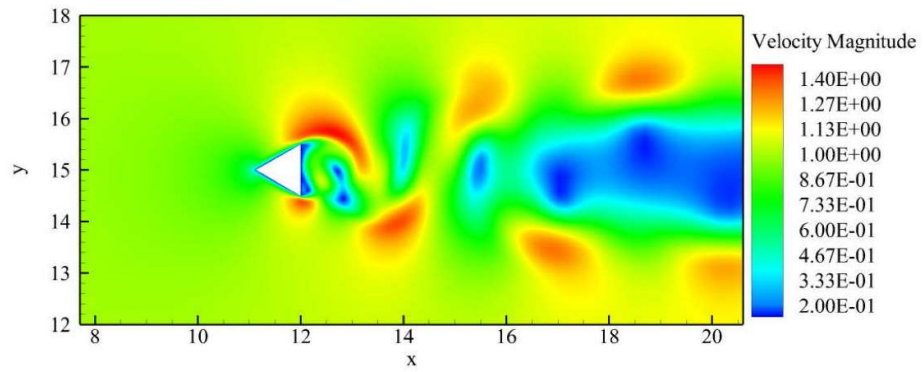
Re = 50



Re = 100

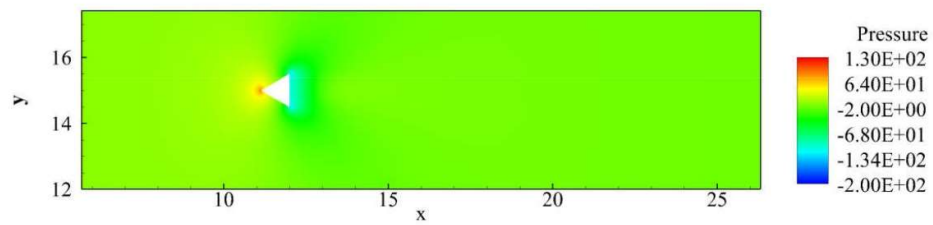
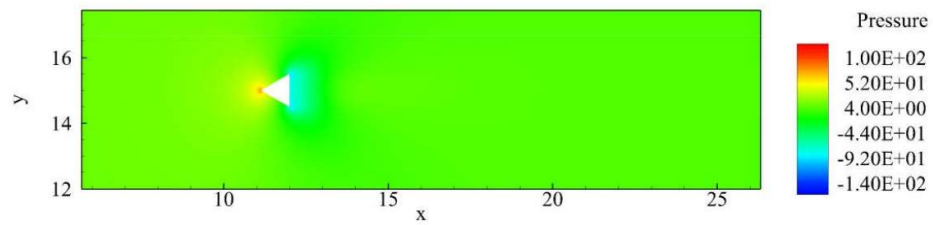
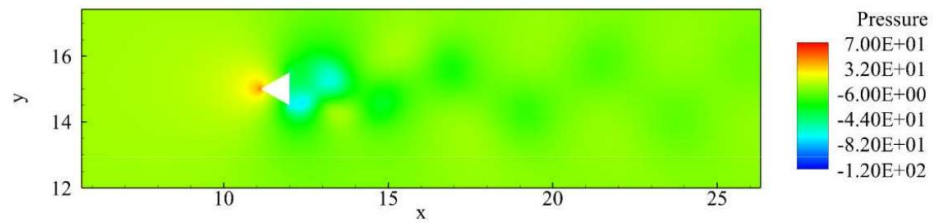
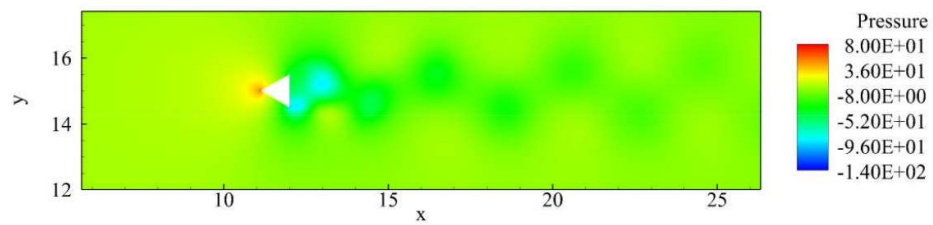
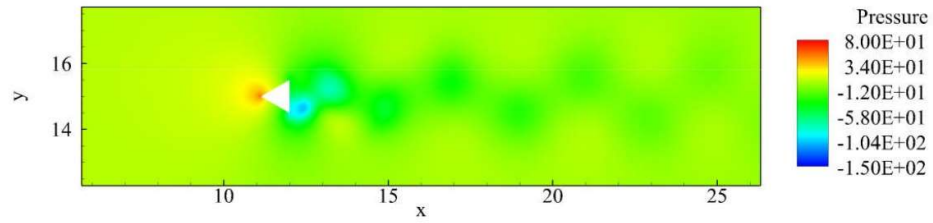


Re = 150



APPENDIX-J: PRESSURE CONTOURS FOR WEDGE AT RE = 100 FOR HA

= 0 - 10



APPENDIX-K: VELOCITY CONTOURS FOR WEDGE AT RE = 100 FOR HA

= 0 - 10

